State of Oregon
Oregon Department of Geology and Mineral Industries
Sarah L. Lewis, Interim State Geologist

GEOLOGIC MAP 122

GEOLOGIC MAP OF THE HARNEY 7.5' QUADRANGLE, HARNEY COUNTY, OREGON

by Robert A. Houston[1], Jason D. McClaughry[2], Carlie J.M. Azzopardi[3], and Mark L. Ferns[4]

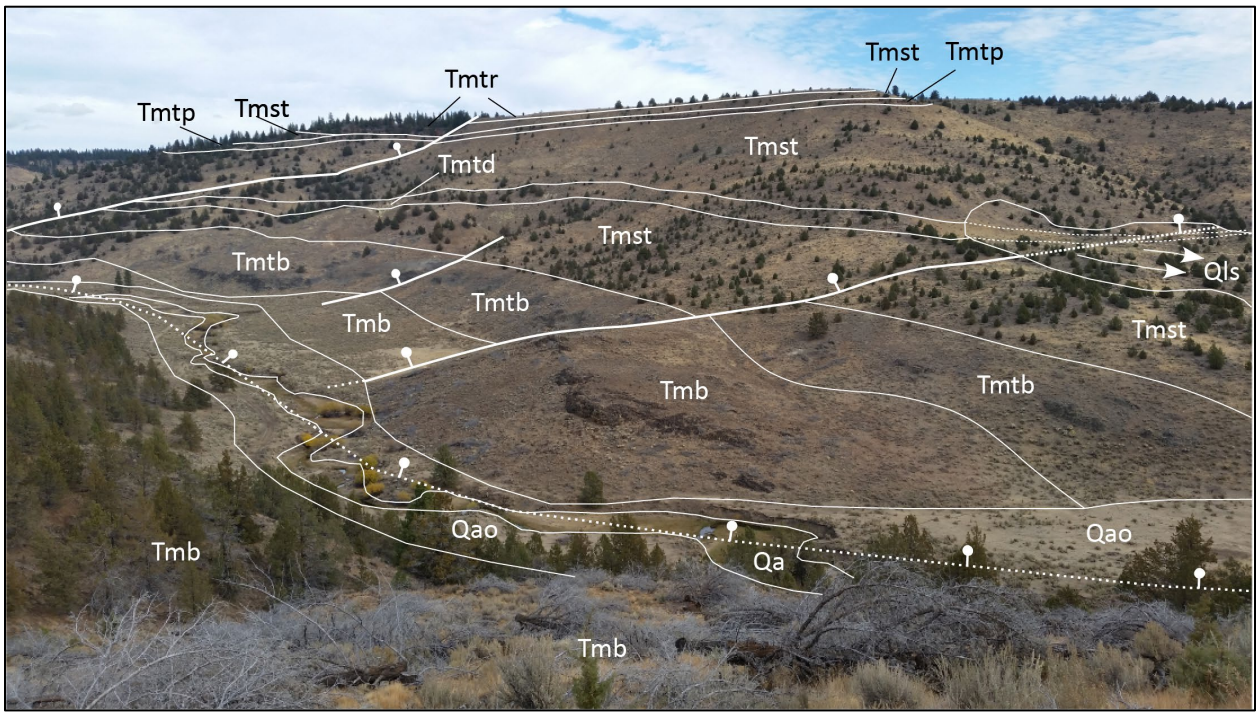

2021

[1] Oregon Department of Geology and Mineral Industries, Springfield Field Office, Springfield Interagency Office, 3106 Pierce Pkwy D, Springfield, OR 97477
[2] Oregon Department of Geology and Mineral Industries, Baker City Field Office, Baker County Courthouse, 1995 3rd Street, Ste. 130, Baker City, OR 97814
[3] Oregon Department of Geology and Mineral Industries, 800 NE Oregon Street, Suite 965, Portland, OR 97232
[4] Retired, formerly at Oregon Department of Geology and Mineral Industries, Baker City Field Office, Baker County Courthouse, 1995 3rd Street, Ste. 130, Baker City, OR 97814

NOTICE

WHAT'S IN THIS REPORT?

This publication provides an updated and spatially accurate geologic framework for the Harney 7.5' quadrangle as part of a multi-year study of the geology of the larger Harney Basin. Geologic data in the publication provide significant new details about the volcanic and structural geologic history of the area and the geologic conditions controlling the distribution of water resources, aggregate and other mineral resources, and geologic hazards.

*Cover photograph: View northeast (upstream) along the Cow Creek drainage (43.69520187, −118.7679977). The valley here is underlain by a complex stratigraphic succession. The lower part of the succession is composed of middle Miocene basalt and basaltic andesite (**Tmb**) lava flows. The upper part of the succession consists of a tuff breccia (**Tmtb**), tuffaceous sedimentary rocks (**Tmst**), Devine Canyon Ash-flow Tuff (**Tmtd**), and Prater Creek Ash-flow Tuff (**Tmtp**). Locally, the Rattlesnake Tuff (**Tmtr**) caps the succession, forming a prominent cliff exposure. Photo credit: Robert A. Houston, 2017.*

Expires: 1/31/2022

Oregon Department of Geology and Mineral Industries Geologic Map 122
Published in conformance with ORS 516.030.

For additional information:
Administrative Offices
800 NE Oregon Street, Suite 965
Portland, OR 97232
Telephone (971) 673-1555
Fax (971) 673-1562
www.oregongeology.org
www.oregon.gov/dogami

TABLE OF CONTENTS

LIST OF FIGURES

LIST OF TABLES

GEODATABASE

HA2021_NCGMP09_v10.1.gdb

See the appendix for geodatabase description.
Geodatabase is Esri® version 10.1 format.

SHAPEFILES AND SPREADSHEETS

Shapefiles

Bedding: HA2021_Bedding.shp
Geochemistry: HA2021_Geochemistry.shp
Magnetics: HA2021_Magnetics.shp
Reference map: HA2021_RefMap.shp
Springs: HA2021_Springs.shp
Water wells: HA2021_WaterWells.shp
Cross Section Lines: HA2021_XSectionLines.shp

Spreadsheets

HA2021_DATA.xlsx master file contains:
- HA2021_Bedding.xlsx
- HA2021_Geochemistry.xlsx
- HA2021_Magnetics.xlsx
- HA2021_Springs.xlsx
- HA2021_WaterWells.xlsx

See the digital publication folder for files.
Metadata is embedded in the geodatabase and shapefiles and is also provided as separate .xml format files.

MAP PLATE

Plate. Geologic Map of the Harney 7.5' Quadrangle, Harney County, Oregon, scale 1:24,000

1.0 INTRODUCTION

The Oregon Department of Geology and Mineral Industries (DOGAMI) mapped the geology of the Harney 7.5′ quadrangle, Harney County, Oregon during 2016 and 2017. This mapping is part of a multi-year geologic study of the Harney Basin, designated a high priority by the Oregon Geologic Mapping Advisory Committee (OGMAC; **Figure 1-1**; Plate). Key objectives of this project are to: 1) provide an updated and spatially accurate geologic framework for the Harney 7.5′ quadrangle; 2) correlate geologic units to surrounding areas; 3) improve the understanding of the structural and lithologic controls on groundwater aquifers; and 4) describe the occurrence of geologic resources (aggregate, industrial, mineral, and energy) and geologic hazards within the quadrangle. This study was supported in part by a grant from the STATEMAP component of the U.S. Geological Survey (USGS) National Cooperative Geologic Mapping Program (G16AC00179). Additional funds were provided by the State of Oregon through DOGAMI and the Oregon Water Resources Department (OWRD).

The core products of this study are this report, an accompanying geologic map and cross sections, and an Esri ArcGIS™ ArcMap™ geodatabase. The geodatabase presents new geologic mapping in a digital format, consistent with the USGS National Cooperative Geologic Mapping Program 2009 draft standard format for digital publication of geologic maps, version 1.1 (NCGMP09, 2010). It contains spatial information about geologic polygons, contacts, and structures, and basic data about each geologic unit such as age, lithology, mineralogy, and structure. The geologic map and cross sections, showing the distribution of bedrock lithology, critical structural relations, and surficial geology are at a scale of 1:24,000 (Plate).

Figure 1-1. Location map of the Harney 7.5′ quadrangle (*following page*), showing the status of geologic mapping completed, in progress, and planned in the Harney Basin. Deep pink area encompasses 2015 to 2016 geologic mapping in the Harney 7.5′ quadrangle (this study). Blue quadrangles were mapped by DOGAMI with funding from STATEMAP between 2015 and 2020 (Niewendorp and others, 2018; Houston and others, 2018; McClaughry and others, 2019, 2020). Yellow quadrangles include geologic maps completed by the USGS (Minor and others, 1987a,b; Johnson, 1994, 1996; Sherrod and Johnson, 1994). Orange quadrangles include geologic mapping completed or in progress by Portland State University (EdMap). Light pink quadrangles include targets of future geologic mapping by DOGAMI. Blue line is the Harney Basin hydrologic boundary. Asterisks are landmarks and labeled as follows: AL – Alkali Lake; AR – Antelope Reservoir; BV – Bear Valley; BR – Beulah Reservoir; BC – Buchanan; BB – Burns Butte; CH – Capehart Lake; CR – Castle Rock; CW – Cow Lakes; CN – Crane; CG – Cougar Mountain; CM – Cottonwood Mountain; CL – Crump Lake; DC – Diamond Craters; DM – Dry Mountain; GB – Glass Buttes; GL – Goose Lake; HL – Harney Lake; HM – Horsehead Mountain; IR – Ingle Mountain; IM – Iron Mountain; JC – Jordan Craters; JR – Juniper Ridge; LA – Lake Abert; LO – Lake Owyhee; LW – Lawen; LJ – Little Juniper Mountain; LV – Logan Valley; ML – Malheur Lake; MNWR – Malheur National Wildlife Refuge; NHS – Neil Hot Springs; SL – Silver Lake; SM – Sheep Mountain; WM – Wagontire Mountain; WRP – Wrights Point; WR – Warm Springs Reservoir.

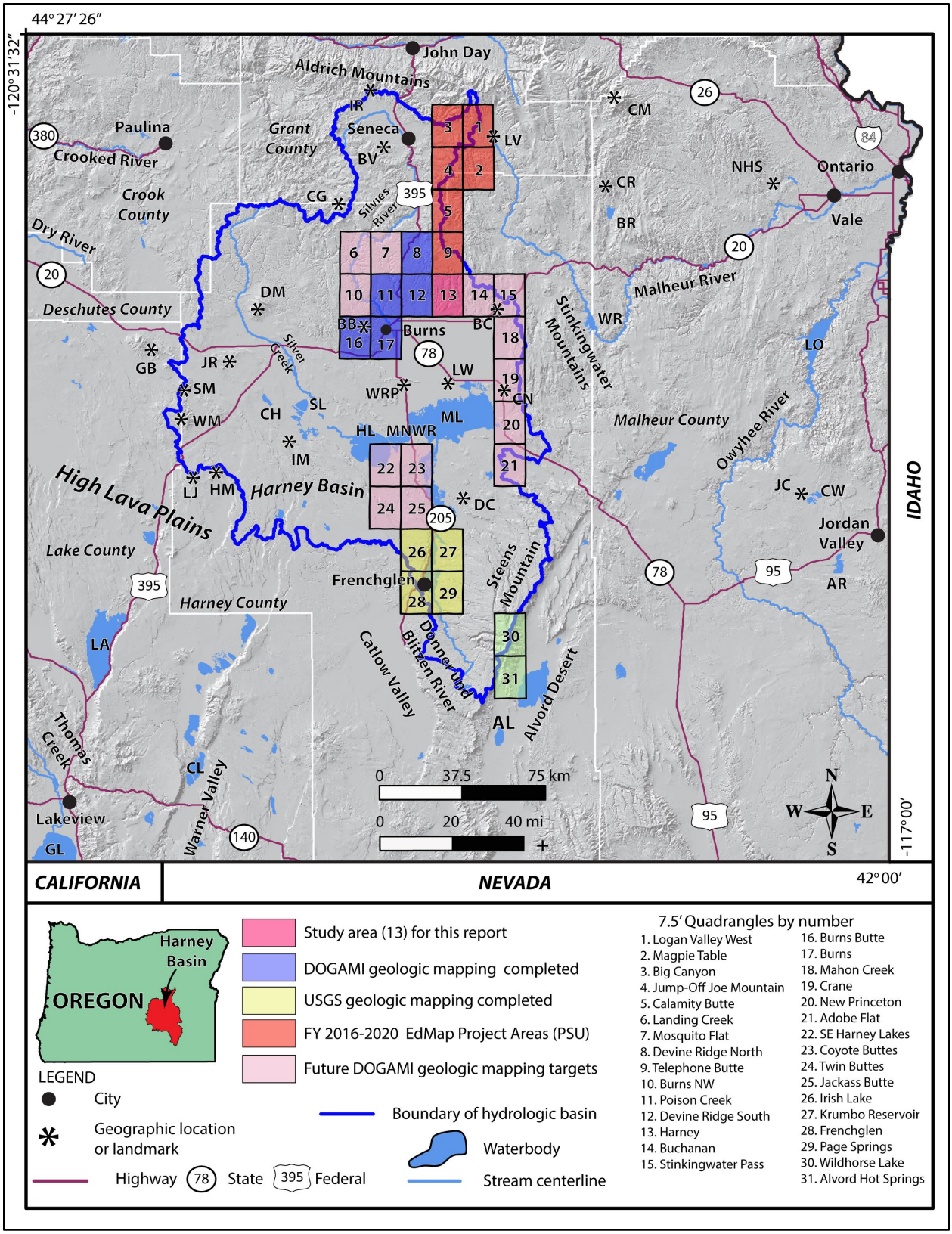
44° 27′ 26″
-120° 31′ 32″
-117° 00′
42° 00′
John Day
Aldrich Mountains
Paulina
Crooked River
Grant County
Seneca
Crook County
Dry River
Deschutes County
Silvies River
Burns
Silver Creek
Stinkingwater Mountains
Malheur River
Malheur County
Owyhee River
Ontario
Vale
NHS
CM
CR
BR
WR
LO
LW
WRP
ML
CN
DM
BB
BC
GB
JR
SM
WM
CH
SL
HL
MNWR
IM
LJ
HM
Harney Basin
High Lava Plains
DC
Lake County
Harney County
Frenchglen
Steens Mountain
Catlow Valley
Blitzen River
Donner und Blitzen
Alvord Desert
AL
AR
JC
CW
Jordan Valley
IDAHO
LA
CL
Thomas Creek
Warner Valley
Lakeview
GL
IR
BV
LV
CG
0 37.5 75 km
0 20 40 mi
N
W
E
S
CALIFORNIA
NEVADA
Harney Basin
OREGON
LEGEND
City
Geographic location or landmark
Highway 78 State 395 Federal
Study area (13) for this report
DOGAMI geologic mapping completed
USGS geologic mapping completed
FY 2016-2020 EdMap Project Areas (PSU)
Future DOGAMI geologic mapping targets
Boundary of hydrologic basin
Waterbody
Stream centerline
7.5′ Quadrangles by number
1. Logan Valley West
2. Magpie Table
3. Big Canyon
4. Jump-Off Joe Mountain
5. Calamity Butte
6. Landing Creek
7. Mosquito Flat
8. Devine Ridge North
9. Telephone Butte
10. Burns NW
11. Poison Creek
12. Devine Ridge South
13. Harney
14. Buchanan
15. Stinkingwater Pass
16. Burns Butte
17. Burns
18. Mahon Creek
19. Crane
20. New Princeton
21. Adobe Flat
22. SE Harney Lakes
23. Coyote Buttes
24. Twin Buttes
25. Jackass Butte
26. Irish Lake
27. Krumbo Reservoir
28. Frenchglen
29. Page Springs
30. Wildhorse Lake
31. Alvord Hot Springs

2.0 GEOGRAPHIC, ECOLOGIC, AND REGIONAL GEOLOGIC SETTINGS

The Harney Basin encompasses an area of ~13,566 km^2 (5,247 mi^2) in southeastern Oregon (**Figure 1-1**). The basin is internally drained and fed by several creeks and rivers, including Silver Creek, Silvies River, and the Donner und Blitzen River (**Figure 1-1**). These tributaries drain into numerous plains, marshes, and lakes, including Harney and Malheur Lakes, which lie near the geographic center of the basin. Topographic relief is substantial, ranging from a high of 2,967 m (9,733 ft) at the summit of Steens Mountain to a low of 1,248 m (4,093 ft) at Harney Lake in the center of the basin. Climate in the Harney Basin is semi-arid.

The Harney Basin straddles the boundary between the Blue Mountains, High Lava Plains, and Basin and Range physiographic provinces (Walker and MacLeod, 1991; **Figure 2-1**). The Blue Mountains Uplift province (BMU) extends into the northern part of the Harney Basin (**Figure 2-1**). The High Lava Plains province (HLP) transects the central part of the basin and is characterized by multiple episodes of late Miocene and younger bimodal volcanism (MacLeod and others, 1976; Jordan and others, 2004). The northern part of the Basin and Range province (BRP) extends into the southern third of the basin and is marked by large displacement (>150 m [>500 feet]) north-northeast to northwest-striking normal faults (e.g., Winter Rim fault, Abert Rim fault, Hart Mountain fault, Steens Mountain fault). BRP deformation began during the Miocene (~17 Ma; Donath, 1962; Thompson and Burke, 1974).

The Brothers fault zone (BFZ) lies across the southern part of the basin as a wide diffuse zone, interpreted as an intracontinental transform fault, separating the extended crust of the BRP from comparatively un-extended BMU crust to the north (Lawrence, 1976; **Figure 2-1**). The Steens fault extends across the eastern end of the BFZ. The western end is obscured by Holocene ash deposits (Lawrence, 1976). Lawrence described the BFZ as a series of longer (as much as 20 km [12.4 mi]) discontinuous en echelon faults (Reidel shears) striking ~N.50°W. and less abundant shorter (5 km [3.1 mi]) N.30°E.-striking faults expressed as horst and graben structures (Lawrence, 1976). Faults in the BFZ largely dip steeply northeast, downdropping regional stratigraphy down to the northeast. Iademarco (2009) and Trench (2008) suggested en echelon faults in the BFZ formed from ~7 Ma to 5 Ma. Trench (2008) suggested east-west extension in the Basin and Range Province is transitioned to the BFZ by way of dextral oblique strike-slip horsetail fractures and structural clockwise rotation about a pole located in northeastern Oregon.

The stratigraphic sequence in the Harney Basin includes a diverse assemblage of middle Miocene and younger lavas, fluvial and lacustrine sedimentary rocks, and widespread ash-flow tuffs that unconformably overlie a deeply eroded basement of Eocene to late Oligocene volcanic and sedimentary rocks and pre-Cenozoic accreted terranes (**Figure 2-2**). Significant geologic units in the Harney Basin include the 16.7 Ma Steens Basalt of the Columbia River Basalt Group (CRBG; Camp and others, 2013), middle to late Miocene ash-flow tuffs, and late Miocene and Pliocene basaltic lava flows of the High Lava Plains Province. Rocks of the Steens Basalt, the earliest lavas to erupt as part of the CRBG, are exposed in the southern part of the Harney Basin and cover much of southeastern Oregon and parts of southwestern Idaho to northern Nevada (**Figure 2-2**). The ~17 to 16 Ma Picture Gorge Basalt (Cahoon and others, 2020) of the CRBG largely occurs in north-central Oregon and extends south to the northern part of the Harney Basin (Cahoon and Streck, 2017). Three voluminous tuffs, the 9.63 Ma Devine Canyon Ash-flow Tuff (Ford and others, 2013; S. L. Isom and M. J. Streck, unpub. data, 2017), 8.41 Ma Prater Creek Ash-flow Tuff (Jordan and others, 2004), and 7.05 Ma Rattlesnake Tuff (Streck and Grunder, 1995), overlie the CRBG and are important stratigraphic markers where exposed. The areal extent of the Rattlesnake Tuff is as much as 40,000 km^2 (15,444 miles^2). The caldera sources for these tuffs are not exposed and but are

thought on the basis of thickness and distribution to reside in the Harney Basin to the south and southwest of the study area (Greene, 1972; Streck, 1994; Khatiwada and Keller, 2015). Locally, Pliocene olivine-basalts of the High Lava Plains and several late Pleistocene to Holocene volcanic fields that occur along the northwest-striking BFZ locally overlie the ash-flow tuffs (**Figure 2-2**). Central and marginal parts of the Harney Basin are covered by sequences of Quaternary sediments (<100 m [330 ft] thick). The northern region of the basin can be generally described as a south dipping block on the flank of the Strawberry Mountains. Pre-Tertiary basement rocks are exposed less than 8 km (5 mi) to the northwest of the study area (**Figure 2-2**).

Figure 2-1. Physiographic province map of Oregon, showing location of the Brothers fault zone, selected Basin and Range faults, and the study area. Abbreviations: CR – Coast Range; HC – High Cascades; KM – Klamath Mountains; WC – Western Cascades; WV – Willamette Valley. Solid black lines demarcate physiographic provinces (after Walker, 1977). Blue lines are selected major Basin and Range type normal faults, showing normal displacement direction (ball and bar on downdropped block). Red line marks the location of the Harney hydrologic basin. Basemap: 10-m hillshade DEM.

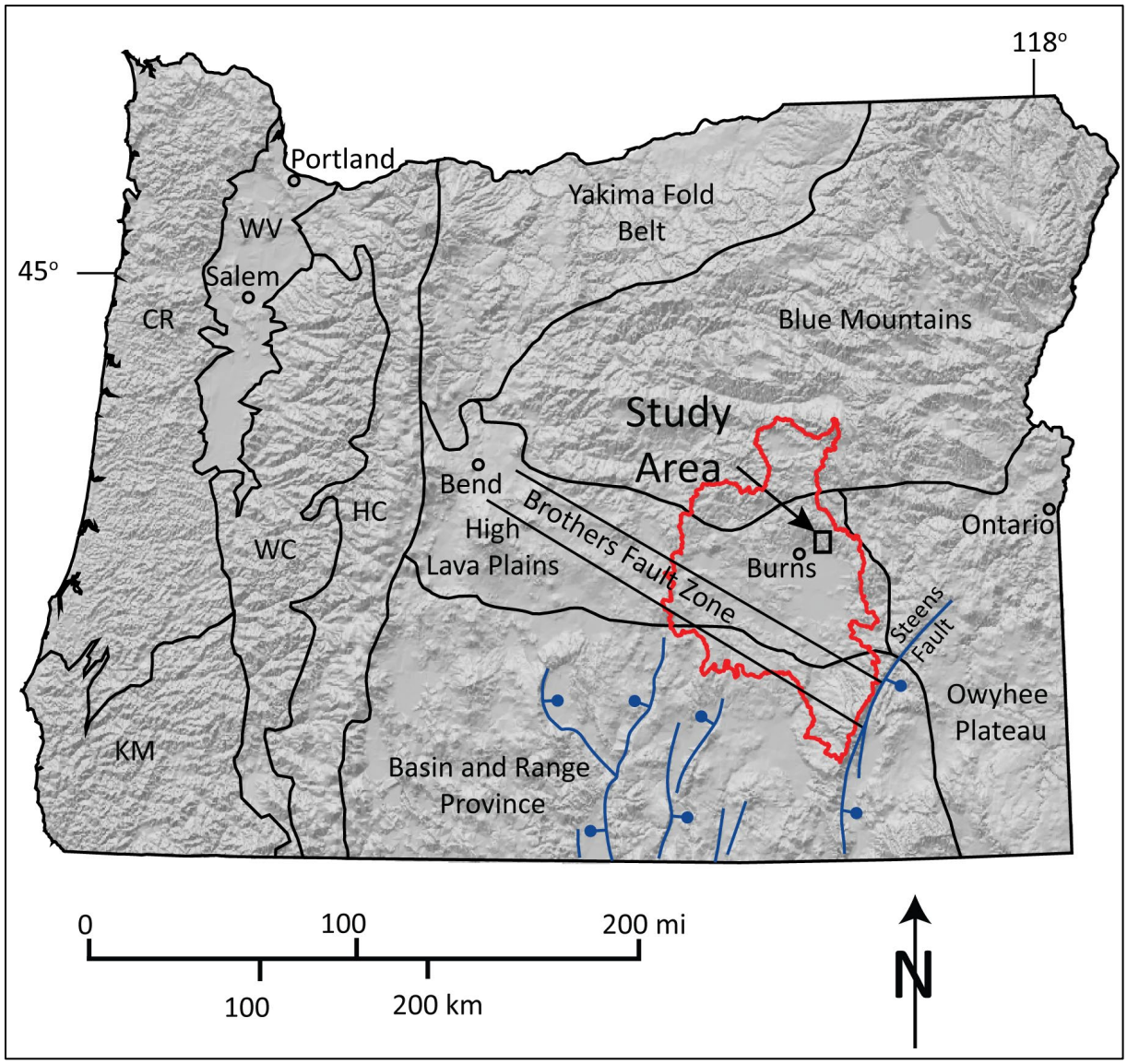

Figure 2-2. Generalized geologic map of southeastern Oregon, after compiled data of Smith and Roe (2015). Red-outlined quadrangle is the study area. The blue line marks the location of the Harney hydrologic basin.

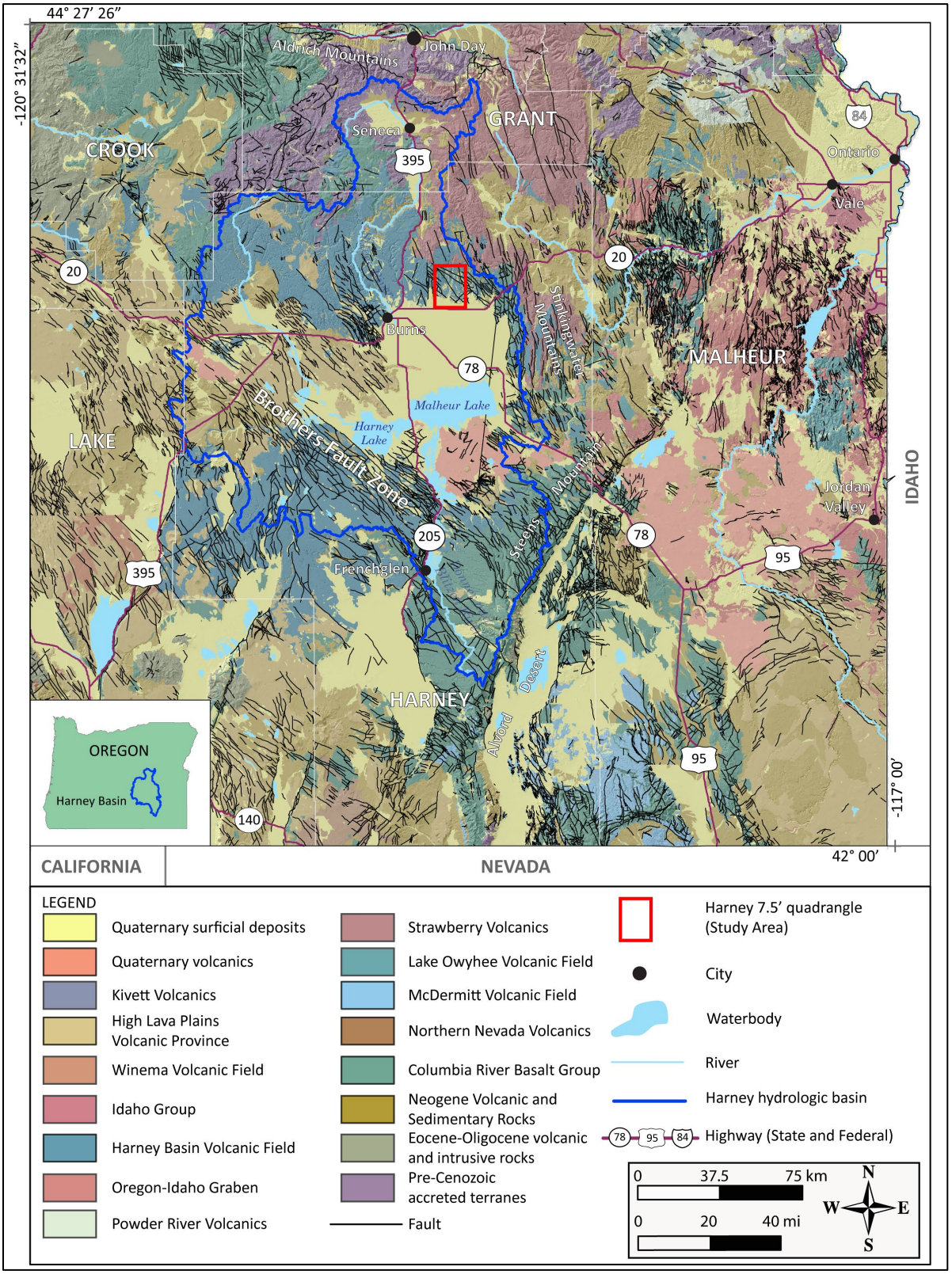

3.0 PREVIOUS WORK

This report builds on previous regional geologic mapping, groundwater studies, and natural resource investigations (**Figure 3-1**). Earlier geologic maps and reports displaying the bedrock geology in and adjacent to the study area include those by Piper and others (1939), Greene (1972), Greene and others (1972), Brown and others (1980a,b), Brown (1982), McGrane (1985), Walker and MacLeod (1991), Smith and Roe (2015), S. L. Isom and M. J. Streck (unpublished data, 2017), Niewendorp and others (2018), Houston and others (2018), and M. Cruz and M. J. Streck (unpublished data, 2018)(**Figure 3-1**). Additional scientific investigations consulted during this study include Russell (1884), Wagner (1944 unpublished report, Valley View Prospect [cinnabar, geodes], DOGAMI), Leonard (1970), Wallace and Calkins (1956), Walker and Repenning (1965), Brown and Thayer (1966), Walker (1970), Greene (1973), Niem (1974), Lawrence (1976), Walker (1979), Gray and others (1983), Minor and others (1987a,b), Sherrod and Johnson (1994), Sheppard (1994), MacLean (1994), Streck (1994), Streck and Grunder (1995), Johnson (1994, 1996, 1998a,b), Jordan (2001), Jordan and others (2002), Camp and others (2003), Jordan and others (2004), Streck and Ferns (2004), Trench (2008), Meigs and others (2009), Milliard (2010), Ford (2012), Boschmann (2012), Ferns and McClaughry (2013), Camp and others (2013), Ford and others (2013), Streck and others (2015), Khatiwada and Keller (2015), Isom (2017), and McClaughry and others (2019, 2020).

Figure 3-1. Sources of geologic maps consulted during the project. See DataSourcePolys feature class in the geodatabase. Blue line marks the location of the Harney hydrologic basin. The basemap is a 10-m shaded relief DEM.

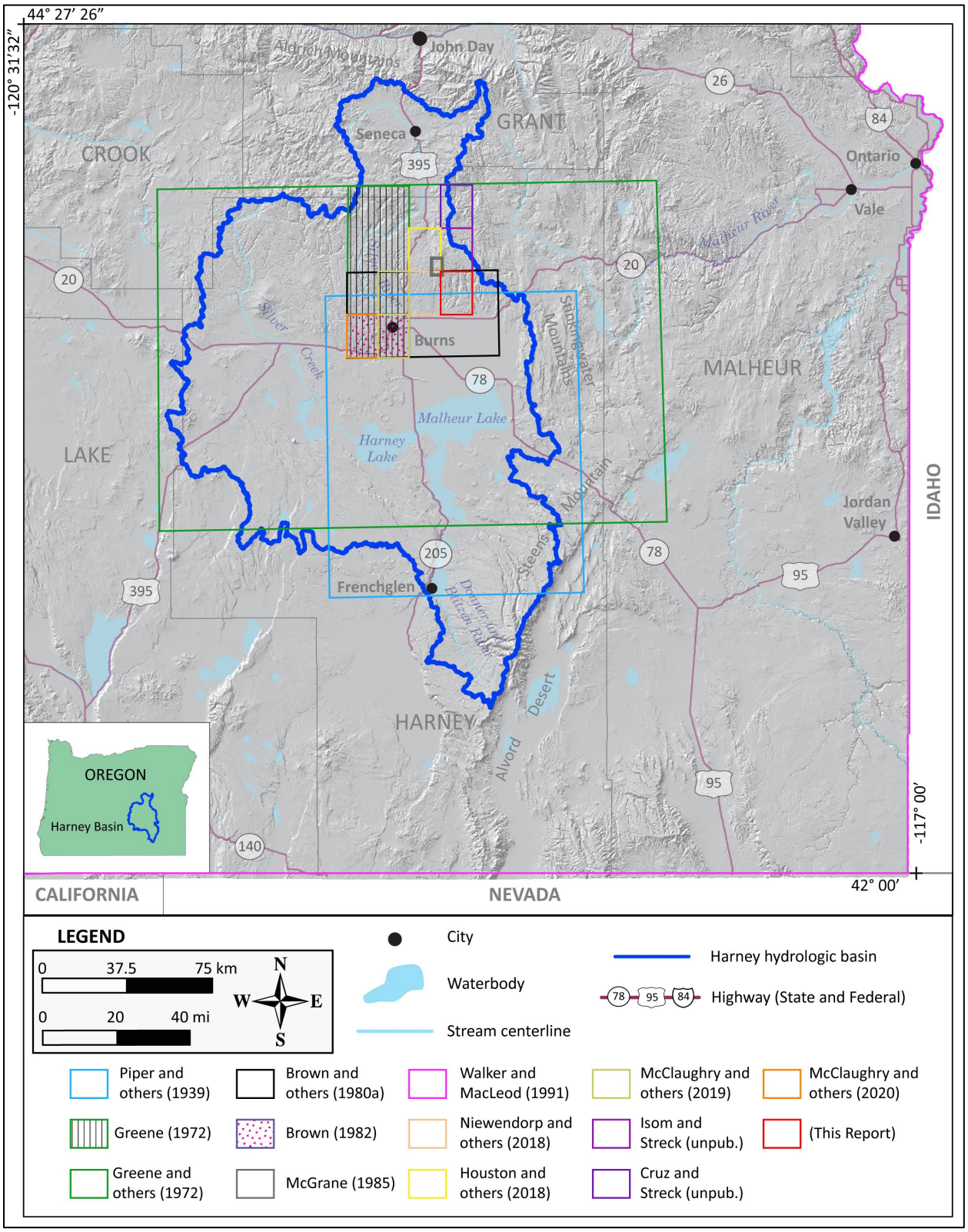

4.0 METHODOLOGY

Geologic data were collected digitally using iGIS™, a Geographic Information Systems software package compatible with Esri ArcGIS™, on a GPS-enabled Apple™ iPad 2. Geologic mapping used shaded relief raster images, USGS digital raster graphics (DRGs), and digital orthophoto imagery (2016) as basemaps. Fieldwork conducted during this study consisted of data collection along roads, combined with transects following lithologic contacts and faults across public and private timber and rangelands. Standard geologic methods for collecting samples and measuring attitudes of inclined bedding, geologic features, and faults were employed. Digitization and the final digital Esri ArcGIS™ format geodatabase was completed at a minimum scale of 1:24,000.

Mapping was supported by new and compiled X-ray fluorescence (XRF) geochemical analyses of whole-rock samples, thin-section petrography, and measurements of natural remanent magnetization (magnetic polarity) (Plate; Appendix). Whole-rock geochemical samples were prepared and analyzed by X-ray fluorescence (XRF) at the Washington State University GeoAnalytical Lab, Pullman, Washington, under the direction of Dr. Scott Boroughs. Analytical procedures for the Washington State University GeoAnalytical Lab are described by Johnson and others (1999) and can be obtained online at https://s3.wp.wsu.edu/uploads/sites/2191/2017/06/Johnson-Hooper-and-Conrey.pdf. Major element determinations are normalized to a 100-percent total on a volatile-free basis and recalculated with total iron expressed as FeO*. Whole-rock geochemical data are useful in classifying volcanic rocks, as many lavas are too fine grained and glassy to be adequately characterized by mineralogical criteria alone. Descriptive rock unit names for volcanic rocks are based in part on the British Geological Survey classification schemes of Gillespie and Styles (1999), Robertson (1999), and Hallsworth and Knox (1999), and normalized major element analyses are plotted on the total alkali ($Na_2O + K_2O$) versus silica (SiO_2) diagram (TAS) of Le Bas and others (1986), Le Bas and Streckeisen (1991), and Le Maitre and others (2004). Magnetic polarity of volcanic units was determined at outcrops using a handheld digital fluxgate magnetometer. Microsoft Excel® spreadsheets tabulating geochemical analyses, magnetic polarity measurements, and strike and dip measurements are provided as part of this publication and are in the Appendix.

In this report, volcanic rocks with fine-grained (<1 mm [0.04 in]; Mackenzie and others, 1997; Le Maitre and others, 2004) average crystal or particle size in the groundmass are characterized in the following manner:

- A coarse groundmass if the average crystal or particle size is <1 mm (0.04 in) and can be determined using the naked eye (>~0.5 mm [0.02 in]).
- A medium groundmass if crystals of average size cannot be determined by eye but can be distinguished by using a hand lens (>~0.05 mm [0.002 in]).
- A fine groundmass if crystals or grains of average size can be determined only by using a microscope, or by hand lens recognition of sparkle or sheen in reflected light, indicating the presence of crystalline groundmass.
- A glassy groundmass if the groundmass has (fresh), or originally had (altered), groundmass with the characteristics of glass (e.g., conchoidal fracture; sharp, transparent edges; vitreous luster; etc.).
- Mixtures of crystalline and glassy groundmass are described as intersertal; ratios of glass to crystalline materials may be indicated by textural terms including holocrystalline, hypocrystalline, hyalophitic, hyalopilitic, and holohyaline.

- Microphenocrysts are defined as crystals larger than the overall groundmass and <1 mm across (0.04).

Grain size of clastic sedimentary rocks is described following the Wentworth (1922) scale. Hand samples of unconsolidated sediments and clastic sedimentary rocks were compared in the field and/or in the laboratory to graphical representations (comparator) of the Wentworth scale to determine average representative grain size in various parts of a respective sedimentary geologic unit. Colors given for hand-sample descriptions are from the Geological Society of America Rock-Color Chart Committee (1991).

Subsurface geology shown in the geologic cross sections incorporates lithologic interpretations from water well records available through the Oregon Water Resources Department (OWRD) Groundwater Resource Information Distribution (GRID) system (Plate; Appendix). An attempt was made to locate water wells and other drill holes that have well logs archived by OWRD. Approximate locations were estimated by using a combination of sources, including internal OWRD databases of located wells, Google Earth™, tax lot maps, street addresses, and aerial photographs. The accuracy of the locations ranges widely, from errors of 0.7 mi (1.1 km) possible for wells located only by section and plotted at the section centroid to a few tens of feet for wells located by address or tax lot number on a city lot with bearing and distance from a corner. For each well, the number of the well log (Well Log ID) is indicated in the database. This number can be combined with the first four letters of the county name (e.g., HARN-51852), to retrieve an image of the well log from the OWRD web site (https://apps.wrd.state.or.us/apps/gw/well_log/). A database of eight well logs with interpreted subsurface geologic units for the Harney 7.5′ quadrangle is provided (Appendix).

Geographic map coordinates (decimal degree, datum = WGS84) are provided for outcrop photographs in report figures, allowing the interested reader to visit these sites in the field or to remotely visualize the area using Google Earth™. Coordinates can be entered into the "Fly to" box (e.g., 45.661323, -121.471230) in the search toolbar and Google Earth™ will automatically locate and focus on the specified site.

5.0 EXPLANATION OF MAP UNITS

The suite of terrestrial sedimentary and volcanic bedrock units in the Harney 7.5′ quadrangle ranges in age from upper Miocene to upper Oligocene (**Figure 5-1**; Plate). Bedrock geologic units are locally covered along drainages and on some slopes in the project area by Pleistocene and Holocene surficial deposits. Widely separated stratigraphic units were grouped based on apparent stratigraphic position, lithology, and chemical composition. Unit names follow local stratigraphic nomenclature when available, but when formal rock names are lacking, informal names are given because of composition or sites of good exposure. **Figure 5-1** depicts a time-rock chart showing age ranges for Cenozoic bedrock and Quaternary surficial units.

5.1 Overview of map units

UPPER CENOZOIC SURFICIAL DEPOSITS

Qf modern fill and construction material (upper Holocene)
Qa alluvium (Holocene and Upper Pleistocene[?])
Qaf fan deposits (Holocene and Upper Pleistocene[?])
Qls landslide deposits (Holocene and Upper Pleistocene[?])
Qao older alluvium (Holocene and Upper Pleistocene[?])

Qlo loess (Holocene and Upper Pleistocene[?])

Angular unconformity to disconformity

UPPER CENOZOIC VOLCANIC AND SEDIMENTARY ROCKS

LOWER PLEISTOCENE TO UPPER MIOCENE SEDIMENTARY ROCKS

Harney Formation

QTst sedimentary rocks (lower Pleistocene[?] to upper Miocene[?])

Angular unconformity to disconformity

UPPER MIOCENE VOLCANIC AND SEDIMENTARY ROCKS

Tmtr Rattlesnake Tuff (upper Miocene) 7.05 ± 0.01 Ma ($^{40}Ar/^{39}Ar$; outside study area); 7.093 ± 0.015 Ma ($^{40}Ar/^{39}Ar$; outside study area)

Angular unconformity

Tmtp Prater Creek Ash-flow Tuff (upper Miocene) 8.41 ± 0.16 Ma ($^{40}Ar/^{39}Ar$; outside study area); 8.48 ± 0.05 Ma ($^{40}Ar/^{39}Ar$; outside study area)

Angular unconformity

Tmtd Devine Canyon Ash-flow Tuff (upper Miocene) 9.63 ± 0.05 Ma ($^{40}Ar/^{39}Ar$; outside study area), 9.74 ± 0.02 Ma ($^{40}Ar/^{39}Ar$; outside study area)

Tmst tuffaceous sedimentary rocks (upper Miocene and middle Miocene[?])

Disconformity

MIDDLE AND LOWER MIOCENE VOLCANIC ROCKS

Tmtb tuff breccia (middle Miocene)

Tmt pumice tuff (middle Miocene)

Tmtl pumice-lithic tuff (middle Miocene)

Tmdc Dinner Creek Tuff (middle Miocene or lower Miocene) 15.9 ± 0.09 Ma ($^{40}Ar/^{39}Ar$; outside study area); 16.16 ± 0.02 Ma ($^{40}Ar/^{39}Ar$; outside study area)

Tmb basalt and basaltic andesite lava flows (middle Miocene and lower Miocene)

Angular unconformity to disconformity

LOWER CENOZOIC VOLCANIC AND SEDIMENTARY ROCKS

Toa andesite (upper Oligocene) 24.75 ± 0.15 Ma ($^{40}Ar/^{39}Ar$; outside study area)

Tor rhyolite (upper Oligocene[?])

Toda dacite (upper Oligocene[?])

Figure 5-1. Time-rock chart of the Harney 7.5’ quadrangle showing the 19 geologic units shown on the geologic map and in geologic cross sections in the Harney 7.5’ quadrangle.

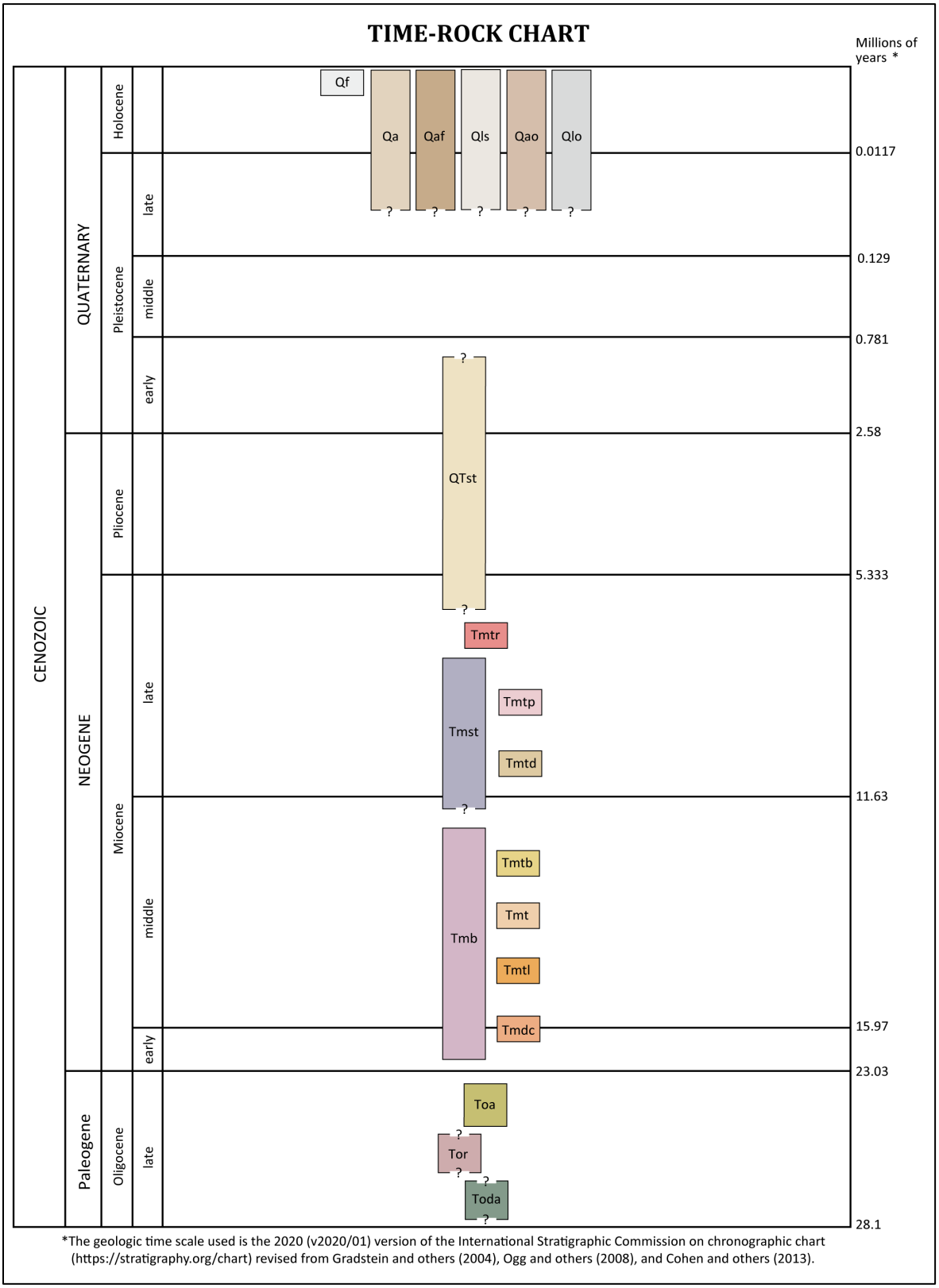

5.2 Upper Cenozoic surficial deposits

Upper Cenozoic sedimentary and volcanic rocks are locally covered by Upper Pleistocene and Holocene surficial deposits in the Harney 7.5′ quadrangle, including alluvial, landslide, and fan deposits (**Figure 5-1**; Plate 1). Surficial units within the project area are delineated on the basis of geomorphology as interpreted from a combination of field observations, topographic maps, 5-m structure from motion (SFM) generated DEMs, 10-m DEMs, and 2016 U.S. Department of Agriculture National Agriculture Imagery Program (NAIP) orthophotos.

Qf **modern fill and construction material (upper Holocene)**—Artificial or constructed fill deposits of poorly sorted and crudely layered mixed gravel, sand, clay, and other engineered fill (Plate). These deposits (**Qf**) usually contain rounded to angular clasts ranging from small pebbles as much as several meters across. The orientation of clasts is typically less uniform than is found in naturally occurring imbricated or bedding-parallel gravel. Deposits mapped as modern fill and construction material (**Qf**) in the study area are generally associated with railroad grades, dams and levees, road embankments, causeways, culvert fills, and mined land (Plate). The thickness of fill-deposits (**Qf**) may exceed 30 m (98 ft). Unit **Qf** is assigned a late Holocene age.

Qa **alluvium (Holocene and Upper Pleistocene[?])**—Unconsolidated gravel, sand, silt, and clay deposited along active stream channels and on adjacent floodplains (**Figure 5-2;** Plate). Gravel deposited as imbricated, massive to cross-stratified accumulations on smaller mid-channel islands and bars are the most common type of near channel alluvium (**Qa**) along major tributaries, such as Coffee Pot, Rattlesnake, and Cow Creeks. Thickness of alluvial deposits (**Qa**) is generally less than 5 m (16 ft); bedrock units may be locally exposed in the bottoms of stream channels within areas mapped as unit **Qa**. Unit **Qa** is assigned a Late Pleistocene(?) and Holocene age on the basis of stratigraphic position and a lack of more precise age indications.

Figure 5-2. Photograph of older alluvium (Qao) and alluvium (Qa) along Cow Creek (45.460780, -121.234613). The active channel has cut down into the older alluvium (Qao) ~2.5 m (8 ft) at this location. Scale bar is 2.5 m (8 ft) tall.

Qaf **fan deposits (Holocene and Upper Pleistocene[?])**—Unconsolidated, poorly sorted, poorly graded deposits of boulders, cobbles, pebbles, granules, sand, silt, and clay in fan-shaped accumulations at the transition between low-gradient valley floodplains and steeper upland drainages (Plate). Individual fans (**Qaf**) generally cover less than 4 hectares (10 acres). The local thickness of alluvial fan deposits (**Qaf**) is variable but is probably <15 m (<50 ft). Fan deposits (**Qaf**) are considered to be Late Pleistocene(?) and Holocene in age on the basis of stratigraphic position and a lack of more precise age indicators.

Qls **landslide deposits (Holocene and Upper Pleistocene[?])**—Unconsolidated, chaotically mixed masses of rock and soil deposited by landslides (e.g., slides, debris flows, rock avalanches; Plate). Landslide terrain is characterized by sloping hummocky surfaces. Landslides (**Qls**) are often traceable uphill to head scarps or failure surfaces. Individual landslides (**Qls**) mapped are as small as 0.1 hectares (0.4 acres) and as large as 138 hectares (341 acres). Thickness of the landslide deposits (**Qls**) is highly varied but may be more than several tens of meters in larger deposits. Landslide deposits (**Qls**) are typically referred to as clay, boulders, rock, or rock and clay in water well logs (Appendix). Landslide deposits (**Qls**) range in age from Late Pleistocene(?) to those that have been recurrently active in the late Holocene. Large areas mapped as landslide deposits (**Qls**) typically include many discrete deposits of varying age that are not differentiated here.

Qao **older alluvium (Holocene and Upper Pleistocene[?])**—Moderately dissected, unconsolidated, well- to poorly-sorted and stratified gravel, sand, silt, and clay deposited in active stream channels and on adjoining flood plains (**Figure 5-2**; Plate). Unit **Qao** is recognized and mapped along Coffee Pot Creek, Rattlesnake Creek, and Cow Creek and related tributaries, where deposits reside adjacent to incised drainages filled with younger Quaternary alluvium (**Qa**)(Plate). Thickness of unit **Qao** likely does not exceed 6 m (20 ft). Unit **Qao** is assigned a Late Pleistocene(?) and Holocene age on the basis of stratigraphic position and a lack of more precise age indications.

Qlo **loess (Holocene and Upper Pleistocene[?])**—Very fine grained, massive sand and clay mantling upland surfaces in the southwestern part of the study area (Plate). Thickness of unit **Qlo** ranges from thin veneers ≤1 m thick (3.3 ft) to as much as 6 m (20 ft) thick. The distribution of loess (**Qlo**) is identified on the basis of field observations, a 5-m SFM generated DEM, and 2014 NAIP orthophotos (Plate). Thinner or geographically restricted deposits (**Qlo**) have not been mapped where the underlying geology can be reasonably inferred or is known to be present at or near the surface. Unit **Qlo** is assigned a Late Pleistocene(?) and Holocene age on the basis of stratigraphic position.

Angular unconformity to disconformity

5.3 Upper Cenozoic volcanic and sedimentary rocks

Mapped upper Cenozoic units in the Harney 7.5′ quadrangle include upper Miocene to lower Pleistocene(?) sedimentary rocks (**QTst**) overlying three laterally extensive upper Miocene rhyolitic ash-flow tuffs (**Tmtr**, **Tmtp**, **Tmtd**)(Plate). Ash-flow tuffs were deposited concurrently with a sequence of tuffaceous sedimentary rocks (**Tmst**)(Plate). These rocks overlie a lower to middle Miocene succession of basalt and basaltic andesite lava flows (**Tmb**), interstratified with the ~16 Ma Dinner Creek Tuff (**Tmdc**) and three other mapped tuffs (**Tmtl**, **Tmt**, **Tmtb**)(Plate). The lowermost exposed part of the stratigraphic section in the study area is composed of late Oligocene andesite (**Toa**), dacite (**Toda**), and rhyolite (**Tor**). Whole-rock XRF geochemical analyses were obtained from 93 samples of Cenozoic volcanic and intrusive rocks in the Harney 7.5′ quadrangle (Plate; Appendix). Representative major- and trace-element data for these units are shown in **Figure 5-3**, **Figure 5-4**, and **Table 5-1** (see geochemical data in the Geochemistry feature class in the geodatabase, shapefile named *HA2021_Geochemistry.shp*, and spreadsheet named *HA2021_Geochemistry*).

Figure 5-3. Total alkalis ($Na_2O + K_2O$) versus silica (SiO_2) plot classification (TAS), showing whole-rock XRF analyses on volcanic rocks from the upper Miocene to upper Oligocene volcanic rocks in the Harney 7.5' quadrangle (normalized to 100 percent anhydrous). Fields and rock names are from Le Bas and others (1986) and Le Maitre and others (1989). Red-dashed line is the dividing line between alkaline, subalkaline/tholeiitic fields after Cox and others (1979). Plot includes 93 analyses obtained for this study and those compiled from previous studies (MacLean, 1994; Ford, 2012; M. Ferns, unpublished data, 2015; Houston and others, 2018; Niewendorp and others, 2018; McClaughry and others, 2019, 2020). The letters A and B indicate two pumice populations that characterize tuff breccia (Tmtb).

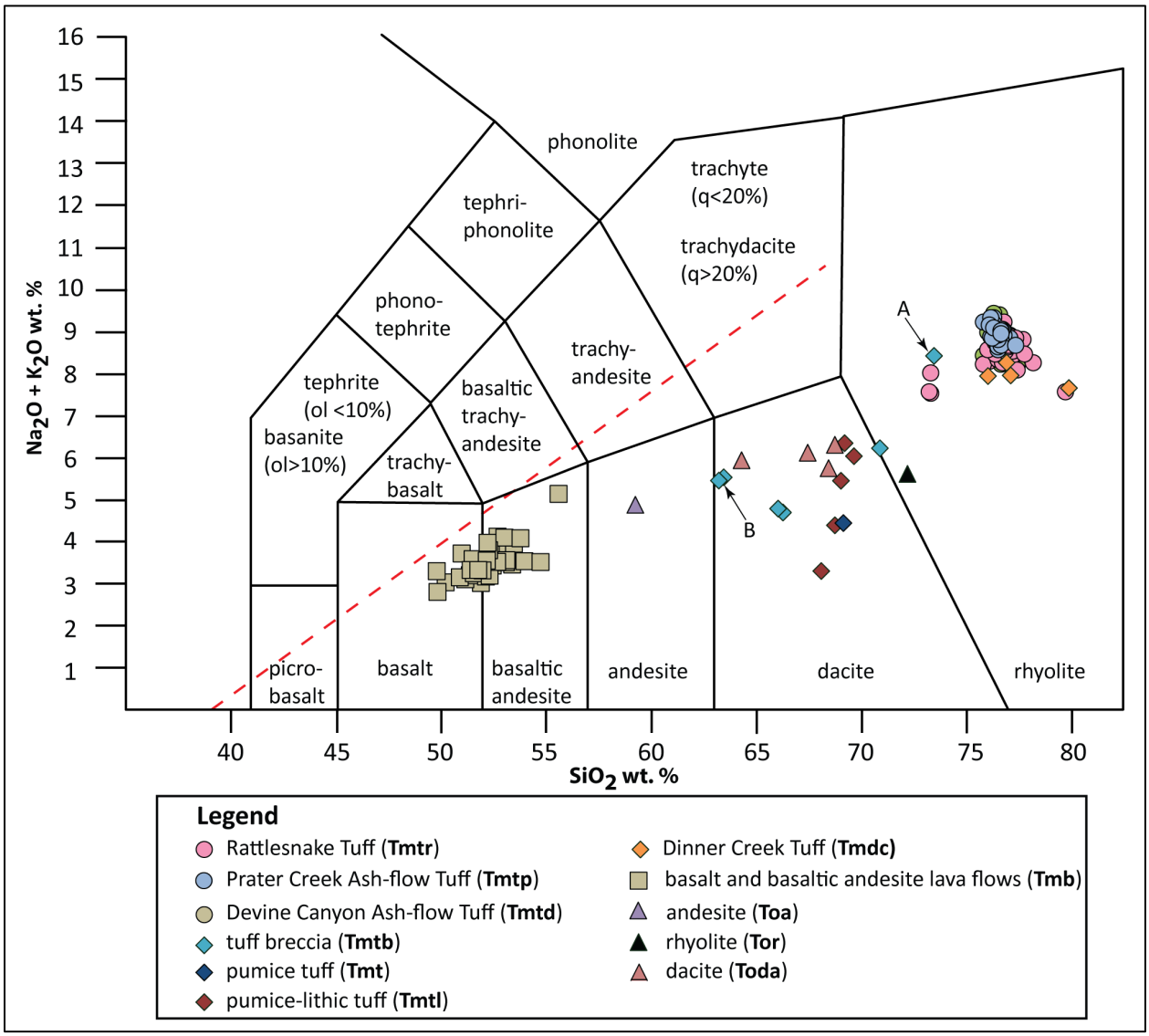

Figure 5-4. Chemical variation diagram (zirconium versus niobium) showing geochemical groupings for Cenozoic volcanic rocks in the Harney 7.5’ quadrangle. Plot includes 93 analyses obtained for this study and those compiled from previous studies (MacLean, 1994; Ford, 2012; M. Ferns, unpublished data, 2015; Houston and others, 2018; Niewendorp and others, 2018; McClaughry and others, 2019, 2020).

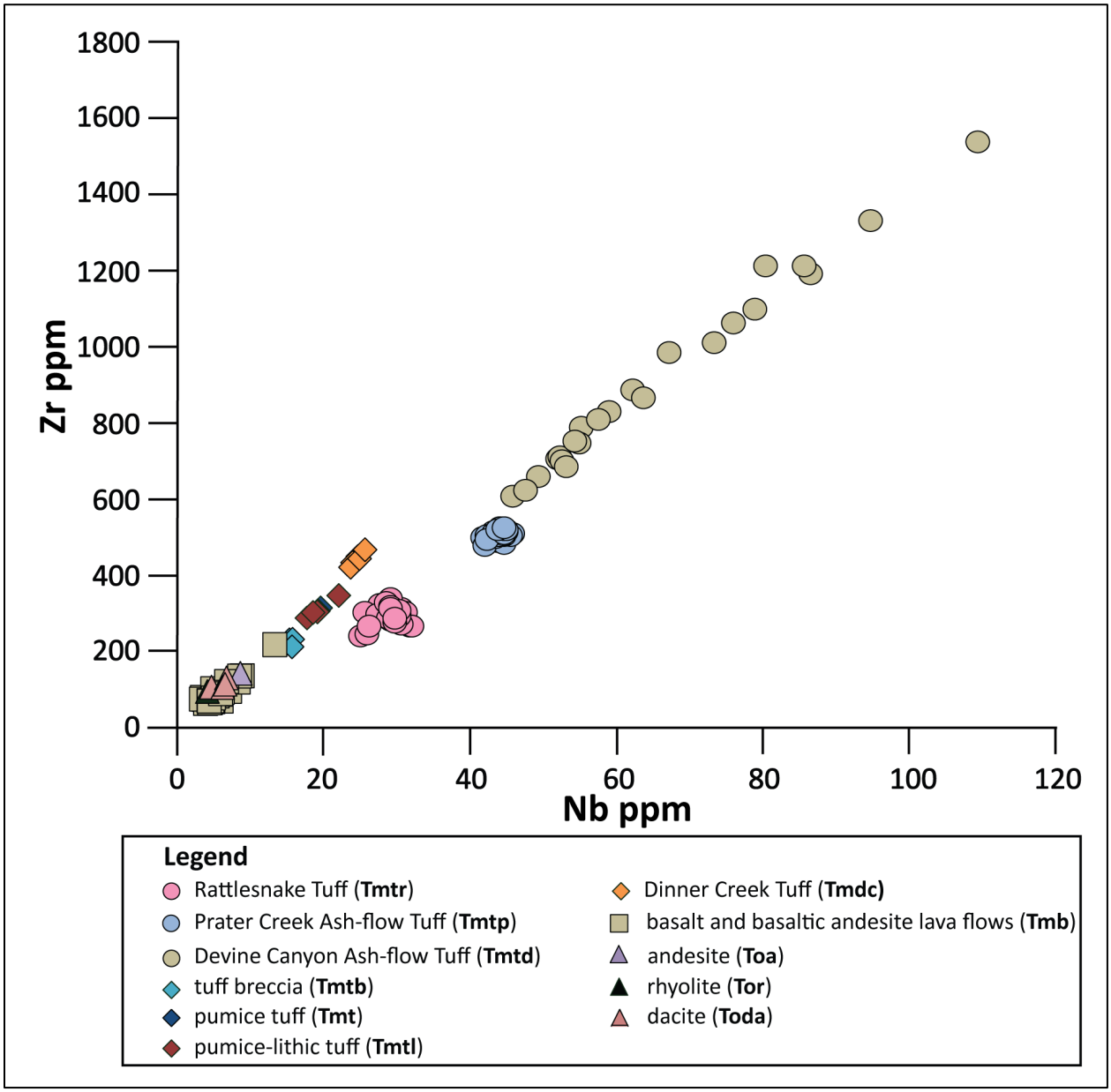

Table 5-1. Representative XRF analyses for late Oligocene to late Miocene volcanic rocks sampled from the Harney 7.5' quadrangle.

Sample no.	HAH101-16	HAH099-16	HAH176-16	HAH179-16	HAH199-16	HAH162-16	HAH058-16	HAH026-16	HAH061-16	HAH157-16	HAH065-16	HAH147-16
Formation	na	na	na	na	na	na	na	na	na	na	na	na
Map_Unit_Name	dacite	rhyolite	andesite	basalt-basaltic andesite lava flows	basalt basaltic andesite lava flows	Dinner Creek Tuff	pumice- lithic tuff	pumice tuff	tuff breccia	Devine Canyon Ash-flow Tuff	Prater Creek Ash-flow Tuff	Rattlesnake Tuff
Map_Unit_Label	Toda	Tor	Toa	Tmb	Tmb	Tmdc	Tmtl	Tmt	Tmtb	Tmtd	Tmtp	Tmtr
UTM_N (NAD 83)	4844889	4844993	4839384	4839497	4844955	4843352	4840877	4844336	4839930	4841422	4839848	4839019
UTM_E (NAD 83)	349541	349889	357578	357534	356668	349805	354222	354867	354359	350563	353812	350233
Age (Ma)	nd	nd	nd	nd	nd	~16	nd	nd	~14.88	~9.63	~8.41	~7.05
Map_No.	G75	G79	G11	G15	G77	G62	G44	G68	G36	G46	G28	G9
Oxides, weight percent												
SiO_2	67.47	72.21	59.27	49.87	52.24	76.93	69.66	69.16	66.29	76.61	76.55	76.99
TiO_2	0.579	0.407	1.311	1.065	1.109	0.196	0.661	0.819	1.395	0.182	0.152	0.159
Al_2O_3	16.52	14.95	15.27	16.88	18.29	12.88	14.42	15.60	14.84	10.70	11.81	12.23
FeO*	4.01	2.91	8.22	10.21	9.67	1.35	5.99	7.27	7.48	2.73	2.23	1.53
MnO	0.046	0.021	0.190	0.184	0.173	0.018	0.105	0.194	0.116	0.055	0.014	0.066
MgO	0.60	0.22	3.69	8.47	4.19	0.05	1.04	0.65	1.50	0.12	0.17	0.16
CaO	4.48	3.57	6.77	10.29	10.03	0.32	2.00	1.80	3.31	0.22	0.11	0.19
Na_2O	3.86	3.50	3.12	2.55	3.13	4.37	2.41	1.88	2.19	2.84	4.42	4.15
K_2O	2.24	2.10	1.75	0.25	0.83	3.88	3.61	2.55	2.49	6.54	4.55	4.51
P_2O_5	0.194	0.117	0.406	0.246	0.332	0.012	0.103	0.077	0.385	0.001	0.002	0.019
Total_I	97.23	97.54	98.00	97.47	97.46	98.31	92.52	90.32	91.78	96.58	98.90	98.86
LOI	2.24	1.67	1.30	2.00	1.65	0.83	6.72	9.02	7.28	2.65	0.77	0.49
Trace elements, parts per million												
Ni	20	10	49	161	107	1	6	10	9	2	3	3
Cr	28	10	71	243	77	4	8	5	9	3	2	4
Sc	10	8	25	32	29	4	16	20	17	1	2	4
V	97	48	173	251	235	9	31	30	75	5	4	6
Ba	1,141	1,739	710	212	504	1,419	1,077	1,141	1,109	34	90	639
Rb	39	37	35	4	9	75	60	49	51	138	103	92
Sr	585	454	280	296	458	28	147	147	248	4	12	13
Zr	112	93	140	73	87	466	304	313	229	1,205	502	304
Y	9	9	36	22	26	75	60	69	45	145	57	83
Nb	6.5	4.1	8.6	3.3	5.9	25.6	19.2	19.5	15.3	80.8	44.3	30.8
Ga	18	15	18	17	18	22	20	22	19	28	22	20
Cu	48	41	41	93	112	4	13	21	10	2	6	5
Zn	53	38	98	81	94	102	151	143	130	234	92	87
Pb	10	11	7	2	4	19	14	15	11	34	19	18
La	21	18	16	10	12	46	36	44	29	86	46	38
Ce	35	27	37	18	31	70	77	85	66	181	89	77
Th	4	4	4	0	1	8	6	7	5	14	9	8
Nd	16	12	21	13	16	45	40	51	36	90	42	47
U	2	0	3	0	0	3	3	3	2	4	3	4

Major element determinations have been normalized to a 100-percent total on a volatile-free basis and recalculated with total iron expressed as FeO*; nd – no data for radiometric ages, na - not applicable or no information about formation. LOI, Loss on Ignition; Total_I, original analytical total.

5.3.1 Lower Pleistocene to Upper Miocene sedimentary rocks

5.3.1.1 Harney Formation

QTst **sedimentary rocks (lower Pleistocene[?] to upper Miocene[?])**—Semi-consolidated tuffaceous mud-stone, siltstone, sandstone, and conglomerate (Plate). The unit (**QTst**) locally contains well to poorly sorted, fine- to medium-grained sandstone that exhibit planar laminations or trough cross-stratification. Sandstone beds contain ripple marks and minor carbonaceous detritus. Sandstone beds are generally less than 1 m (3 ft) thick. At Wright's Point, located ~25 km (15.5 miles) southwest from the study area, Niem (1974) noted the occurrence of several fossil fish bones, including vertebrae and ribs, within some of the coarser-grained sandstone beds. No fossils were identified in the study area. The unit (**QTst**) is recognized and mapped on the basis of lithology and stratigraphic position above the Rattlesnake Tuff (**Tmtr**). Within the Harney 7.5′ quadrangle the basal contact is poorly exposed and the upper parts of the unit have been removed by erosion. Total thickness of unit **QTst** in the study area is ≤27 m (90 ft).

Unit **QTst** is equivalent to the Harney Formation as redefined by Walker (1979), and is correlative, in part, to the Harney Formation of Piper and others (1939), QTtg (terrace gravels) of Greene (1972) and Greene and others (1972), QTg (pediment gravel) and QTs (tuffaceous sedimentary rocks) of Walker (1977), and QTsg (Pliocene to Pleistocene[?] tuffaceous sedimentary rocks) of Brown and others (1980a) and Brown (1982). According to Walker (1979), sedimentary rocks equivalent to **QTst** are present in the type section of the Harney Formation at Wright Point, ~6.2 km (~3.8 mi) to the southeast of the Burns 7.5′ quadrangle. The unit is assigned an upper Miocene(?) to lower Pleistocene(?) age on the basis of stratigraphic position.

Angular unconformity to disconformity

5.3.2 Upper Miocene volcanic and sedimentary rocks

Tmtr **Rattlesnake Tuff (upper Miocene)**— Vitric, phenocryst poor, pumice and lithic rich rhyolitic ash-flow tuff (SiO_2 = 75.84 to 78.18 weight percent; K_2O = 4.12 to 5.91 weight percent; Zr = 238 to 333 ppm; Nb = 25.4 to 32.5 ppm; *n* = 33 analyses in the northern Harney Basin, 21 outside study area) forming an extensive cover across older upper Miocene rocks in the study area (**Figure 5-3**, **Figure 5-4**, **Figure 5-5**; **Table 5-1**; Plate; Appendix). Over much of the study area, unit **Tmtr** forms distinctive cliffs and rimrock that can be easily traced in DEMs and air photographs (**Figure 5-5a**; Plate). Crystallization facies include vapor phase, pervasively devitrified zone, and a spherulite and lithophysal zone (Streck and Grunder, 1995; **Figure 5-5b**, **Figure 5-6a,b**). The basal contact and associated non-welded, laminated basal surge deposits are poorly exposed and are overlain by a densely welded vitric tuff (**Figure 5-5b**). Locally, lithophysae increase in abundance up section from a <2 m (6.5 ft) thick basal vitrophyre zone. The lithophysal zone grades upward to a hackly jointed, massively bedded tuff with a eutaxitic texture defined by aligned fiamme. Devitrified, moderately flattened black, white, and banded fiamme occur up to 10 cm (3.9 in) in diameter (**Figure 5-5c**, **Figure 5-6a**). Poly-compositional lithic fragments consist of angular, moderate reddish brown (10R 4/6) fragments as much as 1 cm (0.5 in) in length that are supported in a devitrified glass shard and crystal groundmass (**Figure 5-6e,f**). The tuff (**Tmtr)** is 10 to 20 m (32 to 65 ft) thick in the study area and occurs as a single cooling unit. Typical hand samples of the Rattlesnake Tuff (**Tmtr**) are very pale orange (10YR 8/2), to very light gray (N7), to medium gray (N5), and light brownish gray (5YR 6/1), and aphyric to very sparsely porphyritic. Phenocryst content is ≤1 percent (vol.) for the bulk tuff. The tuff (**Tmtr**) contains microphenocrysts and phenocrysts ≤2 mm (0.01 in) of clear, subhedral to euhedral anorthoclase and sanidine, clear, subhedral plagioclase, clear, subhedral quartz, and dusky green (5G 3/2), anhedral clinopyroxene (ferrohedenbergite), distributed within a vitric groundmass (**Figure 5-6c-f**). The original vitroclastic texture of the tuff (**Tmtr**) is retained but is locally overprinted by very fine elongated crystals forming axiolitic structures.

The Rattlesnake Tuff (**Tmtr**) has reversed magnetic polarity (Parker, 1974; Thormahlen, 1984; Smith, 1986a,b; Streck, 1994) and is assigned a late Miocene age on the basis of stratigraphic position and $^{40}Ar/^{39}Ar$ ages of 7.05 ± 0.01 (sanidine from pumice; sample HP-91-12; Streck, 1994; Streck and Grunder, 1995) and 7.093 ± 0.015 Ma (sanidine; sample HP-91-12; Jordan and others, 2004)**.** Unit (**Tmtr**) is equivalent to the Rattlesnake Ash-flow Tuff formally described by Walker (1979) and later renamed to Rattlesnake Tuff by Streck and Grunder (1995). Even though no caldera source related to the tuff is exposed, from pumice fragment size and distance correlations, Streck (1994) proposed a vent located near Capehart Lake in the western Harney Basin.

Figure 5-5. Outcrop photographs of the Rattlesnake Tuff (Tmtr) along Coffeepot Creek. (A) Typical outcrop of Rattlesnake Tuff forming a prominent cliff exposure over tuffaceous sedimentary rocks (Tmst) and the Prater Creek Ash-Flow Tuff (Tmtp). View is looking north (43.67906, -118.85921). (B) Outcrop of spherulitic Rattlesnake Tuff (Tmtr)(43.66999, –118.86599). Hammer for scale is 28 cm (11 in) long. (C) Pumice-rich vitric tuff (Tmtr), containing partially collapsed white (N9) and black (N1) pumice fragments (43.66999, –118.86599). Hammer head for scale is 10 cm (4 in) wide. Photo credits: Robert A. Houston, 2016.

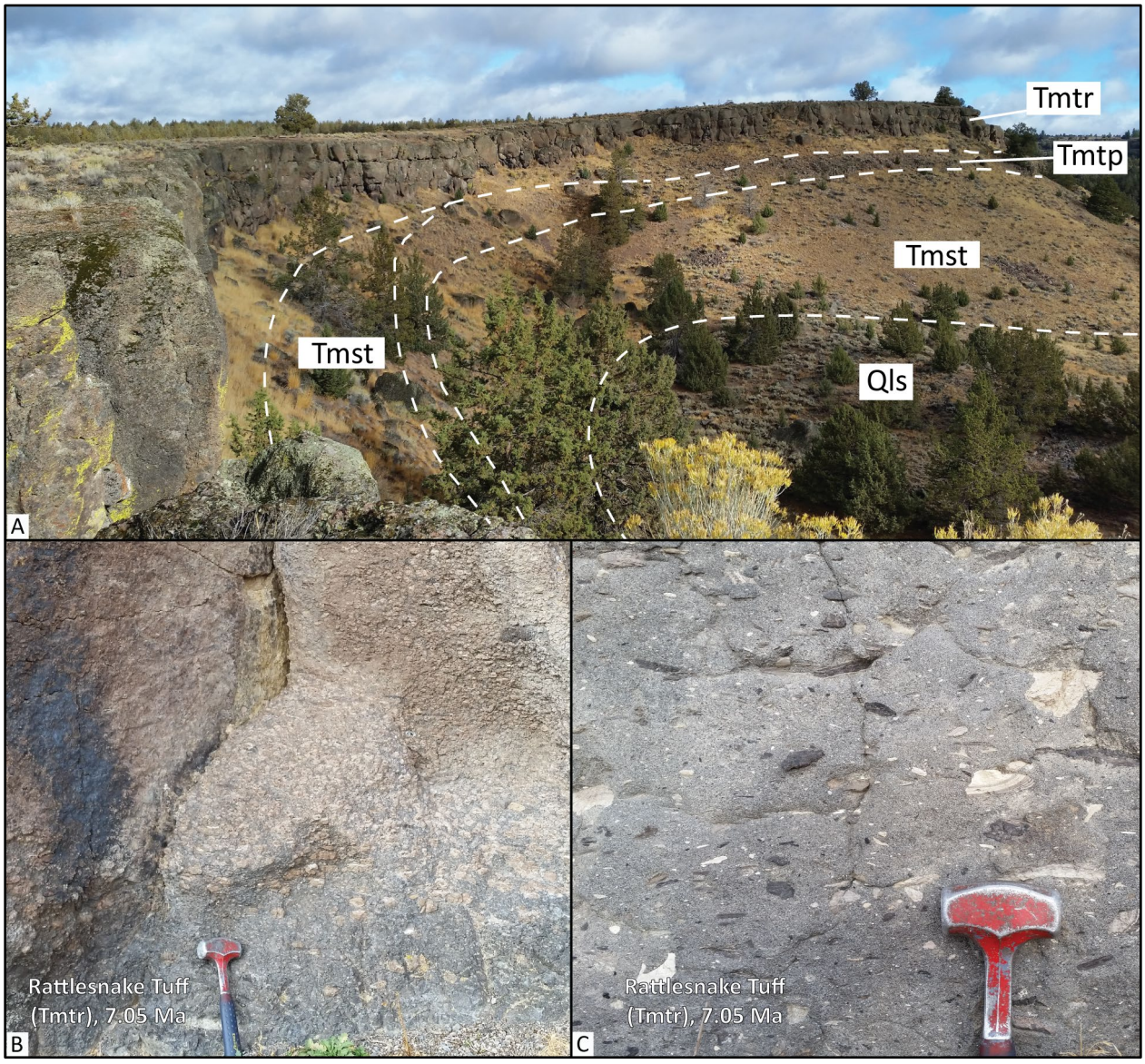

Figure 5-6. Photographs showing texture in the Rattlesnake Tuff (Tmtr). (A) Partially welded tuff (Tmtr) with banded pumice and fiamme. (B) Lithophysal tuff (Tmtr). Scale bar in (A) and (B) is 2.5 cm (1 in). (C) Anorthoclase (an) and clinopyroxene (cpx) microphenocrysts within a vitric groundmass (sample HAH0170-16). Plane-polarized light. (D) Same view as (C) under cross-polarized light. (E) Photomicrograph of a mafic lithic fragment, anorthoclase (an), and quartz (qtz) in glass shards. Plane-polarized light. (F) Same view as (D) under cross-polarized light. Scale bar in (C-F) is 1 mm (0.04 in). Photo credits: (A–B) Jason D. McClaughry, 2018; (C-F) Robert A. Houston, 2017.

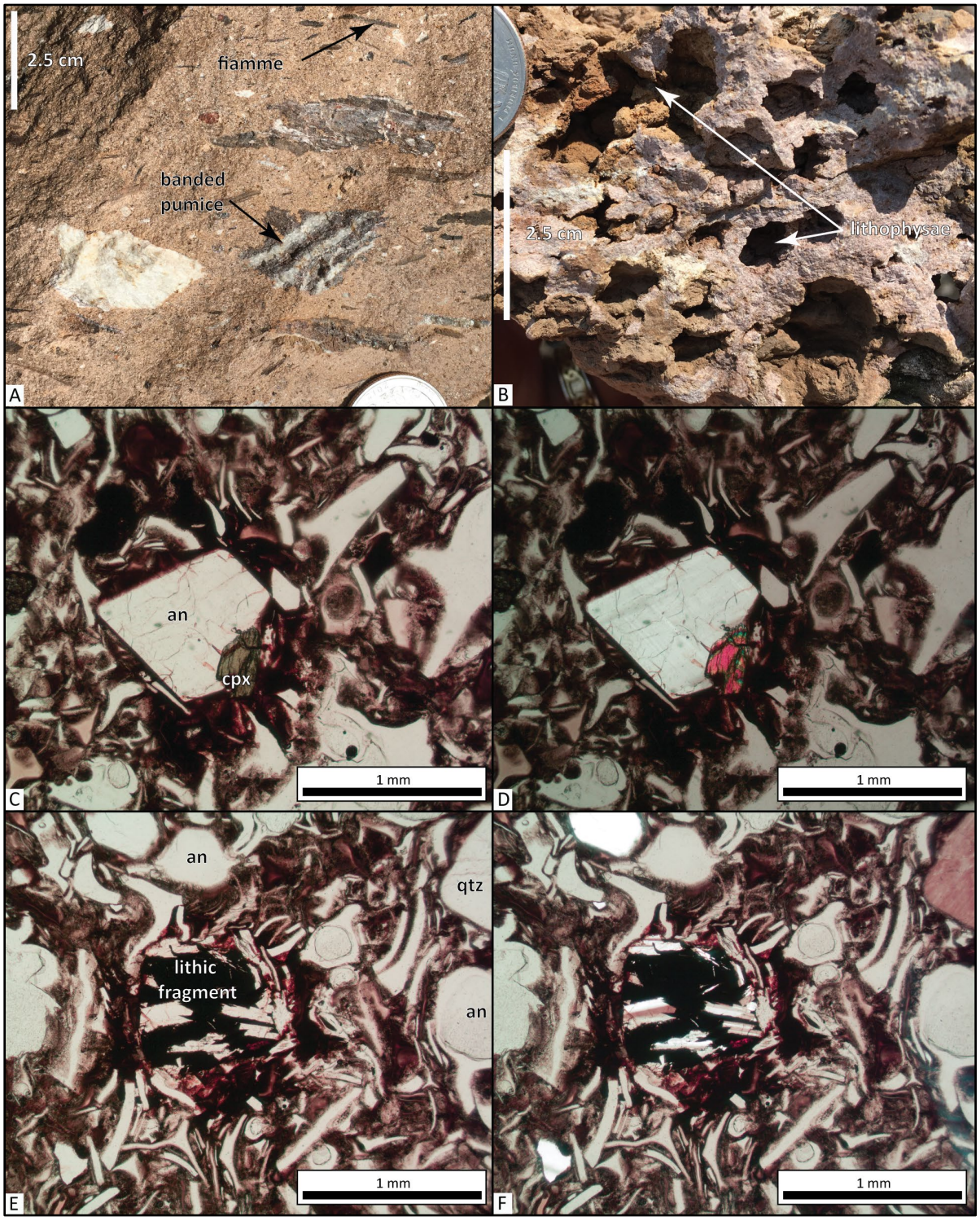

Angular unconformity

Tmtp **Prater Creek Ash-flow Tuff (upper Miocene)**—Devitrified, welded, lithophysal, crystal poor rhyolitic ash-flow tuff (SiO_2 = 75.81 to 77.35 weight percent; K_2O = 4.47 to 5.99 weight percent; Zr = 475 to 521 ppm; Nb = 42.2 to 46.2 ppm; *n* = 59 analyses in the northern Harney Basin, 41 outside study area) cropping out as a single cooling unit in cliff exposures in the study area (**Figure 5-3**, **Figure 5-4**, **Figure 5-7**; **Table 5-1**; Plate; Appendix). The tuff (**Tmtp**) is massive and densely welded, exhibiting eutaxitic texture and distinctive platy jointing (**Figure 5-7b**, **Figure 5-8**, **Figure 5-9**). Locally, a lithophysal section of the tuff (**Tmtp**) exhibits lenticular or crescent-shaped vesicles in the plane of compaction foliation. Abundant flattened pumice fragments (fiamme) range in size up to 5 cm (2 in) with a compaction ratio of 10:1 (**Figure 5-9c,d**). Lithics are a minor constituent (<3 percent) and consist of angular poly-compositional lithic fragments as much as 2 cm (0.78 in) in length (**Figure 5-9e,f**). Maximum thickness of the tuff (**Tmtp**) is ~10 to 20 m (32 to 65 ft). Typical hand samples of the Prater Creek Ash-flow Tuff (**Tmtp**) are pale blue (5PB 7/2), pinkish gray (5YR 8/1), light brown (5YR 5/2), to moderate reddish brown (10R 4/6)(**Figure 5-8**). The tuff (**Tmtp**) contains <1 percent (vol.) crystal fragments of sanidine and quartz ≤0.5 mm (<0.01 in) across, within a devitrified glass-shard groundmass (**Figure 5-9**). The tuff (**Tmtp**) commonly exhibits a distinctive spotted texture, and locally is zeolitized.

The Prater Creek Ash-flow Tuff (**Tmtp**) is assigned a late Miocene age on the basis of stratigraphic position and isotopic ages. Jordan and others (2004) reported an $^{40}Ar/^{39}Ar$ isochron age of 8.41 ± 0.16 Ma and $^{40}Ar/^{39}Ar$ plateau and integrated ages of 8.46 ± 0.09 Ma (matrix; sample PC-1). Streck and others (1999) reported a similar $^{40}Ar/^{39}Ar$ age of 8.48 ± 0.05 Ma (devitrified whole rock) for the Prater Creek Ash-flow Tuff (**Tmtp**). The tuff (**Tmtp**) was informally named the welded tuff of Prater Creek by Greene (1972) and Greene and others (1972) and was formally recognized as the Prater Creek Ash-flow Tuff by Walker (1979). Unit **Tmtp** is partly equivalent to Td (Danforth Formation) of Piper and others (1939) and (silicic ash-flow tuff) of Walker (1977). Equivalent to unit Tmtp (Prater Creek Ash-flow Tuff) of Brown and others (1980a) and Brown (1982). The Prater Creek Ash-flow Tuff (**Tmtp**) was erupted from the Silvies River caldera near Burns, ~16.5 km (10 mi) southwest of the study area (McClaughry and others, 2019, 2020).

Figure 5-7. Outcrop photographs of the Prater Creek Ash-Flow Tuff (Tmtp). (A) Cliff-forming outcrop of unit Tmtp between the overlying Rattlesnake Tuff (Tmtr) and underlying tuffaceous sedimentary rocks (Tmst). View is looking north (43.68510, −118.85900). (B) Unit Tmtp with platy jointing. The cliff exposure is 5 m (16 ft) high. View is looking north (43.69839, −118.85900). Photo credits: Robert A. Houston, 2016.

Figure 5-8. Hand sample of the Prater Creek Ash-Flow Tuff (Tmtp). In hand sample, the devitrified welded ash groundmass contains minor collapsed pumice, lithic fragments, and rare sanidine crystals. Scale bar is 5 cm (2 in). Sample number: HAH064-16. Photo credit: Robert A. Houston, 2016.

Figure 5-9. Photographs showing texture in the Prater Creek Ash-flow Tuff (Tmtp). (A) Broken sanidine (sa) crystal in a eutaxitic, devitrified groundmass of vitric ash and glass shards (sample HAH023-16). Plane-polarized light. (B) Same view as (A) under cross-polarized light. (C) Two collapsed pumice fiamme, exhibiting a 20:1 compaction ratio (sample HAH064-16). Plane-polarized light. (D) Same view as (C) under cross-polarized light. (E) Lithic fragment, likely of Devine Canyon Ash-flow Tuff (Tmtd), in the Prater Creek Ash-flow Tuff (Tmtp)(sample HAH064-16). Compaction flow foliation is evident along the margins of the clast. Plane-polarized light. (F) Same view as (E) under cross-polarized light. Scale bar in (A-F) is 1 mm (0.04 in). Photo credits: Robert A. Houston, 2017.

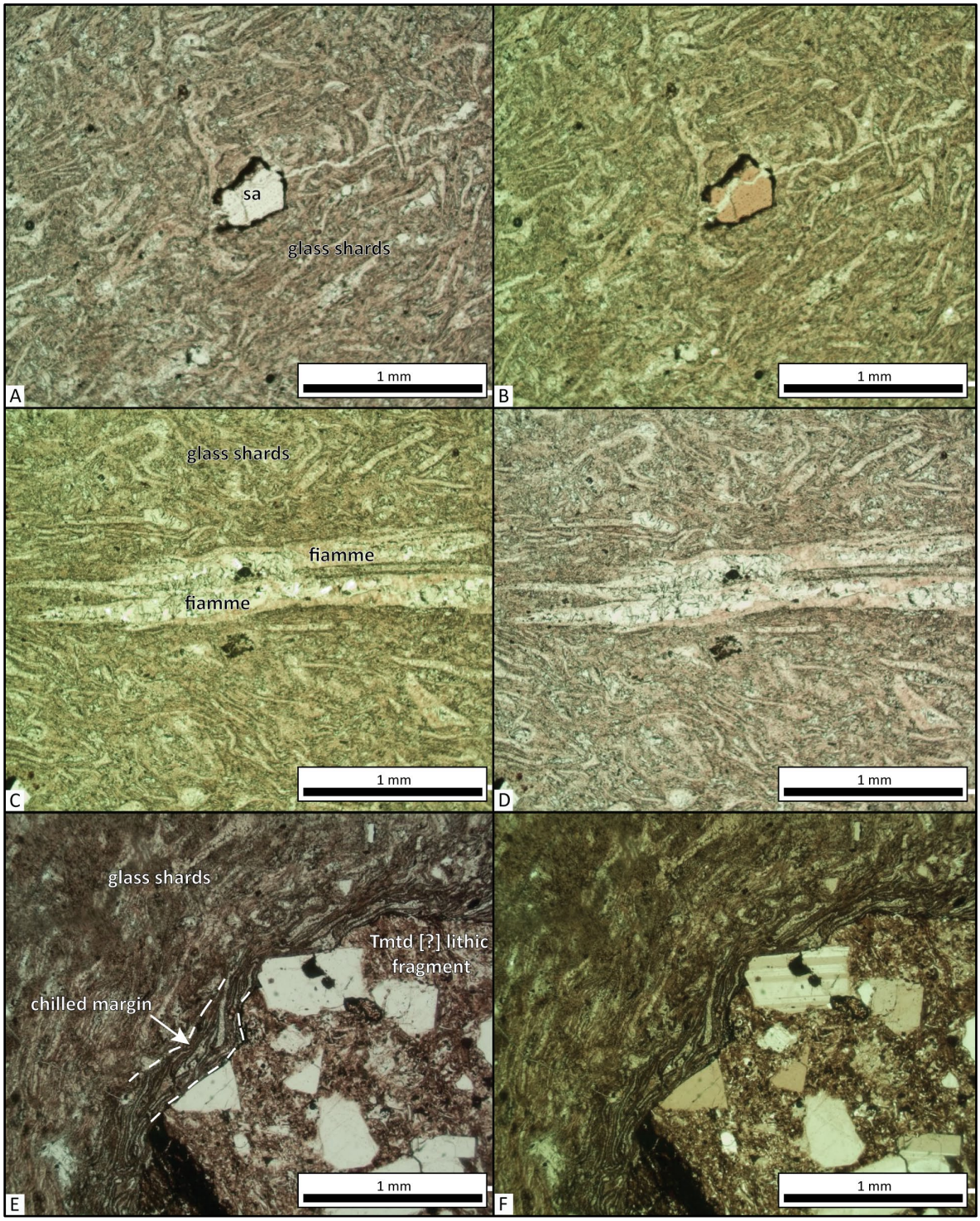

Angular unconformity

Tmtd **Devine Canyon Ash-flow Tuff (upper Miocene)**—Devitrified, welded to non-welded, lithophysal, crystal rich, vitric rhyolitic ash-flow tuff (SiO_2 = 75.84 to 77.40 weight percent; K_2O = 4.42 to 6.81 weight percent; Zr = 604 to 1531 ppm; Nb = 46.3 to 109.7 ppm; *n* = 22 analyses in the northern Harney Basin, 18 outside study area) mapped in the northern and eastern parts of the study area (**Figure 5-3**, **Figure 5-4**, **Figure 5-10**; **Table 5-1**; Plate; Appendix). In the study area, two phases of the ash-flow tuff (**Tmtd**) are recognized; a strongly welded cliff-former and a non-welded slope-former (**Figure 5-10**). Outcrops of the strongly welded vitric zone occur in the northern part of the study area. The strongly welded vitric phase contains large (up to 30 cm [12 in]), flattened, glassy pumice fiamme exhibiting compaction ratios up to 15:1 (**Figure 5-10a,b**). The cliff-forming strongly welded zone weathers to form a distinctive apron of very large boulders up to 10 m (30 ft) in diameter)(**Figure 5-11**). In the eastern part of the quadrangle, the ash-flow tuff (**Tmtd**) occurs as an altered, non-welded phase (**Figure 5-10c,d**). The poorly exposed nonwelded slope forming phase contains poorly sorted, large crystal-rich inflated pumice fragments up to 30 cm (12 in) in diameter (**Figure 5-10c,d**). The tuff (**Tmtd**) weathers to produce alkali feldspar–rich soil, which is useful to map the unit in areas of poor exposure (**Figure 5-12a**). At some locations, the extent of the non-welded phase was mapped on the distribution of ~0.3 m (1 ft) high ant colony mounds composed entirely of coarse alkali feldspar crystals. Thickness of unit **Tmtd** in the study area is ≤10 m (30 ft). Typical hand samples of the Devine Canyon Ash-Flow Tuff (**Tmtd**) are light gray (N7 to N8) to greenish gray (5GY 5-6/1). Where outcrops are abundant in phenocrysts, the rock is medium to light gray (N5-N7) to pinkish, yellowish, and greenish gray (5 YR 8/1, 5Y 8/1, 5GY 6/1), with a streaked and mottled appearance (**Figure 5-12b**). Petrographically, the tuff (**Tmtd**) contains as much as 30 percent (vol.) crystals and crystal fragments of dominantly alkali feldspar (sanidine; Greene, 1973; Smith and MacKenzie, 1958), ≤7 percent (vol.) clear quartz, and rare dark greenish yellow (10Y 6/6) pyroxene, ilmenite, and magnetite (**Figure 5-12c,d**). Greene (1973) noted that alkali feldspar and quartz generally increase in abundance up section. Most of the phenocrysts are broken and exhibit rounding or embayment textures (**Figure 5-12c,d**). Additionally, the unit (**Tmtd**) contains lithic fragments.

The Devine Canyon Ash-flow Tuff (**Tmtd**) is assigned a late Miocene age on the basis of stratigraphic position and $^{40}Ar/^{39}Ar$ ages of 9.74 ± 0.02 Ma (Jordan and others, 2004) and 9.63 ± 0.05 Ma (Ford and others, 2013). Informally named the welded tuff of Devine Canyon by Greene (1972) and Greene and others (1972); formally recognized as the Devine Canyon Ash-flow Tuff by Walker (1979). Partly equivalent to Td (Danforth Formation) of Piper and others (1939) and Tat (silicic ash-flow tuff) of Walker (1977). The Devine Canyon Ash-flow Tuff (**Tmtd**) is presumed to have been erupted from a concealed source within the Harney Basin (Greene, 1973; Parker, 1974; Walker, 1974, 1979; Meigs and others, 2009; Ford and others, 2013; Khatiwada and Keller, 2015; Isom, 2017).

Figure 5-10. Outcrop photographs of the Devine Canyon Ash-Flow Tuff (Tmtd) along upper Coffeepot Creek. (A) Strongly welded, crystal rich, vitric ash-flow tuff (Tmtd) containing glassy, flattened pumice fiamme, with a 10:1 average compaction ratio (43.73979, −118.81700). (B) Crystal-rich pumice fiamme are as long as 45 cm (18 in). Same outcrop as in (A). Pencil for scale in (A) and (B) is 15 cm (6 in) long. (C) Nonwelded crystal rich ash-flow tuff (Tmtd)(43.73942, −118.81603). Outcrops of the nonwelded phase are limited. The inflated pumice fragments have a zirconium abundance of ~1,000 ppm Zr. Hammer for scale is 30 cm (12 in) tall. (D) Inflated pumice fragments in hand sample (sample HAH011-16) collected from the outcrop pictured in (C). Bubble walls and alkali feldspar crystals are visible without magnification. U.S. quarter coin for scale is 2.5 cm (1 in) across. Photo credits: Robert A. Houston, 2016.

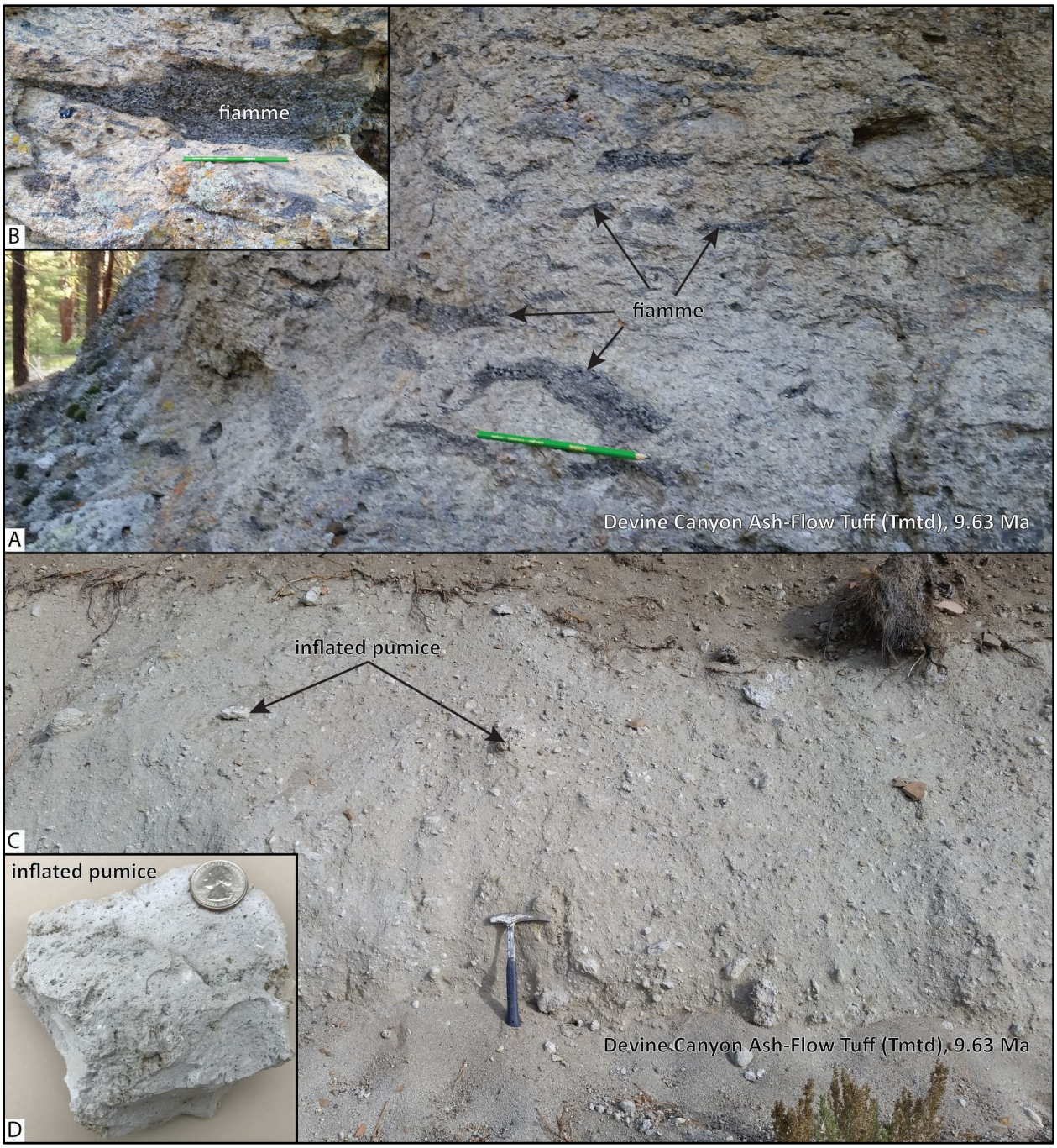

Figure 5-11. Cliff forming outcrops of unit Tmtd shed large distinctive boulders downslope. This weathering pattern is distinctive and recognizable in aerial photography. The boulder in the center of the photograph is ~5 m (16.5 ft) in height (43.75619, −118.81700). Photo credit: Robert A. Houston, 2016.

Figure 5-12. Hand sample and thin section photographs showing the Devine Canyon Ash-flow Tuff (Tmtd). (A) Crystal-rich sand eroding from outcrops of Tmtd. (B) Hand sample of strongly welded, devitrified, crystal-rich tuff. Scale bar in (A) and (B) is 2.5 m (1 in). (C) Subhedral to anhedral alkali feldspar (af) and rounded quartz (qtz) phenocrysts distributed within a vitric groundmass of glass shards (sample HAH011-16). Plane-polarized light. (D) Same view as (C), under cross-polarized light. Scale bar in (C) and (D) is 1 mm (0.04 in) in length. Photo credit: (A-B) Jason D. McClaughry, 2018; (C-D) Robert A. Houston, 2017.

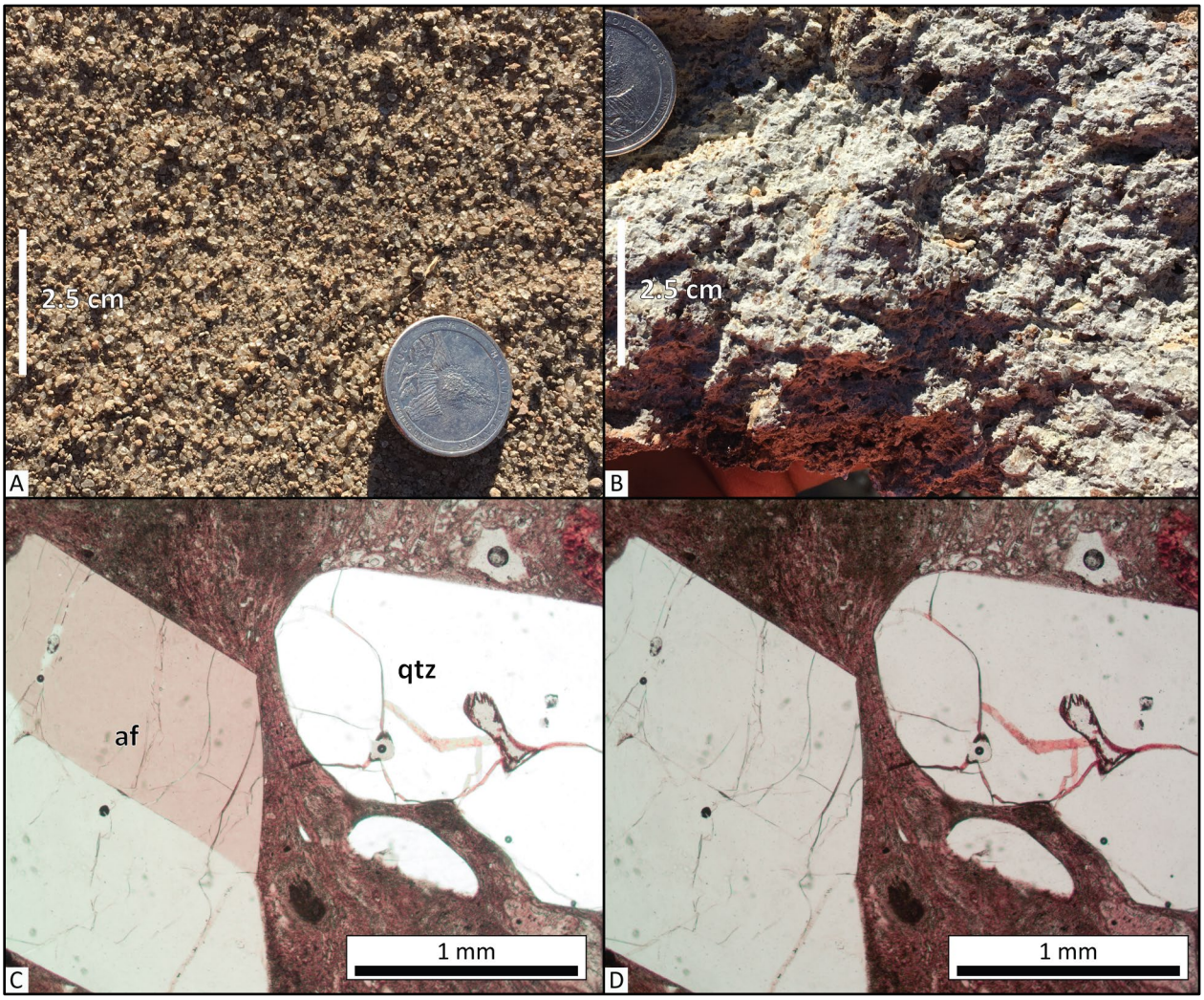

Tmst **tuffaceous sedimentary rocks (upper Miocene and middle Miocene[?])**—Tuffaceous mudstone, siltstone, sandstone, and conglomerate and reworked tuff (**Figure 5-13**). Fine to coarse grained, thinly bedded and well- to poorly-sorted sandstone layers contain ripple marks and trough cross-bedding (**Figure 5-13b,c**). A significant percentage of tuffaceous material is present throughout the unit (**Tmst**)(**Figure 5-13b**). Conglomerate sequences are generally ≤1 m (3 ft) thick (**Figure 5-13a,d,e**). Locally, tuffaceous sedimentary rocks contain fossil rootlet molds (**Figure 5-13f**). Unit **Tmst** is as much as 110 m (360 ft) thick. The basal contact is poorly exposed.

Tuffaceous sedimentary rocks (**Tmst**) are assigned a middle Miocene(?) and late Miocene age. The unit (**Tmst**) is mapped below the Devine Canyon Ash-flow Tuff (**Tmtd**), is interbedded with the Prater Creek Ash-flow Tuff (**Tmtp**), and lies below the Rattlesnake Tuff (**Tmtr**). Precise age of the unit is unknown in areas where exposure is poor, and direct relations to interbedded and precisely dated tuff marker beds are unclear. Unit **Tmst** is partially equivalent to Td (Danforth Formation) of Piper and others (1939); Tst (sedimentary rocks) of Greene (1972); Tst (tuffaceous sedimentary rocks) of Greene and others (1972); overlying sedimentary rocks of Tdv (welded tuff of Devine Canyon) of Greene (1972); overlying sedimentary rocks of Tdv (welded tuff of Devine Canyon) of Greene and others (1972); Tst (tuffaceous sedimentary rocks and tuff) of Walker (1977); Tmst-1, -2, and -3 (tuffaceous sedimentary rocks) of Brown and others (1980).

Figure 5-13. Outcrops of tuffaceous sedimentary rocks (Tmst) in the study area (*following page*). (A) Bedded mudstone, siltstone, and conglomerate. Conglomerate is clast supported and contains tough cross-stratified sandstone lenses (43.67229, −118.86499). View is looking north. (B) Thin bedded and laminated tuffaceous sandstone (43.70780, −118.81099). View is looking west. (C) Trough cross-stratified sandstone lenses (43.67229, −118.86499). (D) Poorly-sorted sandstone and conglomerate lenses (43.67229, −118.86499). (E) Reworked tuff overlies a poorly sorted, clast-supported conglomerate (43.70780, −118.81099). View is looking west. Hammer for scale in photographs (A) to (E) is 28 cm (11 in) long. (F) Massive, tuffaceous siltstone bed, as much as 2 m (6 ft) thick, contains plant rootlet molds (43.66979, −118.86000). Blue handle to hammer for scale is 10 cm (4 in) tall. Photo credits: Robert A. Houston, 2016.

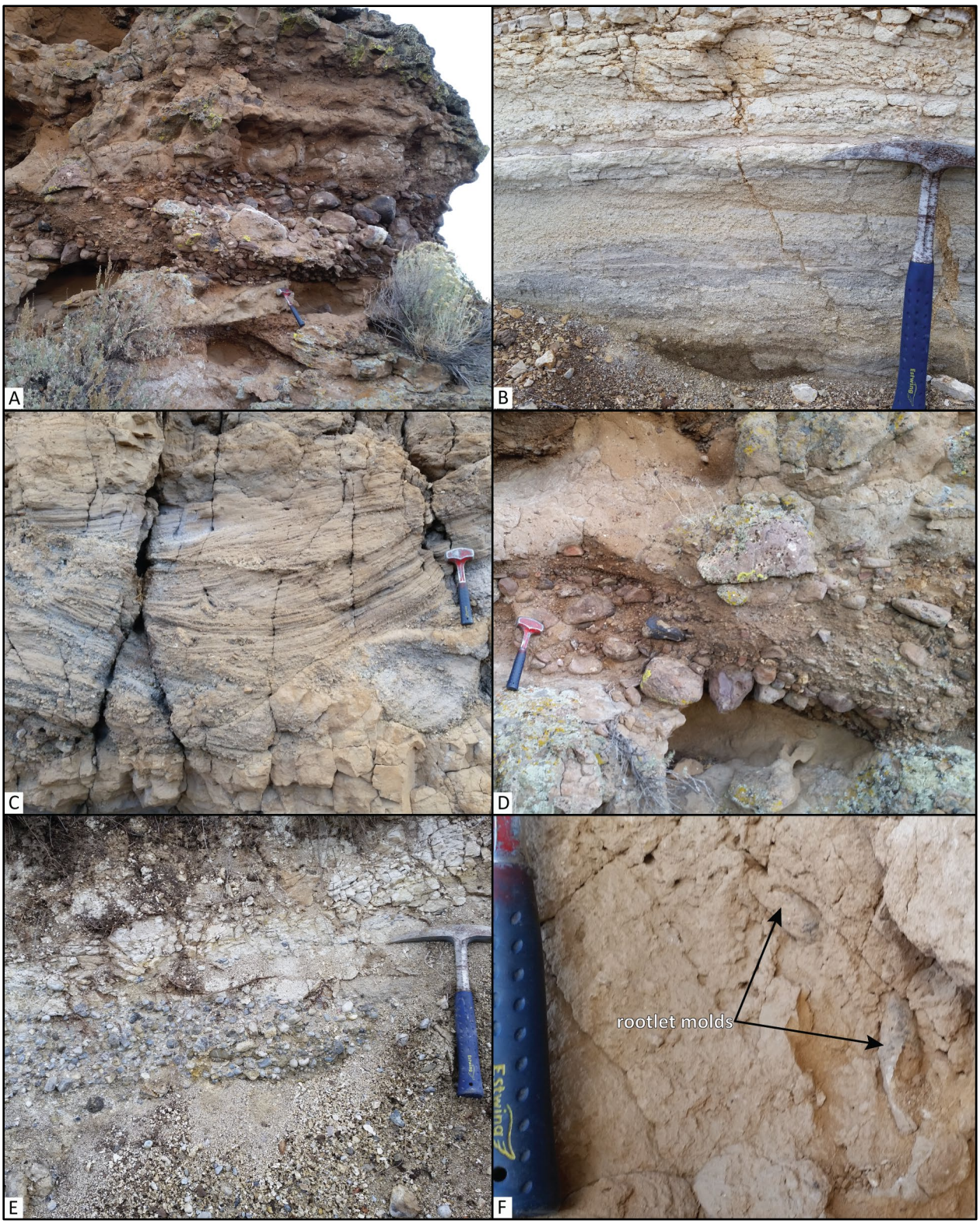
A
B
C
D
E
F
rootlet molds

Angular unconformity

5.3.1 Middle and lower Miocene volcanic rocks

Tmtb **tuff breccia (middle Miocene)**—Crystal poor, pumice- and lithic-rich dacitic to rhyolitic tuff breccia (SiO_2 = 63.47 to 70.90 weight percent; K_2O = 2.40 to 3.88 weight percent; Ba = 1,058 to 1,237 ppm; Zr = 218 to 307 ppm; Nb = 14.2 to 19.5 ppm; *n* = 4 analyses) mapped along the hill slopes of Rattlesnake Creek and Cow Creek drainages (**Figure 5-3**, **Figure 5-4**, **Figure 5-14**; **Table 5-1**; Plate; Appendix). The tuff breccia (**Tmtb**) has a reversely graded, lithic-rich base, containing common and conspicuous dark gray (N3) pumice fragments as much as 10 cm (4 in) across (**Figure 5-14b**). The tuff breccia (**Tmtb**) transitions from a very pale orange tan (10YR 8/2) basal phase, characterized by a higher percentage of white (N9) to pinkish gray (5YR 8/1) pumice, to a dark gray (N3) tuff dominated by dark gray (N3) dacitic pumice fragments (**Figure 5-14b**). A white (N9) to pinkish gray (5YR 8/1) pumice fragment analyzed is rhyolitic (SiO_2 = 73.47 weight percent; *n* = 1 analysis), with moderate amounts of barium (Ba = 412 ppm), zirconium (Zr = 447 ppm), and niobium (Nb = 24.6 ppm)(point A on **Figure 5-3**, **Table 5-1**; Plate; Appendix). A dark gray (N3) pumice fragment analyzed is dacitic (SiO_2 = 63.24 weight percent; *n* = 1 analysis), with relatively high amounts of barium (Ba = 1,185 ppm) and lower amounts of zirconium (Zr = 210 ppm) and niobium (Nb = 15.6 ppm)(point B on **Figure 5-3**, **Table 5-1**; Plate; Appendix). Mafic globules (SiO_2 = 56 weight percent) described by Streck and others (2015) are texturally similar to the dark gray (N3) pumice fragments (SiO_2 = 63.24 weight percent), but are more mafic in composition. The tuff breccia (**Tmtb**) is interbedded with the upper parts of basalt and basaltic andesite lava flows of unit **Tmb**. Unit **Tmtb** is as thick as 12 to 18 m (40 to 60 ft). Typical hand samples of the tuff breccia (**Tmtb**) are grayish blue (5PB 5/2), containing two populations of conspicuous dark gray (N3) and white (N9) to pinkish gray (5YR 8/1) pumice fragments (**Figure 5-14b**, **Figure 5-15a**). Both lithic and pumice fragments are abundant throughout the unit. In thin section, the breccia (**Tmtb**) groundmass contains sparse anhedral anorthoclase as long as 3 mm (0.12 in)(**Figure 5-15b-e**)(Streck and others, 2015; Cruz, 2017).

The tuff breccia (**Tmtb**) is assigned a middle Miocene age on the basis of stratigraphic position. Stratigraphic position, combined with outcrop, textural, and geochemical similarities suggest that the tuff breccia (**Tmtb**) may be equivalent to the ash-flow tuff near Buchanan of Greene and others (1972; unit Ttb), Strawberry Volcanics marker tuff bed of Woods (1976), Buchanan ash-flow tuff of Brown and others (1980; unit Tmtb), and the Dinner Creek Tuff, cooling unit 4 of Streck and others (2015).

Figure 5-14. Tuff breccia (Tmtb) cropping out along the Rattlesnake and Cow Creek drainages. (A) Dark gray, crystal poor, pumice and lithic rich, devitrified ash-flow tuff (43.69860, −118.80200). (B) Lithics and both dark gray (N3) and white (N9) to pinkish gray (5YR 8/1) pumice fragments are abundant throughout unit Tmtb (43.69810, −118.80699). Scale bar is 10 cm (4 in) long. Photo credits: Robert A. Houston, 2016.

Figure 5-15. Photographs showing texture in the tuff breccia (Tmtb). (A) Unit Tmtb hand sample with dark gray (N3) and white (N9) to pinkish gray (5YR 8/1) pumice fragments. (B) Pumice and rare anorthoclase feldspar (an) phenocryst. Plane-polarized light. (C) Same view as (B) under cross-polarized light. (D) Tuffaceous and mafic lithic fragments are sub to well rounded, indicating considerable abrasion during the eruptive phase. Plane-polarized light. (E) Same view as (D) under cross-polarized light. Scale bar in (B-E) is 1 mm (0.04 in). Photo credits: Robert A. Houston, 2017.

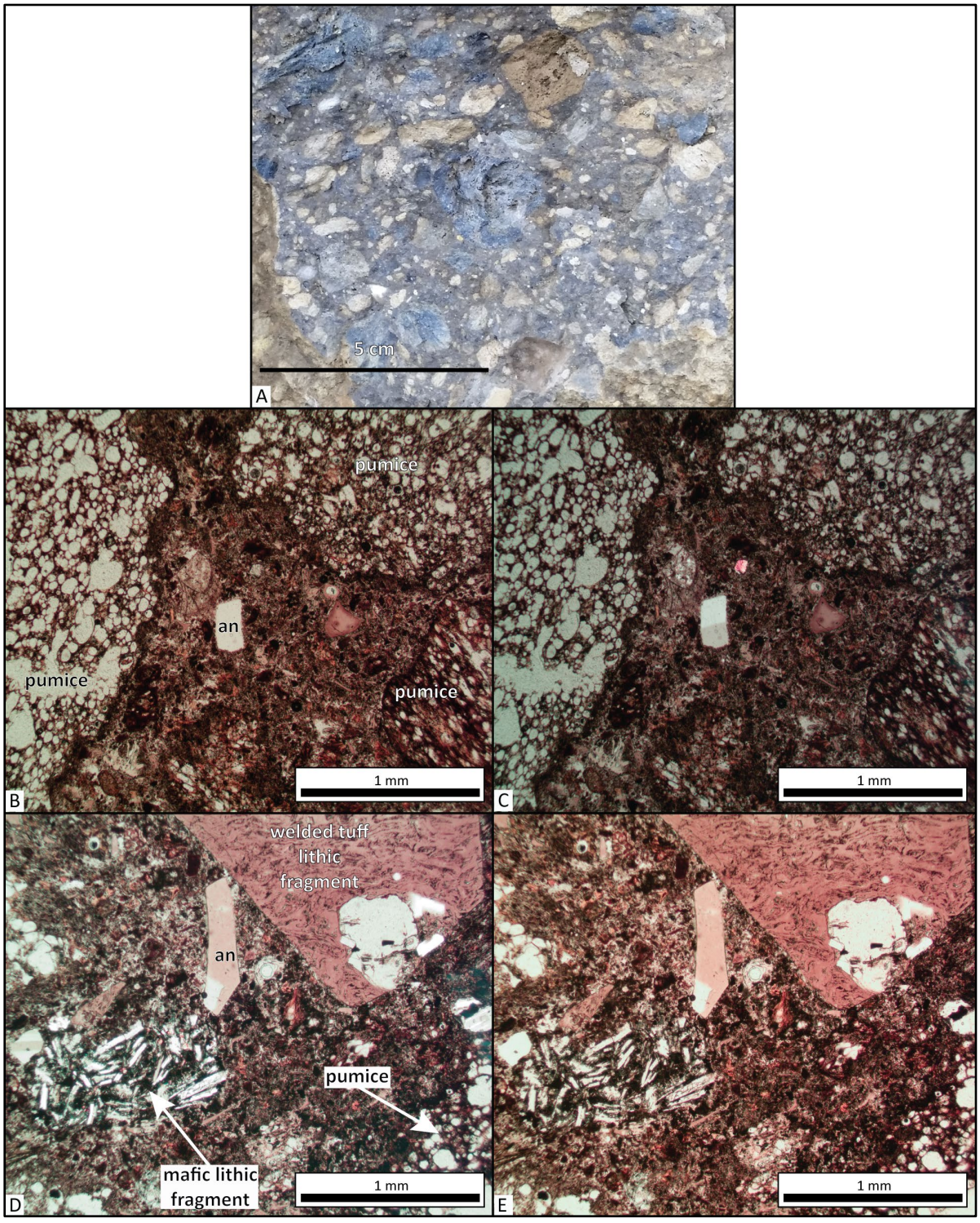

Tmt **pumice tuff (middle Miocene)**—Massive, very pale orange (10YR 8/2) to grayish-orange (10YR 7/4), devitrified crystal-poor dacitic tuff (SiO_2 = 69.16 weight percent; K_2O = 2.55 weight percent; Ba = 1,140 ppm; Zr = 312 ppm; Nb = 19.5 ppm; *n* = 1 analysis) mapped along Rattlesnake Creek (**Figure 5-3**, **Figure 5-4**, **Figure 5-16**; **Table 5-1**; Plate; Appendix). The pumice tuff (**Tmt**) is locally moderately welded and contains inflated pumice and minor lithic fragments up to 3 cm (1 in) in diameter (**Figure 5-16b**). Thickness of unit **Tmt** is as much as 4 to 6 m (13 to 19 ft). In thin section, feldspar phenocrysts up to 0.5 mm (0.19 in) are surrounded by a devitrified groundmass of ash and brecciated lithic fragments. Unit **Tmt** is interbedded with basalt and basaltic andesite lava flows of unit **Tmb**, and lies between tuff units **Tmtb** and **Tmtl** (**Figure 5-16c**). Therefore, the pumice tuff (**Tmt**) is assigned a middle Miocene age.

Figure 5-16. Pumice tuff (Tmt) cropping out in the Rattlesnake and Cow Creek drainages. (A) Devitrified ash-flow tuff (Tmt) (43.73759, –118.80200). Scale bar is 3 m (10 ft) high. (B) Close-up photograph at the outcrop in (A) of moderately welded, devitrified, crystal-poor tuff, containing inflated pumice and lithic fragments up to 1 cm (0.4 in). (C) Upper baked contact between basalt and basaltic andesite lava flows (Tmb) and pumice tuff (Tmt)(43.73789, –118.80200). Hammer for scale in (B) and (C) is 28 cm (11 in) long. Photo credits: Robert A. Houston, 2016.

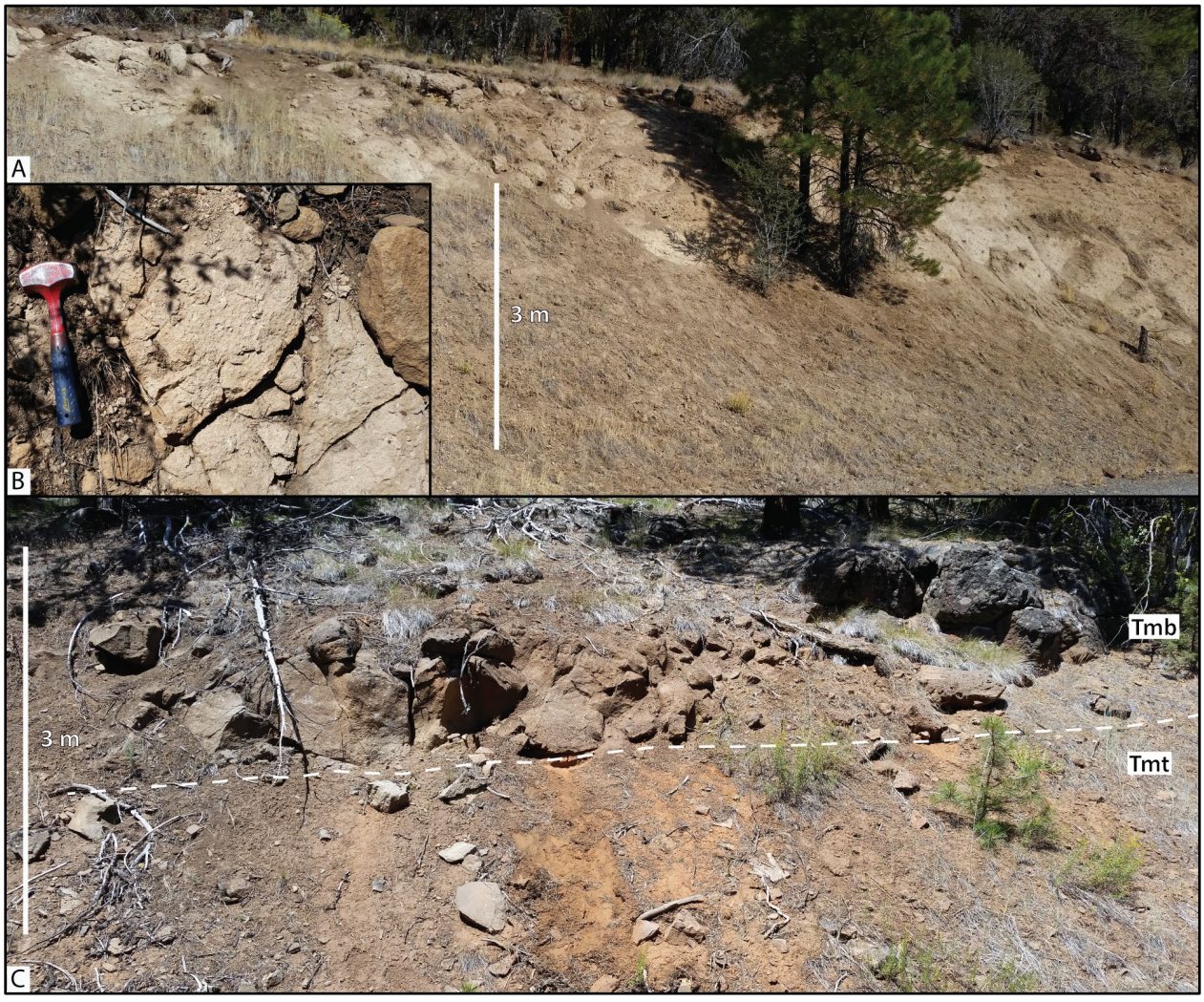

Tmtl **pumice-lithic tuff (middle Miocene)**—Massive, crystal poor, pumice- and lithic-rich dacitic tuff (SiO_2 = 68.11 to 69.66 weight percent; K_2O = 2.68 to 3.61 weight percent; Ba = 1,076 to 1,417 ppm; Zr = 302 to 345 ppm; Nb = 19.1 to 22 ppm; *n* = 5 analyses) cropping out discontinuously along Rattlesnake Creek (**Figure 5-3**, **Figure 5-4**, **Figure 5-17**; **Table 5-1**; Plate; Appendix). Unit **Tmtl** locally contains a basal pumice rich and lithic poor air-fall tuff section, as much as 6 m thick (20 ft), that is overlain by a moderately welded pumice and lithic rich ash-flow tuff (**Figure 5-17a**). The nonwelded airfall section contains graded pumice fragments up to 1 cm (0.4 in) in diameter. The overlying moderately welded pumice and lithic rich ash-flow tuff is pinkish gray (5YR 8/1) and contains abundant white pumice (N9) and minor lithic fragments within a groundmass of altered ash (**Figure 5-17**). Unit **Tmtl** is as thick as 20 to 25 m (64 to 82 ft). The tuff (**Tmtl**) is interbedded with the upper parts of basalt and basaltic andesite lava flows of unit **Tmb**. Typical hand samples of the tuff (**Tmtl**) contain angular light gray (N8 to N7) pumice fragments up to 2 cm (0.75 in) and minor lithic fragments (**Figure 5-18**). In thin section, the tuff contains ≤1 percent (vol.) fragmented, angular, anhedral feldspar crystals ≤1 mm (0.04 in), contained in a groundmass of ash, brecciated tuff, and lithic fragments (**Figure 5-18**).

Unit **Tmtl** is assigned a middle Miocene age on the basis of stratigraphic position. Stratigraphic position, combined with outcrop, textural, and geochemical similarities suggest that the tuff (**Tmtl**) may be equivalent to the Dinner Creek Tuff, cooling unit 2 of Streck and others (2015).

Figure 5-17. Pumice-lithic tuff (Tmtl) cropping out along the Rattlesnake and Cow Creek drainages. (A) Ash-flow and air-fall tuff in unit Tmtl overlying basalt and basaltic andesite lava flows (Tmb)(43.70119, −118.80699). Scale bar is 3 m (10 ft) tall. (B) Close up view of the contact between ash-flow and air-fall tuff (Tmtl)(43.70130157, −118.80699). Scale bar is 1 m (3.3 ft) tall. (C) Welded ash-flow tuff in unit Tmtl (43.70199, −118.80699). Scale bar is 20 cm (8 in) tall. Photo credits: Robert A. Houston, 2016.

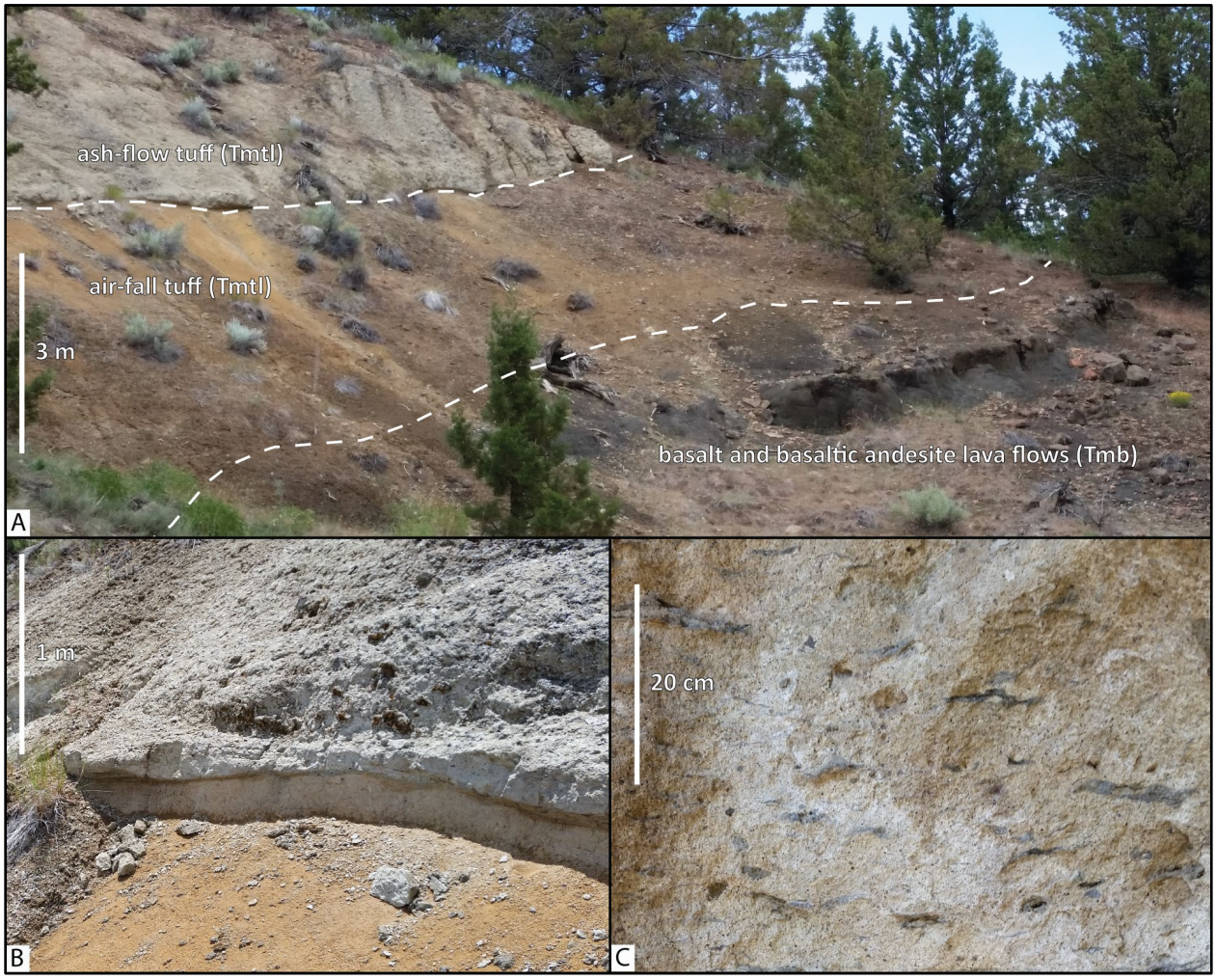

Figure 5-18. Photographs showing texture in the pumice-lithic tuff (Tmtl). (A) Thin section of pumice-lithic tuff with sparse plagioclase (pl) phenocrysts surrounded by a groundmass of ash, pumice, and lithic fragments (sample HAH058-16). Plane-polarized light. (B) Same view as (A) under cross-polarized light. (C) Thin section of pumice-lithic tuff showing vitric groundmass composed of glass shards, crystal and lithic fragments, flow-banded obsidian, and tuffaceous brecciated fragments (sample HAH058-16). (D) Same view as (C) under cross-polarized light. Scale bar in (A-D) is 1 mm (0.04 in). Photo credits: Robert A. Houston, 2017.

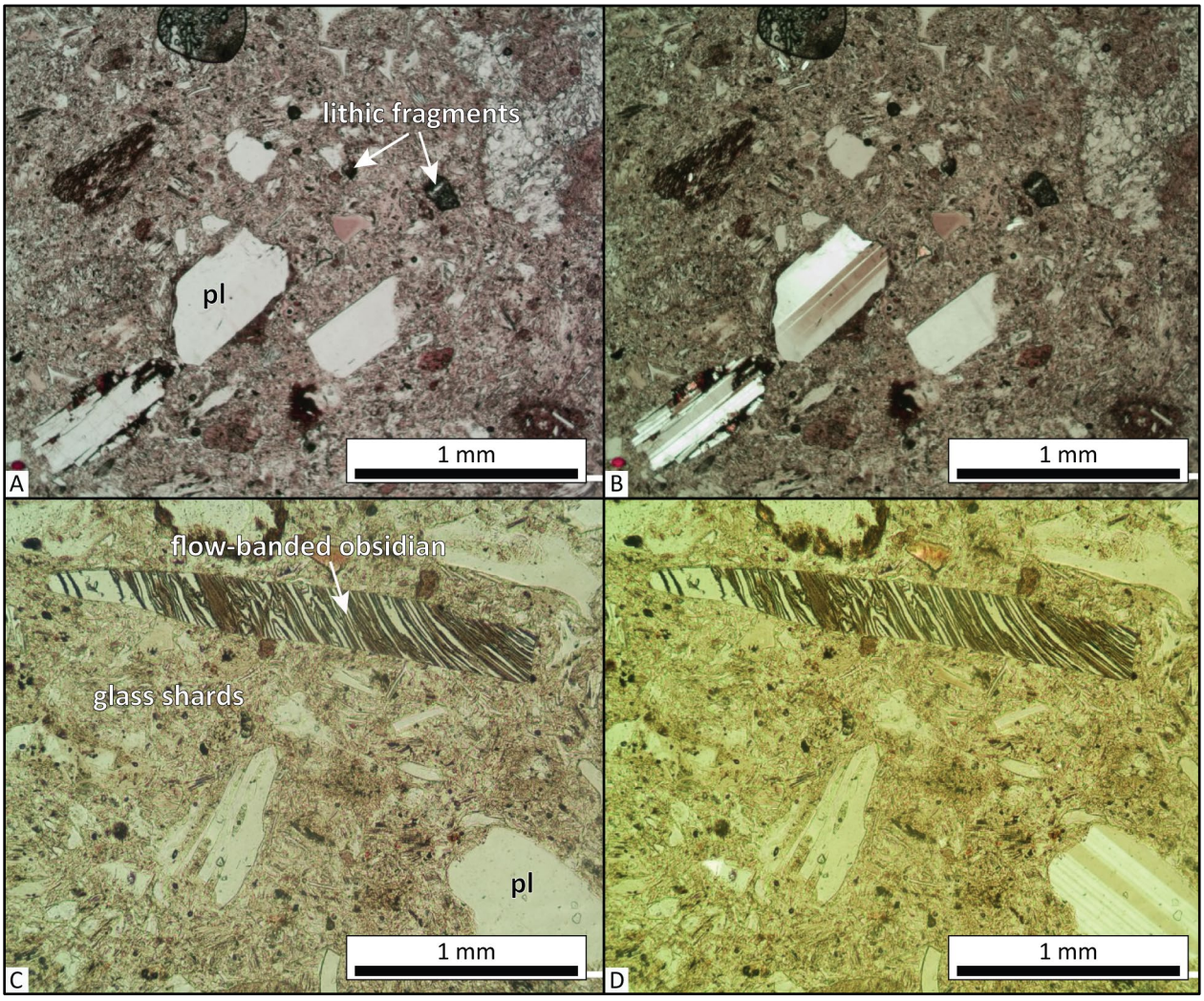

Tmdc **Dinner Creek Tuff (middle Miocene or lower Miocene)**—Massive, crystal poor, pumice and lithic rich, moderately to strongly welded rhyolitic ash-flow tuff (SiO_2 = 76.04 to 76.93 weight percent; K_2O = 3.65 to 3.88 weight percent; Ba = 1,417 to 1,418 ppm; Zr = 442 to 466 ppm; Nb = 24.8 to 25.6 ppm; *n* = 4 analyses) mapped along the Mill Creek drainage (**Figure 5-3**, **Figure 5-4**; **Table 5-1**; Plate; Appendix). Thickness of the tuff (**Tmdc**) ranges from 10 to 20 m (32 to 65 ft). The tuff (**Tmdc**) is interbedded with basalt and basaltic andesite lava flows of unit **Tmb**. Typical hand samples of the tuff are pinkish gray (5YR 8/1), containing angular white (N9) to light gray (N7) pumices up to 2.5 cm (1 in) and lithic fragments up to 3 cm (1.2 in) in diameter. The tuff (**Tmdc**) contains ≤5 percent (vol.), angular fragments of anhedral plagioclase, clinopyroxene, and minor quartz ≤2 mm (0.08 in) in a grayish red (5R 4/2) devitrified ash groundmass.

Unit **Tmdc** is assigned an early Miocene or late Miocene age on the basis of stratigraphic position. Stratigraphic position, combined with outcrop, textural, and geochemical similarities indicate that the tuff (**Tmdc**) is equivalent to the Dinner Creek Welded Ash-flow Tuff of Kittleman and others (1965), Dinner Creek Welded Tuff of Greene and others (1972), Dinner Creek Tuff (unit Td) of Ferns and others (1993), and Dinner Creek Tuff, cooling unit 1 of Streck and others (2015). Streck and others (2015) reported $^{40}Ar/^{39}Ar$ ages of 15.9 ± 0.09 Ma and 16.16 ± 0.02 Ma for the Dinner Creek Tuff, cooling unit 1.

Tmb **basalt and basaltic andesite lava flows (middle Miocene and lower Miocene)**—Chiefly a flow-on-flow succession of aphyric to olivine-, clinopyroxene-, and plagioclase-microporphyritic basalt and basaltic andesite lava flows (SiO_2 = 49.82 to 55.62 weight percent; K_2O = 0.30 to 1.80 weight percent; MgO = 2.93 to 8.47 weight percent; *n* = 37 analyses) mapped across the northern half of the study area (**Figure 5-3**, **Figure 5-4**, **Figure 5-19**, **Figure 5-20**; **Table 5-1**; Plate; Appendix). Lava flows forming unit **Tmb** are typically blocky jointed (**Figure 5-19a**); vertical vesicle cylinders are common (**Figure 5-19b**). Individual unit **Tmb** lava flows are as thick as 10 m (32 ft). Collectively, the total thickness of unit **Tmb** in the Harney 7.5′ quadrangle is as much as 240 m (800 ft). Unit **Tmb** is interbedded with four tuff units, including units **Tmdc**, **Tmtl**, **Tmt**, and **Tmtb** (**Figure 5-20**). Typical hand samples of the basalt and basaltic andesite lava flows (**Tmb)** are medium gray (N5) to pale-red purple (5RP 6/2), containing ~40 to 50 percent (vol.) subhedral plagioclase laths ≤2 mm (0.08 in), ~30 percent (vol.) poikilitic clinopyroxene, and ≤10 percent (vol.) iddingsitized olivine within a fine-grained holocrystalline to hypocrystalline groundmass (**Figure 5-21**).

Unit **Tmb** is assigned an early and middle Miocene age on the basis of stratigraphic position, interbedded with the Dinner Creek Tuff, cooling unit 1 (**Tmdc**). Stratigraphic position, combined with outcrop, textural, and geochemical similarities indicate that the basalt and basaltic andesite unit **Tmb** is made up of lava flows correlative to parts of the Grand Ronde Basalt, Steens Basalt, and Picture Gorge Basalt of the regionally extensive Columbia River Basalt Group.

Figure 5-19. Basalt and basaltic andesite lava flows (Tmb). (A) Blocky basaltic andesite lava flow (Tmb). Hammer for scale is 28 cm (11 in) long (43.73699, −118.80300). (B) Multiple vesicle cylinders (white arrows), formed by gas-filter pressing above a rising lower solidification front (Anderson and other, 1984; Manga and Stone, 1994, Goff, 1996), are present in unit Tmb lava flows. Pen for scale is 15 cm (6 in) long (43.73699,−118.80300). Photo credits: Robert A. Houston, 2016.

Figure 5-20. Baked lower contacts of basalt and basaltic andesite lava flows (Tmb). (A) Unit Tmb lava flow overlying pumice lithic tuff (Tmtl)(43.69673, −118.77217). (B) Unit Tmb lava flow overlying pumice tuff (Tmt)(43.73726,−118.80216). Hammer for scale in (A) and (B) is 28 cm (11 in) long. Photo credits: Robert A. Houston, 2016.

Figure 5-21. Photographs of texture in basalt and basaltic andesite lava flows (Tmb). (A) Microcrystalline basaltic andesite (Tmb). (B) Microporphyritic basaltic. Scale bars in (A) and (B) are 2.5 cm (1 in). (C) Thin section of basaltic andesite with plagioclase (pl), poikilitic clinopyroxene (cpx), olivine (ol), and opaques (sample HAH187-16). Plane-polarized light. (D) Same view as (C) under cross-polarized light. (E) Thin section of basalt with plagioclase (pl), poikilitic clinopyroxene (cpx), and opaques (sample HAH183-16). Plane-polarized light. (F) Same view as (E) under cross-polarized light. Scale bars in (C-F) are 1 mm (0.04 in). Photo credits: Robert A. Houston, 2017.

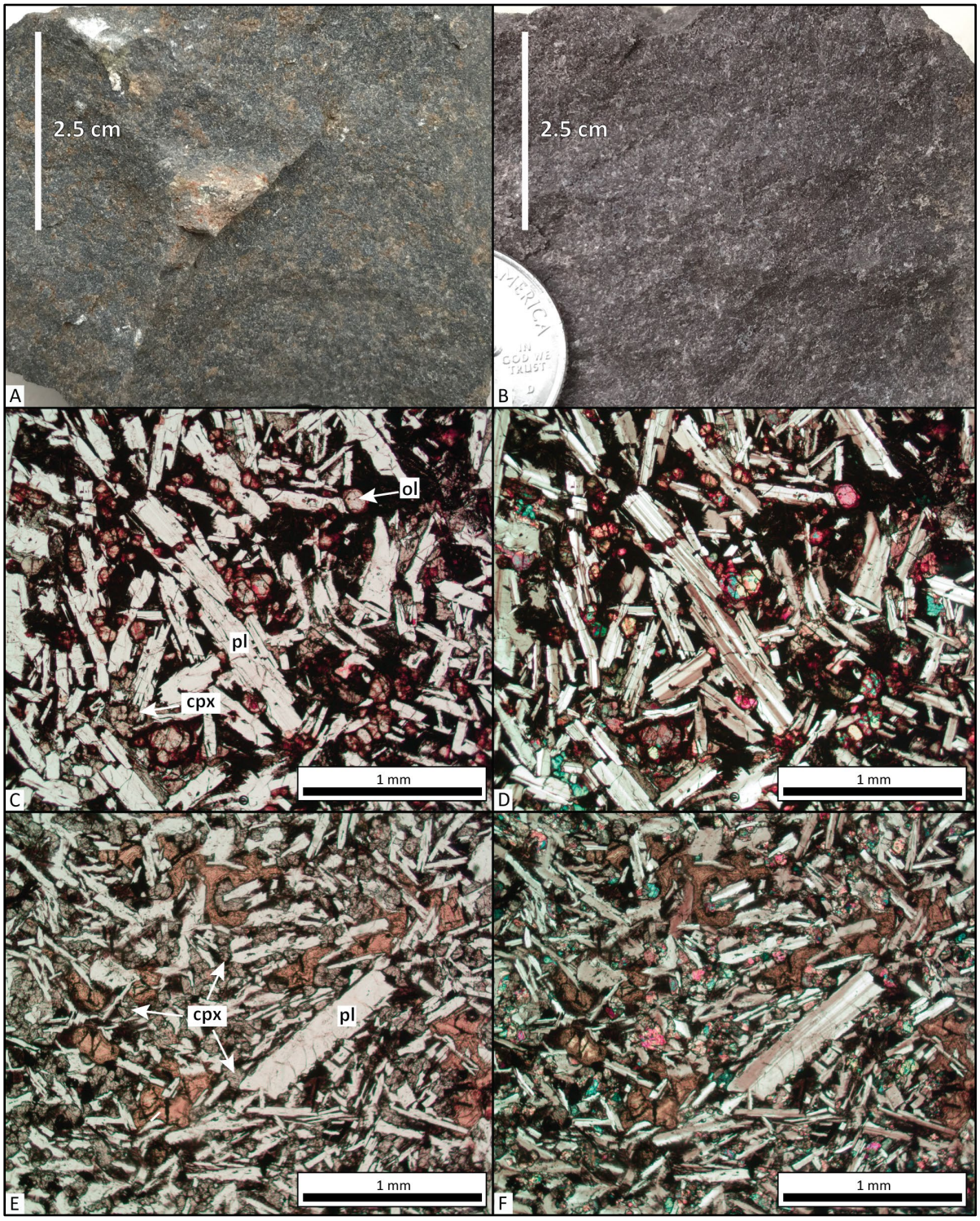

Angular unconformity to disconformity

5.4 Lower Cenozoic volcanic and sedimentary rocks

Toa **andesite (upper Oligocene)**—Andesite lava flows (SiO_2 = 59.27 weight percent; K_2O = 1.75 weight percent; Zr = 140 ppm; Nb = 8.6 ppm; *n* = 1 analysis) mapped beneath basalt and basaltic andesite lava flows along Cow Creek (**Figure 5-3**, **Figure 5-4**, **Table 5-1**; Plate; Appendix). Individual unit **Toa** lava flows range from 5 to 10 m (16 to 32 ft) thick, with a collective total exposed thickness of as much as 76 m (250 ft). The base of unit **Toa** is not exposed. Typical hand samples are medium gray (N5), containing ~60 percent (vol.) subhedral plagioclase microphenocrysts ≤1 mm (0.04 in), contained within a fine-grained holocrystalline groundmass (**Figure 5-22**).

Unit **Toa** has reversed magnetic polarity and is assigned a late Oligocene age on the basis of stratigraphic position and isotopic age. Houston and others (2018) reported an $^{40}Ar/^{39}Ar$ age of 24.75 ± 0.15 Ma for unit **Toa** andesite in the Devine Ridge North 7.5' quadrangle directly to the northwest of the study area (**Figure 1-1**).

Figure 5-22. Photographs of texture in andesite (Toa)(*following page*). (A) Vesicular andesite containing minor subhedral plagioclase laths (sample HAH176-16). Scale bar is 2.5 cm (1 in) tall. (B) Thin section of andesite (Toa) where a plagioclase (pl) phenocryst is surrounded by a fine-grained crystalline groundmass of plagioclase and poikilitic clinopyroxene. Plane-polarized light. (C) Same view as (B) under cross-polarized light. Scale bars in (B-C) are 1 mm (0.04 in). Photo credits: Robert A. Houston, 2017.

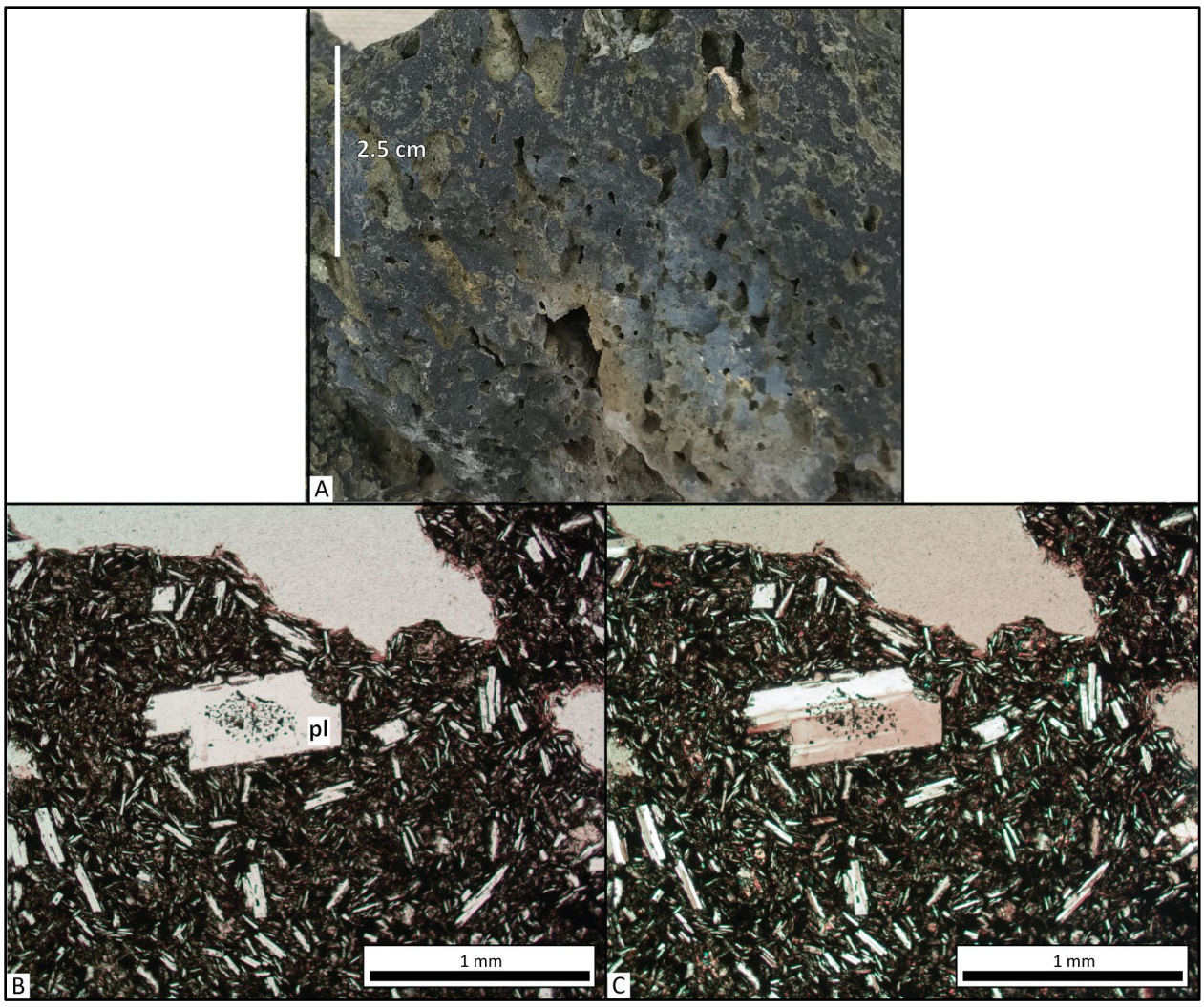

Tor **rhyolite (upper Oligocene[?])**—Quartz-, sanidine-, and biotite-phyric rhyolitic dike or plug (SiO_2 = 72.20 weight percent; K_2O = 2.09 weight percent; Zr = 93 ppm; Nb = 4.1 ppm; *n* = 1 analysis) mapped in the northwest part of the study area (**Figure 5-3**, **Figure 5-4**, **Table 5-1**; Plate; Appendix). Locally, the rhyolite is silicified, containing numerous chalcedony-filled fractures with no apparent brecciation. To the west and northwest in the Devine Ridge South and Devine Ridge North 7.5' quadrangles, McGrane (1985) noted that both rhyolitic and quartz porphyry dikes are spatially, temporally, and genetically related to the epithermal gold mineralization at the Idol City mining district (Niewendorp and others, 2018; Houston and others, 2018). Typical hand samples of the rhyolite (**Tor**) are light gray (N7) to medium light gray (N6) containing 10 to 15 percent (vol.) subhedral to euhedral, embayed quartz phenocrysts ≤2 mm (0.08 in), euhedral to subhedral sanidine, and biotite set within a very-fine-grained microcrystalline groundmass.

Unit **Tor** is assigned a late Oligocene(?) age on the basis of stratigraphic position.

Toda **dacite (upper Oligocene[?])**—Plagioclase- and quartz-phyric dacite (SiO_2 = 64.32 to 68.75 weight percent; K_2O = 2.06 to 2.45 weight percent; Zr = 103 to 128 ppm; Nb = 4.6 to 6.6 ppm; *n* = 4 analyses) mapped in the northwest part of the study area (**Figure 5-3**, **Figure 5-4**, **Figure 5-23**; **Table 5-1**; Plate; Appendix). These are the oldest rocks mapped in the Harney 7.5′ quadrangle. Within the study area, unit **Toda** is made up of individual dacite lava flows as thick as 5 to 10 m (16 to 32 ft). Contacts between lava flows area locally separated by thin paleosols, containing petrified wood and silicified nodules (**Figure 5-23**). Collectively unit **Toda** is as thick as 20 m (64 ft). In the study area, the dacite (**Toda**) is overlain by basalt and basaltic andesite lava flows (**Tmb**) and the Devine Canyon Ash-Flow Tuff (**Tmtd**). The lower part of the dacite (**Toda**) is not exposed in the quadrangle, so is queried where shown in cross section (Plate). Typical hand samples of the dacite (**Toda**) are dark gray (N3), containing ~25 percent (vol.) euhedral to subhedral plagioclase phenocrysts ≤5 mm (0.2 in), ≤5 percent (vol.) clinopyroxene ≤1 mm (0.04 in), and ≤1 percent (vol.) quartz ≤1 mm (0.04 in), set within a fine-grained microcrystalline groundmass (**Figure 5-24**).

The dacite (**Toda**) has normal magnetic polarity and is assigned a late Oligocene(?) age on the basis of stratigraphic position. Isom (2017) mapped six texturally and geochemically similar dacite units in the adjacent Telephone Butte 7.5' quadrangle (**Figure 1-1**) and obtained a U-Pb age of 22.83 ± 0014 Ma for the dacite of Black Rock. The dacite is equivalent to dacite (unit Toda) described by Houston and others (2018) and Niewendorp and others (2018) in the adjacent Devine Ridge North and Devine Ridge South 7.5'quadrangles.

Figure 5-23. Dacite lava flows (Toda). Typical exposure dacite of upper Mill Creek (Toda)(43.74280, −118.86400). Dashed white line shows the contact between individual lava flows in unit Toda. The contact is recognized by a thin paleosol containing petrified wood and silicified nodules.

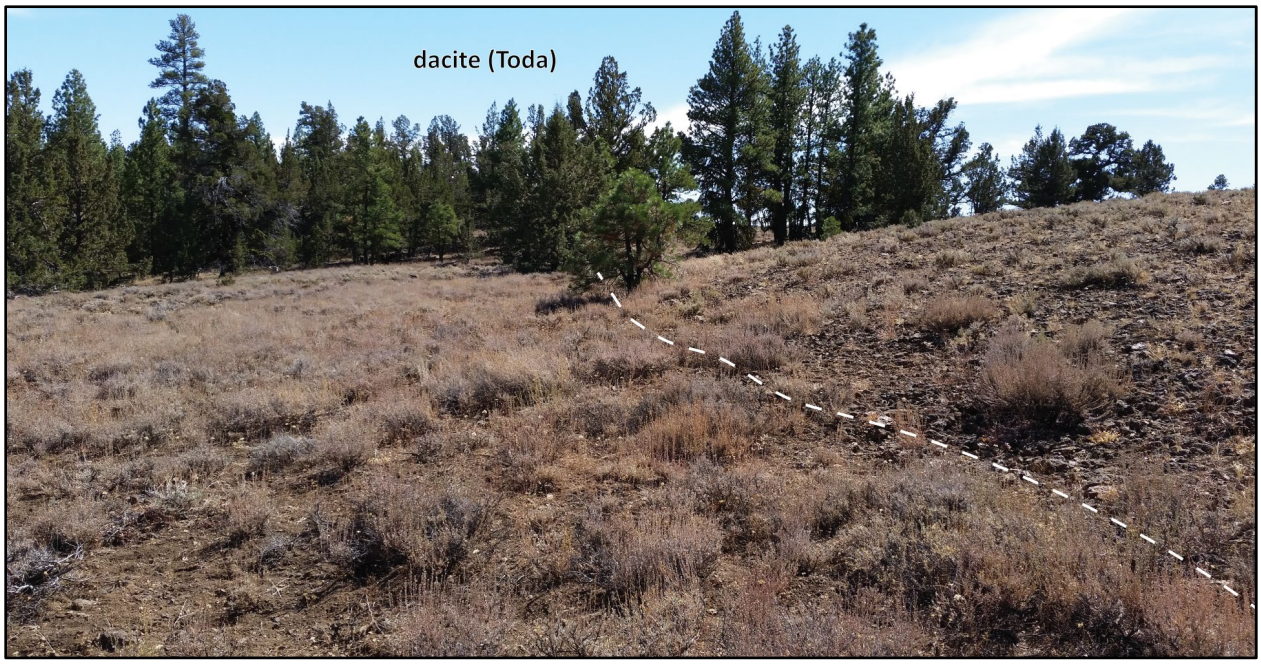

Figure 5-24. Thin section photographs of texture in dacite (Toda) (A) Clinopyroxene (cpx) phenocrysts surrounded by a fine-grained holocrystalline groundmass of plagioclase (pl)(sample HAH095-16). Plane-polarized light. (B) Same view as (A) under cross-polarized light. Plane-polarized light. (D) Euhedral clinopyroxene phenocryst surrounded by a fine-grained holocrystalline groundmass of plagioclase. Same view as (C) under cross-polarized light. Scale bars in (A-D) are 1 mm (0.04 in). Photo credits: Robert A. Houston, 2017.

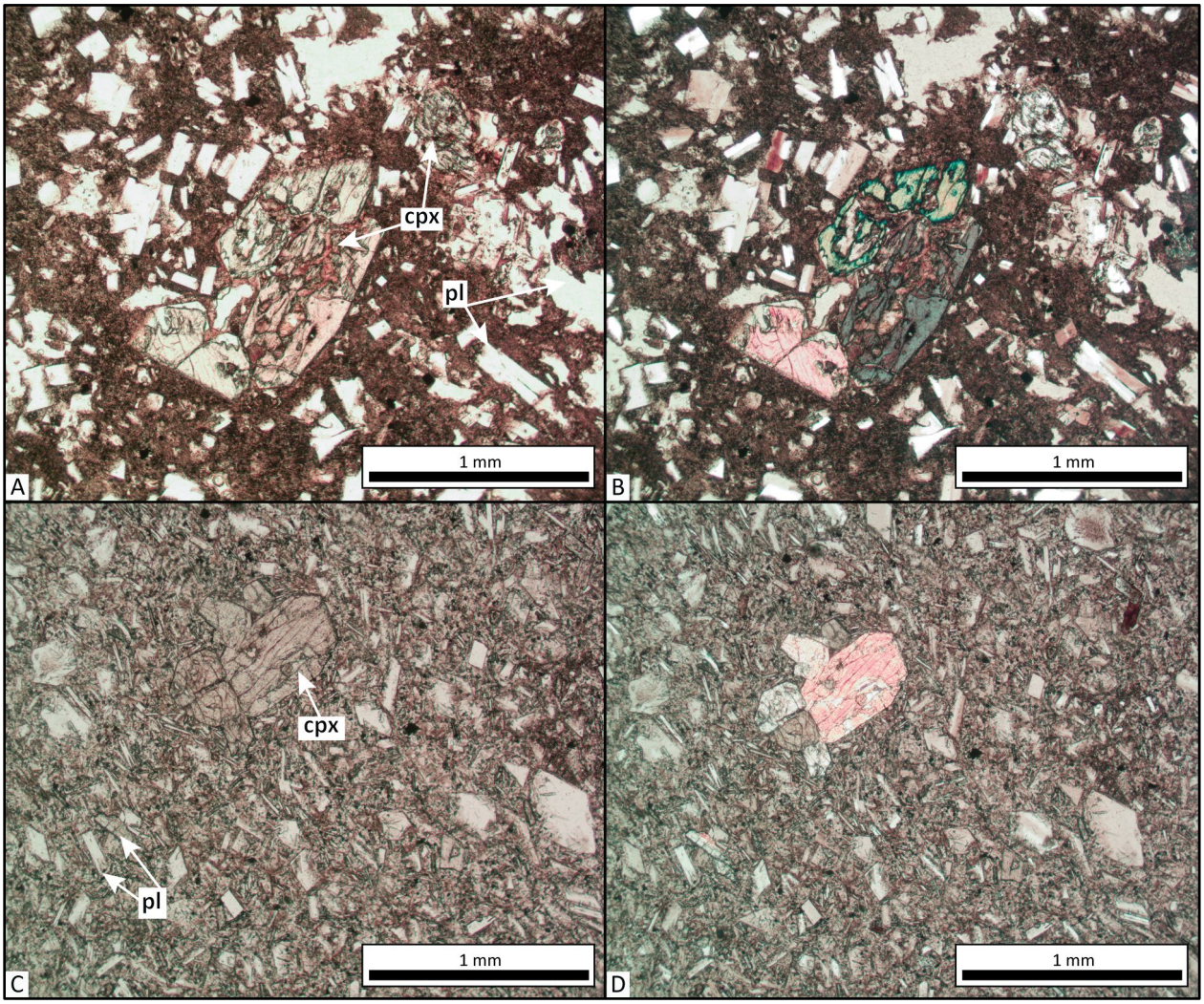

6.0 STRUCTURE

6.1 Introduction

Geologic structure in the Harney 7.5′ quadrangle is defined by the mapped distribution of geologic units, faults, topographic lineaments (as observed in SFM DEMs, 10-m DEMs, and 2016 NAIP orthophotos), folds, and bedding attitudes (Plate). Primary structural features (e.g., slickensides or fault breccia) are rarely observed in the field. Fault zones, such as those shown on the Plate, are recognized on the basis of offset geologic contacts, missing units, topographic lineaments as indicators of possible movement, breccia zones, and analysis of subsurface lithologic data obtained from water well logs.

The Harney 7.5′ quadrangle lies in a moderately deformed structural area of the northern Harney Basin, ~60 km (36 mi) northeast of the BFZ (**Figure 1-1**, **Figure 2-1**, **Figure 2-2**). Rocks in the northern part of the Harney Basin are gently folded along generally south-southwest-trending fold axes, and are cut by a dominant set of steeply dipping, normal and normal oblique northwest-striking faults, and a lesser number of north-striking and east-northeast–striking faults that are interpreted as conjugate Riedel shears (Niewendorp and others, 2018; Houston and others, 2018)(**Figure 6-1**; Plate). Direct observations of horizontal to gently inclined slickensides with shear fracture zones suggest a number of these faults have strike-slip or oblique slip movement (**Figure 6-1**). Faults cut Oligocene to upper Miocene rocks in the Harney 7.5′ quadrangle, and collectively have tilted the rocks gently southwest to west-southwest (**Figure 6-1**). A combination of faulting and some amount of erosion developed a significant paleotopography in the area prior to the deposition of the 9.63 Ma Devine Canyon Ash-flow Tuff (**Tmtd**). Significant faulting in the area continued after deposition of the 7.05 Ma Rattlesnake Tuff (**Tmtr**), but appears to have terminated sometime prior to the beginning of the Quaternary Period (2.58 Ma to present; **Figure 5-1**).

6.2 Faulting in the Harney 7.5′ quadrangle

Stereonet analysis of structural relations in the Harney 7.5′ quadrangle reveals four different periods of deformation: 1) Units **Tmb** to **Tmtd**—faulting and tilting, 2) Units **Tmtd** to **Tmtp**—faulting and tilting, 3) Units **Tmtp** to **Tmtr**—faulting, tilting, and gentle folding, and 4) Units **Tmtr** to present—faulting and tilting (**Figure 6-1**, **Figure 6-2**; Plate). Across these stratigraphic intervals, faulting is coeval with deposition of units, but happens at different rates. The following discussion presents the spatial and temporal distribution of faults, folds, and structural attitudes in the Harney 7.5′ quadrangle.

Within the study area, steeply dipping normal faults are grouped into three populations on the basis of strike orientation: northwest-, northeast-, and north-striking faults (n = 117 faults; Primary: N.4°W. ± 8.5°, Secondary: N.35°E. ± 10°, Ternary: N.5°W. ± 10°; **Figure 6-1a,b**; Plate). Individual primary faults suggest a component of normal rotational slip motion or oblique slip. However, a lack of piercing point offsets makes the quantification of oblique displacement ambiguous. Northwest-striking normal fault populations are generally longer, through-going structures (e.g., Sec. 17 fault; **Figure 6-1a**; Plate). Displacement of units across the northwest-striking normal faults is down on the north, with a few exceptions. Locally, a subset of the primary N.41°W.-striking fault populations appear to exhibit decreasing displacement of unit contacts up section, suggesting these faults remained active during deposition of the stratigraphic section (Plate). Other faults displace unit contacts equally at locations up section, suggesting post-deposition normal dip-slip deformation (Plate). Within the Harney 7.5′ quadrangle, the acute angles between the primary and secondary orientations are interpreted as

conjugate Riedel shears (**Figure 6-1a,b**; Plate). This observation suggests that faulting in the Harney 7.5′ quadrangle may have resulted from the accommodation of strain produced by right-lateral displacement along the BFZ (**Figure 2-1**). Additionally, the northwest-striking faults (R-Riedel shears) coalesce in the Mill Creek fault zone mapped across the northwest corner of the Harney 7.5′ quadrangle (Plate).

Descriptions of selected representative faults, characteristic of the three identified populations are presented in sections 6.2.1, 6.2.2, and 6.2.3 (**Figure 6-1a,b**; Plate).

6.2.1 Northwest-striking normal faults

Mill Creek fault zone (43.74831, -118.87322; **Figure 6-1a**; Plate)—The Mill Creek fault zone is a major north-northwest-striking (~N.20°W. to N.30°W.) zone of fault strands that bound a number of chaotically rotated (up to 90°) fault blocks. Faults strands in the Mill Creek fault zone are mapped to continue northwest into the Devine Ridge South and Devine Ridge North 7.5′ quadrangles, where they merge into north-northwest- to south-southeast-striking faults defining the Trout Creek and Soldier Creek fault zones (Niewendorp and others, 2018; Houston and others, 2018). The Idol City District, an epithermal gold deposit, is located at this zone of convergence. Oligocene rocks in the Idol City District are overprinted by a low-temperature peripheral silicified alteration (veined chalcedony) halo of the small epithermal gold (Houston and others, 2018).

Rattlesnake Creek fault (43.66835, -118.79681; *T22S/R32.5E/Sec. 17;* **Figure 6-1a**; Plate)—The Rattlesnake Creek fault is located in the southeastern part of the study area, adjacent to Rattlesnake Creek. The fault strikes N.20°W. and dips steeply north. Normal dip-slip to normal oblique-slip along the fault offsets the contact between the Prater Creek Ash-flow Tuff (**Tmtp**) and tuffaceous sedimentary rocks (**Tmst**). Displacement of the contact apparently increases from 15 m (49 ft) to 50 m (164 ft) from southeast to northwest, along strike of the fault, suggesting a probable normal to oblique slip displacement vector.

Upper Cow Creek fault (43.70833, -118.75900; *T21S/R32.5E/Sec. 34a*; **Figure 6-1a**; Plate)—The upper Cow Creek fault is located in the eastern part of the study area, adjacent to Cow Creek. The fault strikes ~N.63°W. and dips steeply northeast. Normal dip-slip to normal oblique-slip rotational displacement of the **Tmtp**/**Tmst** contact increases from ~7 m (23 ft) on the west side of the ridge to ~24 m (72 ft) on the east.

Coffeepot Creek fault (43.68501, -118.81740; *T22S/R32.5E/Sec. 7*; **Figure 6-1a**; Plate)—The Coffeepot Creek fault is located in the central part of the study area, adjacent to Rattlesnake Creek. The fault strikes N.42°W. and dips steeply east-northeast. Normal dip-slip displacement offsets the contact between the Prater Creek Ash-flow Tuff (**Tmtp**) and tuffaceous sedimentary rocks (**Tmst**). There is ~14 m (46 ft) of normal dip-slip offset of the **Tmtp**/**Tmst** contact across the fault.

6.2.2 Northeast-striking normal faults

East Cow Creek fault (43.70833, -118.75900; *T21S/R32.5E/Sec. 34b;* **Figure 6-1a**; Plate)—The East Cow Creek fault is located in the eastern part of the study area, adjacent to Cow Creek. The fault strikes ~N.28°E. and dips steeply south. Normal dip-slip displacement offset of the **Tmtr**/**Tmst** unit contact is ~8 m (26 ft).

West Fork Rattlesnake Creek fault (43.73999, -118.81606; *T21S/R32.5E/Sec. 19*; **Figure 6-1a**; Plate)—The West Fork Rattlesnake Creek fault is located in the northern part of the study area, adjacent to West Fork Rattlesnake Creek. The fault strikes ~N.31°E. and dips steeply northwest. There is ~4 m (13 ft) of normal dip-slip displacement offset of the **Tmb**/**Tmtd** unit contacts.

Mill Creek fault (43.67109, -118.85286; *T22S/R32E/Sec. 35;* **Figure 6-1a**; Plate)—The Mill Creek fault is located in the western part of the study area, adjacent to Coffeepot Creek. The fault strikes ~N.26°E. and dips steeply northwest. Normal dip-slip displacement offset of the **Tmst**/**Tmtp**/**Tmtr** unit contacts averages 13 m (42 ft).

6.2.3 North-striking normal faults

Lower Cow Creek fault (43.68599, -118.75771; *T22S/R32.5E/Sec. 10*; **Figure 6-1a**; Plate)—The lower Cow Creek fault is located in the eastern part of the study area and is concealed beneath Cow Creek Quaternary sediments. The inferred fault is based on comparing attitudes and stratigraphic units exposed on adjacent hillslopes of Rattlesnake Creek. The inferred fault strikes ~N.13°W. ±5°, and dips are assumed to be steeply down to the northeast. Structural reconstruction of the stratigraphy suggests normal dip-slip displacement offset of the unit contacts averages 80 m (262 ft) down on the east.

Shellrock Spring fault (43.74877, -118.75600; *T21S/R32.5E/Sec. 15;* **Figure 6-1a**; Plate)—The Shellrock Spring fault is located in the northeastern part of the study area, adjacent to Cow Creek. The fault strikes ~N.6°W. and dips steeply southwest. There is ~64 m (201 ft) of normal dip-slip offset across the fault.

Mortimer Canyon fault (43.69557, -118.78572; *T22S/R32.5E/Sec. 4;* **Figure 6-1a**; Plate)—The Mortimer Canyon fault is located in the east-central part of the study area, adjacent to Cow Creek. The fault strikes ~N.5°E. and dips steeply east. Normal dip-slip displacement of the unit contacts averages ~20 m (65 ft).

6.3 Structural attitudes in the Harney 7.5′ quadrangle

Structural attitudes (primary bedding) with 1° to 10°, southwest to west-southwest dips are common throughout the Harney 7.5′ quadrangle (**Figure 6-2**; Plate). This southward stratigraphic tilt may in part be a product of regional southward tilting resulting from uplift and displacement along the John Day Fault and buttressing along the margin of the BMU, north of the Harney Basin (**Figure 1-1**, **Figure 2-1**, **Figure 2-2**). Steeper structural attitudes were measured in proximity to faults and within the intensely structurally disturbed Mill Creek area in the northwest part of the study area.

Eutaxitic compaction foliation observed in the three major upper Miocene ash-flow tuff units (**Tmtd**, **Tmtp**, **Tmtr**) records similar structural attitudes as measured in the immediately underlying sedimentary rocks (**Tmst**) (**Figure 6-2b,c,g,i**). This observation indicates that within the Harney 7.5′ quadrangle, each ash-flow tuff was deposited on a surface of low topographic relief and eutaxitic foliation can be used as a temporal proxy for paleohorizontal.

Structural attitudes from individual units were collected, grouped, and plotted on equal-area, lower-hemisphere stereonet projections (**Figure 6-2**). Collectively, the mean vector structural attitude recorded across the study area is N.78°E., 10°S. (n = 390 measurements). Further analysis of structural attitudes in individual fault blocks indicats that younger geologic units are tilted to a lesser degree than older underlying units. These observations revealin several subtle angular unconformities between each major ash-flow tuff eruptive cycle. From oldest to youngest, each unit is tilted on average as follows: **Tmtb** (9°S.),

Tmtd (7°S.), **Tmtp** (5°S.), **Tmtr** (2°S.), **Qa** (horizontal) (**Figure 6-2i**). Therefore, angular discordances for the period between ash-flow tuff eruptive cycles is: **Tmtb** to **Tmtd** (2°), **Tmtd** to **Tmtp** (2°), **Tmtp** to **Tmtr** (3°), **Tmtr** to present day horizontal (3°). Because the eruptive cycles are chronologically well constrained, the rate of tilting during the middle to late Miocene can be determined between each eruptive cycle. Between the eruptions of **Tmtb** and **Tmtd**, tilting occurred at a rate of 1° per 2.625 m.y. and substantially increased to 1° tilt per 0.61 m.y. for the following period **Tmtd** to **Tmtp**. The rate of tilting continued to increase to 1° tilt per 0.453 m.y. for the period **Tmtp** to **Tmtr**. For the period following the eruption of **Tmtr** to present day, the rate of tilting significantly slowed to 1° tilt per 2.35 m.y. This drop in the rate of tilting following the eruption of **Tmtr** at 7 Ma is synchronous with regional structural events, including: 1) decrease in slip rates after ~7 Ma in syntectonic basins east of the Harney Basin (Millard, 2010); 2) decrease in extension rates along Basin and Range faults after about 7 Ma to 5.7 Ma (Trench 2008; Meigs and others, 2009); 3) termination of northeast-striking faulting in the Glass Buttes area between 4.7 and 1.39 Ma (Boschmann, 2012); and 4) onset of early High Cascades volcanism and initiation of intra-arc rifting from Mount Jefferson northward to Hood River (Conrey and others, 2002; McClaughry and others, 2012).

Figure 6-1. Distribution of mapped faults in the Harney 7.5′ quadrangle (*following page*). (A) Fault map showing the distribution of faults in the Harney 7.5′ quadrangle. (B) Rose diagram illustrating the dominant northwest-striking structural fabric. Basemap is a 10-m DEM hillshade.

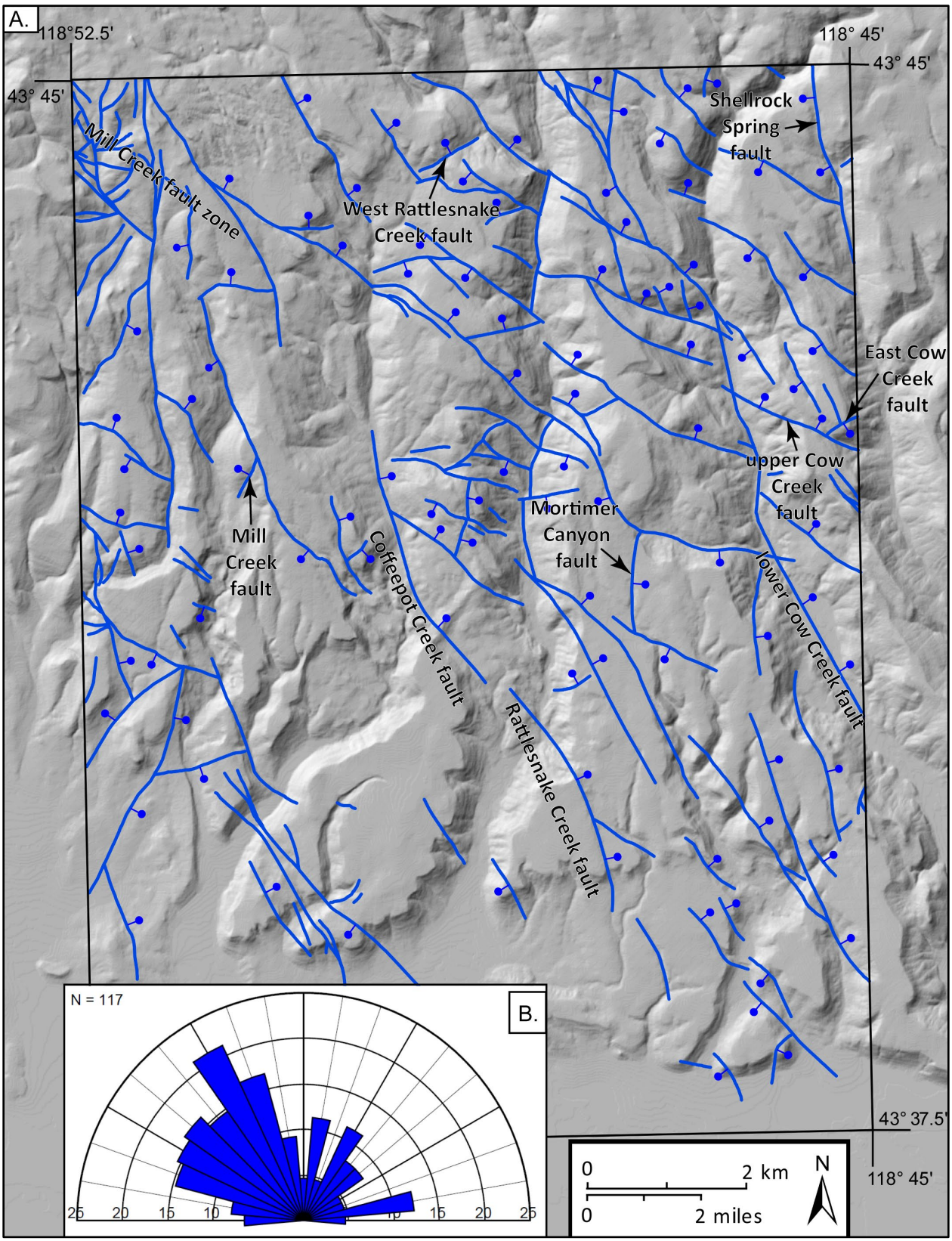
A.
118°52.5'
118° 45'
43° 45'
43° 45'
Mill Creek fault zone
West Rattlesnake Creek fault
Shellrock Spring fault
East Cow Creek fault
upper Cow Creek fault
Mill Creek fault
Coffeepot Creek fault
Mortimer Canyon fault
lower Cow Creek fault
Rattlesnake Creek fault
N = 117
B.
25 20 15 10 5 0 5 10 15 20 25
43° 37.5'
0 2 km
0 2 miles
N
118° 45'

Figure 6-2. Equal-area, lower-hemisphere contoured stereographic pole projections of structural attitudes (*n* = 390 measurements) from the Harney 7.5′ quadrangle. (A–H) Diagrams plot poles to structural attitudes (smaller black dots) with contours at 2 sigma (Kamb method; Kamb, 1956), 98 percent confidence circle, and mean vector pole (larger black dot). Each diagram lists the mean strike and dip in the lower left (e.g., 154° to 33° W), rock type in the upper right, and the number of measurements in the upper left. (I) Diagram shows the mean vector pole and strike and dip for each period of deformation. For this diagram, structural attitudes collected from the tuffaceous sedimentary unit are grouped based on stratigraphic relation, where Tmst occurs below Tmtd; Tmst occurs between Tmtd and Tmtp; and Tmst occurs between Tmtp and Tmtr.

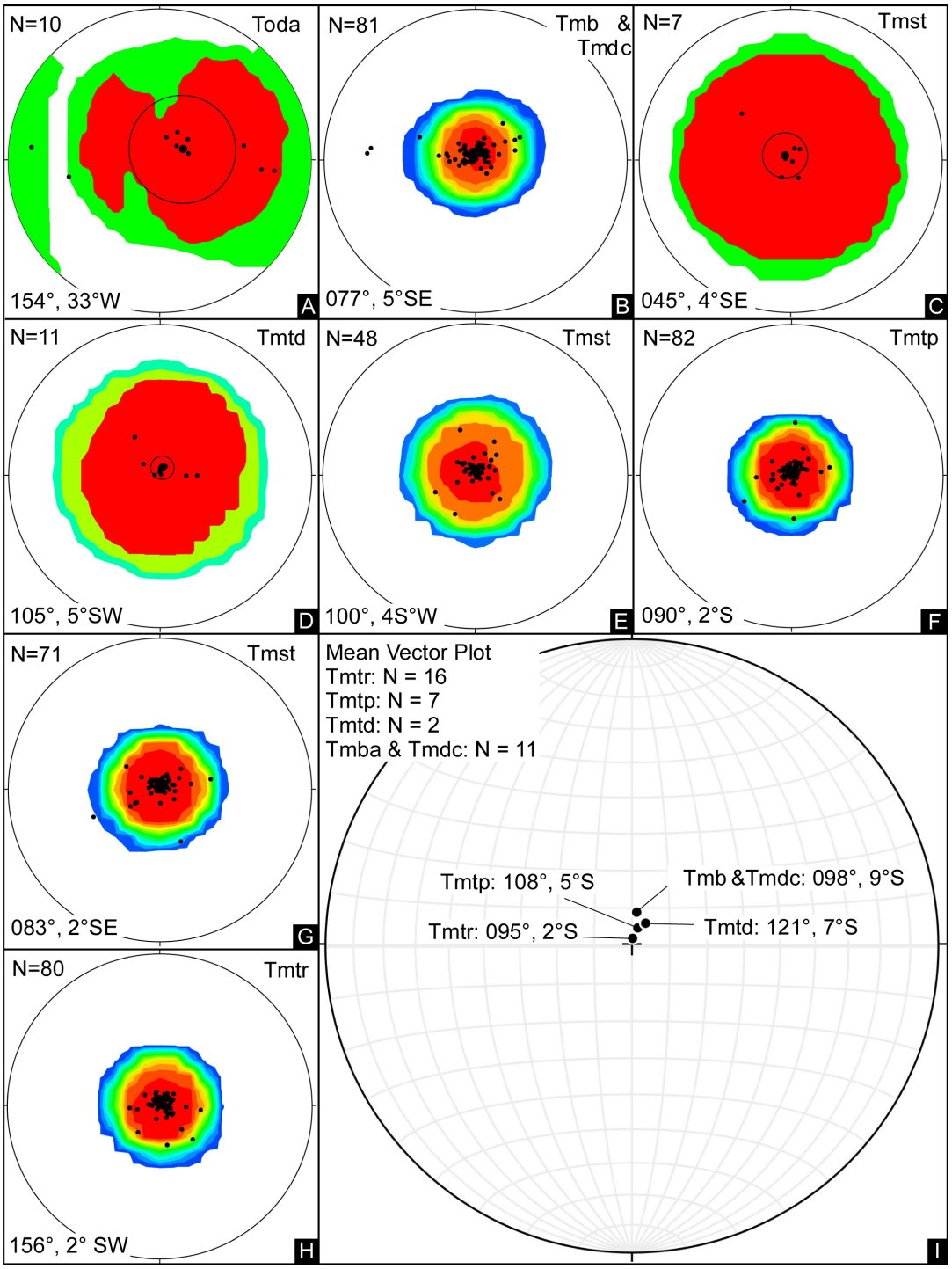

6.4 Folding in the Harney 7.5′ quadrangle

The rocks in the map area are locally folded. The map plate shows a number of gently south-southwest plunging synclines and anticlines mapped in the southern portion of the study area. The contact geometries and attitudes of these folds suggest the folding occurred after emplacement of the 7.05 Ma Rattlesnake Tuff (**Tmtr**). Axes of the folds are cut by high-angle faults.

7.0 GEOLOGIC HISTORY

Cenozoic volcanic and sedimentary rocks and Quaternary surficial deposits mapped in the Harney 7.5′ quadrangle record the volcanic, depositional, and deformational history in this part of the northern Harney basin since the late Oligocene (Plate). The following geologic history discussion presents chronologically major geologic events in the Harney 7.5′ quadrangle.

7.1 Late Miocene to Late Oligocene

Dacite of unit **Toda** is the oldest rock unit mapped in the study area and is likely age equivalent to the 22.83 Ma dacite of Black Rock of Isom (2017; unit Tmbr) and unit Toda dacite of Houston and others (2018) and Niewendorp and others (2018). Rhyolite dikes and irregular bodies (**Tor**) intrude the dacite in the northwest part of the quadrangle (Plate). The age relationship between andesite (**Toa**) and intrusive rhyolite dikes (**Tor**) remains poorly understood, owning to the lack of exposed contact relationships in the Harney 7.5′ quadrangle. Lode ores of the Idol City District, an epithermal gold deposit, are hosted in the dacite (**Toda**), andesite (**Toa**), and rhyolitic dikes (**Tor**). McGrane (1985) reported ages of 21 ± 0.9 Ma (K/Ar) on sericite alteration and 19 ± 0.08 Ma (K/Ar) on a rhyolite dike within the Idol City District. However, altered and mineralized rocks are locally overlain by nonmineralized "fresh" 24.75 Ma andesite (**Toa**), suggesting the hydrothermal ore fluids were emplaced prior to the late Oligocene. Overlying basalt and basaltic andesite lava flows (**Tmb**) are interbedded with four tuffs, including the 16 Ma Dinner Creek Tuff (**Tmdt**), pumice lithic tuff (**Tmtl**), pumice tuff (**Tmt**), and a tuff breccia (**Tmtb**). A combination of faulting and some amount of erosion developed a significant paleo-topography between the dacite (**Toda**) and the 9.63 Ma Devine Canyon Ash-flow Tuff (**Tmtd**).

7.2 Late Miocene to Pliocene

Three voluminous late Miocene ash-flow tuffs are widely exposed and mapped across the Harney Basin. These tuffs, mapped in the Harney 7.5′ quadrangles include: 1) the 9.63/9.74 Ma Devine Canyon Ash-flow Tuff (**Tmtd**), 2) the 8.41 Ma Prater Creek Ash-flow Tuff (**Tmtp**), and 3) the 7.1 Ma Rattlesnake Tuff (**Tmtr**) (Walker, 1979; Streck, 1994; Streck and Grunder, 1995, 2008; Jordan and others, 2004; Ford and others, 2013; McClaughry and others, 2019, 2020; Isom, 2017). The three major late Miocene tuff units, each exceeding 200 km^3 (48 mi^3) in eruptive volume and covering areas ranging from ~9,615 km^2 (~3,713 mi^2) to >35,000 km^2 (>13,500 mi^2) are presumed to have originated from caldera sources lying buried beneath the Harney Basin, including the Silvies River caldera near Burns (McClaughry and others 2019, 2020). Rapidly moving incandescent pyroclastic flows emanating from these calderas completely inundated the landscape of the late Miocene Harney Basin, largely burying evidence for the eruptive sources. Tuffaceous sedimentary rocks (**Tmst**) preserved between ash-flow tuffs represent erosion,

remobilization, transport, and deposition of abundant tuffaceous material in the intervals between caldera-forming eruptions. Some horizons in unit **Tmst** include air-fall tuffs signaling continued regional eruptions and pumice and tuff beds formed during pre-cursor eruptions to caldera-forming ash-flow tuff events.

7.3 Late Miocene to Recent

Uplift of the Blue Mountains to the north and Steens Mountain to the south and downwarping of the Harney Valley into a broad synclinal trough occurred through post-Rattlesnake (**Tmtr**) time (Buwalda, 1921). Drainages in the northern Harney Basin entrenched themselves into the southerly tilted dip-slope, flowing into the valley, forming the shallow Harney and Malheur lakes. These drainages carried locally derived detritus into the basin in the form of clay, sand, and gravel building up basin-fill deposits of considerable thickness.

Late Miocene units in the marginal parts of the Harney Basin, including the southern part of the Harney 7.5′ quadrangle, are covered by sequences of late Pliocene to Quaternary sedimentary rocks (**QTst**). These rocks represent fluvial and lacustrine deposits that partially filled the Harney Basin and followed ancestral drainages 61 to 183 m (200 to 600 ft) above the modern valley floor. Neogene bedrock units in the area are locally covered by surficial units, including older alluvium (**Qoa**), colluvium (**Qc**), fan deposits (**Qaf**), stream channel alluvium (**Qa**), and modern fill (**Qf**). Landslide deposits (**Qls**) are also present in some areas.

8.0 GEOLOGIC RESOURCES

8.1 Aggregate Materials and Industrial Minerals

Aggregate, in the form of crushed rock and gravel, is the major mineral resource mined in the Harney Basin area. Available regional locations for aggregate and crushed rock resources are provided by McClaughry and others (2020) https://www.oregongeology.org/sub/milo/. Aggregate-rock quarry sites within the Harney 7.5′ quadrangle are small pit-run sources located on private lands and on lands administered by the U.S. Forest Service. Quarries are sited mainly within alluvial deposits (**Qa**, **Qao**), tuffaceous sedimentary rock units (**Tmst**), Prater Creek Ash-flow Tuff (**Tmtp**), and the older basalt and basaltic andesite lava flows (**Tmb**). This material is used locally for road construction and maintenance. However, certain localities may be suitable for decorative stone and for use as riprap for stabilization and erosion control purposes. Sand and gravel resources are limited and restricted to unconsolidated alluvial deposits (**Qa**, **Qao**) in Coffee Pot, Rattlesnake, and Cow Creek drainages. No industrial minerals are known to be present in the study area (McClaughry and others, 2020).

Located to the northwest and outside of the study area, placer gravels discovered in 1891 led to the identification and initial development of an epithermal gold deposit named the Idol City District (McClaughry and others, 2020). The Idol City District borders the northwest corner of the Harney 7.5′ quadrangle. The peripheral silicified halo of the district extends into upper Mill Creek in the northwestern corner of the study area, corresponding to an area of focused deformation along a northwest trending shear zone. Locally, colorless, white (N9), to medium bluish gray (5B 5/1) chalcedony occurs as the dominant vein-filling material and lining vesicles. Common open-space cryptocrystalline silica includes massive or banded and to a lesser extent botryoidal textures. The presence of chalcedony and open-space

textures indicates that the depth of emplacement was shallow and fluid temperatures were low (<180°C [356°F]). Additionally, brecciated jasperoid nodules and silicified petrified wood occur at the contact between two dacitic lava flows (**Toda**)(**Figure 5-23**). This occurrence indicates that in addition to vertical fluid movement along faults, silica-rich fluids also moved laterally along permeable lithologic contacts.

8.2 Energy Resources

Geothermal resources are not currently exploited in the Harney 7.5′ quadrangle and, to the knowledge of the authors, no geothermal exploration has occurred in the study area, nor are there surface manifestations of past geothermal waters, such as deposits of siliceous sinter (https://www.oregongeology.org/pubs/dds/p-GILO.htm). However, the study area does host a number of geologic characteristics (e.g., fault zone conduits, stratiform geologic units) that may be favorable for the occurrence of localized geothermal reservoirs at depth. Cow Creek thermal spring is located adjacent to the study area in the Cow Creek drainage (43.66361, -118.74009). The thermal spring is located on a north-northwest trending fault that projects into the Harney 7.5′ quadrangle. A spot measurement of the thermal waters is 22° C (71.6° F) with a flow rate of 850 l/min (225 gpm; Black, 1994). Analysis of the water chemistry recorded 16 mg/l Ca, 86 mg/l HCO_3, 4.0 mg/l SO_4, and1.9 mg/l Cl (Black, 1994).

No oil and gas exploration wells have been drilled in the Harney 7.5′ quadrangle. A limited number of exploratory wells were drilled from the early 1900s into the late 1970s in the Harney basin (McClaughry and others, 2019, 2020). Many wells reported multiple shows of gas. The gas shows were likely of small volume occurring within the basin sediments. All wells were abandoned shortly after completion. Well location and drilling logs are available at https://www.oregongeology.org/mlrr/oilgas-logs.htm.

8.3 Water Resources

A full discussion of the geologic controls on surface and groundwater resources in the Harney 7.5′ quadrangle is beyond the scope of this report. However, field observations and preliminary findings on geologic parameters controlling water resources within the study area are briefly summarized below. For a more in-depth discussion, the reader is referred to previous hydrogeologic investigations conducted by Piper and others (1939), Leonard (1970), Walker (1979), Whitehead (1994), and Gonthier (1985).

In addition to investigating the stratigraphy and structure of the Harney 7.5′ quadrangle, the occurrence and distribution of perennial springs (n = 43) and ephemeral to intermittent springs (n = 49) were compiled by the first author (Appendix). The first author mapped ephemeral to intermittent spring locations on the basis of field observations of locations having temporally constrained groundwater discharge, sites with limited groundwater discharge, morphological expression of a spring, vegetation type and density, signs of temporal wildlife and domestic animal activity.

Coffeepot, Rattlesnake, and Cow Creek surface waters (perennial to intermittent) enter the northern margin of the Harney Basin (Plate). Surface water not locally diverted or evaporated, infiltrates sedimentary rocks in the southern part of the quadrangle (Plate). Clay content and alteration of tuffaceous material likely have reduced the permeability of the tuffaceous sedimentary rock sequence (**Tmst**). Gently southward dipping comparatively permeable lithologies (**Tmtr**, **Tmtp**, **Tmb**), broad, low-amplitude, gently (≤ 7 degree) southward plunging folds, and permeable faults appear to be the best units in terms of permeability and porosity for groundwater recharge. In the Harney 7.5′ quadrangle, for the most part, perennial springs appear to cluster along faults, whereas intermediate and ephemeral springs occur along lithologic contacts, suggesting steeply dipping fault zones are more hydrologically connected than gently tilted lithologic aquifers. Seeps or springs associated with a reduction of slope, that are not related to a

lithologic contact, might suggest a shallower hydraulic connection associated with snow melt and rainfall recharge.

Within the Harney 7.5′ quadrangle, the majority of water wells are drilled to depths of >120 m (400 ft) into sediments and sedimentary rocks (Appendix). The deepest well (HARN 181; Appendix) was drilled to a depth of 268 m (880 ft) into sedimentary rocks containing sequences of claystone, sandstone, gravel, volcanic ash, and pumice. One irrigation well (HARN 189; Appendix) located in the Rattlesnake Creek drainage, adjacent to mapped basaltic lavas (**Tmb**), penetrated the underlying volcanic rocks at depth. All other wells terminated in tuffaceous sedimentary rocks within the study area. Unconsolidated to partly consolidated alluvial sand and gravel deposits, preserved in terraces and floodplains (**Qa**, **Qao**) and on alluvial and debris fans (**Qaf**), likely contain groundwater that typically saturates sediments just above the underlying bedrock platform and is usually in hydraulic connection with nearby streams (Plate; Piper and others, 1939; Leonard, 1970). The deposits are typically thin (<10 m [30 ft]) and likely sinuous, but may be very permeable, except where they contain large amounts of clay and silt (Piper and others, 1939; Leonard, 1970). Alluvial wells developed in permeable sand and gravel intervals, with yields depending on annual precipitation, as compared to relatively impermeable silt-rich sedimentary intervals, are likely favorable targets (Piper and others, 1939).

The location of perennial springs along faults in the study area concentrate groundwater flow where permeabilities are favorable. From the occurrence of springs, water bearing horizons in the study area are generally found at the basal contacts of units **Tmtr**, **Tmtp**, **Tmtd**, and along individual lava flow margins of unit **Tmb** (Plate). These horizons serve as lateral pathways for groundwater flow. Sedimentary interbeds (**Tmst**) between ash-flow tuffs appear to act as either a confining unit or a porous media serving as a pathway for lateral transport of groundwater depending on percent clays. In the northwestern part of the study area, precipitation of chalcedony in fractures likely disrupts groundwater flow. Elsewhere, variability in the alteration and percent fault gouge along faults may leave limited permeable zones that serve as ideal groundwater pathways. Wells completed in tuff beds or unconsolidated tuffaceous sedimentary units are likely to yield only small quantities of water.

Permeable layers within the sedimentary rocks, as well as near-surface volcanic rocks, may be likely targets for groundwater resources. However, the gentle southward tilt of the stratigraphic sequence projects potential zones to deeper drilling depths as distance increase southward into the Harney Basin. Considering the subtle ≤3°, ≤2°, and ≤2° angular unconformities between **Tmtr** and **Tmtp**, **Tmtp** and **Tmtd**, and **Tmtd** and **Tmb** lava flow series, respectively, the economics of reaching deeper lithologic confined aquifers becomes a limiting factor with distance to the south in the Harney Basin. Locally, unconsolidated to partly consolidated alluvial sand and gravel sequences projecting into the Harney Basin likely contain groundwater in hydraulic connection with nearby streams and are likely groundwater targets (Plate; Piper and others, 1939; Leonard, 1970).

9.0 GEOLOGIC HAZARDS

9.1 Landslide Hazards

The downslope movement of rock and soil, in the form of landslides, rock falls, and debris flows, may present a geologic hazard to residents, infrastructure, and transportation corridors in the Harney 7.5′ quadrangle.

9.1.1 Simple and colluvial landslides

Landslide deposits (**Qls**; *n* = 49) were recognized and mapped in the study area. Those landslide deposits (**Qls**) mapped cover ~7.41 percent of the study area. They range in size from those covering less than 1 hectare (2.5 acres) to larger composite features covering areas up to 137 hectares (340 acres). The majority of mapped landslide deposits are deep-seated, earthflow-type features that occur along major drainages, originating on sparsely vegetated, moderately to steep slopes underlain by weakly consolidated tuffaceous sedimentary rocks (**Tmst**; Plate). Many of these slides can be attributed to the combined influences of parallel topographic slope and faulting or bedding dip, undercutting by streams, heavy precipitation, groundwater conditions, and rock type. The generally weakly consolidated nature of the tuffaceous sedimentary units makes this unit especially prone to landslides on gently to steeply inclined slopes. Future landslides should be expected in this unit, particularly in areas of changing vegetation, groundwater conditions, or land use.

Unstable colluvial wedges of soil and rock mantle some slopes in the study area. These deposits typically form when weathered rock particles, ranging in size from clay to boulders, accumulate along a hillside contact. When the mass of the accumulated material reaches a critical size, a triggering event such as heavy rainfall or seismogenic event may initiate the rapid down slope movement of this mass. Areas denuded by fire or other human vegetative removal can especially be at risk from such events.

9.1.2 Rock fall

Rock fall and rockslide hazards may be present in the study area where steep slopes and cliff exposures of **Tmtd**, **Tmtp**, and **Tmtr** occur (Plate). Potential natural triggering mechanisms for rock fall events may include freeze/thaw conditions, heavy rainfall, earthquakes, or extensive devegetation due to fire.

9.1.3 Alluvial and debris-flows

Alluvial fan deposits (**Qaf**) in the study area have been mapped, in particular along Coffee Pot Creek, Rattlesnake Creek, and Cow Creek (Plate). Rapidly moving landslides in the form of debris flows may be expected on both alluvial fans that lie at the mouths of steep-sided, colluvium-filled canyons and upland drainages. The potential for inundation of fan areas by rapidly moving debris flows increases during episodes of intense rainfall that occur after soils have been saturated by fall and early winter rainfall. Redirected drainage and poor construction practices are human activities that could initiate debris flows. Debris flows have the potential to threaten life and may cause extensive damage to property and transportation corridors.

10.0 ACKNOWLEDGMENTS

This project and publication were supported through the STATEMAP component of the National Cooperative Geologic Mapping Program under cooperative agreement number G16AC00179. Additional funds were provided by the State of Oregon through the Oregon Department of Geology and Mineral Industries and the Oregon Water Resources Department. XRF geochemical analyses were prepared and analyzed by Dr. Scott Boroughs at the GeoAnalytical Lab at Washington State University. The authors appreciate informative discussions and field trips with Ivan Gall, Justin Iverson, Jerry Grondin, Darrick Boschmann, and a number of other geologists who provided their expertise on stratigraphy in the Harney Basin. The authors acknowledge a number of area landowners who provided local knowledge and graciously allowed access to private holdings within the study area. Cartography for the map plate was provided Jon Franczyk. Critical and insightful reviews by Darrick Boschmann (OWRD), Clark Niewendorp (DOGAMI-Retired), and Deb Schueller (formerly DOGAMI) greatly enriched the final manuscript, geodatabase, and geologic map.

11.0 REFERENCES

Black, G,L., 1994, Low Temperature Geothermal Database for Oregon, Low-Temperature Geothermal Resources and Technology Transfer Oregon - Phase I Final Report: Oregon Department of Geology and Mineral Industries Open-File Report O-94-08, 340 p., 5 pl., scale 1:100,000. https://www.oregongeology.org/pubs/ofr/O-94-08.pdf

Boschmann, D. E., 2012, Structural and volcanic evolution of the Glass Buttes area, High Lava Plains, Oregon: Corvallis, Oreg., Oregon State University, M.S. thesis, 100 p. https://ir.library.oregonstate.edu/concern/graduate_thesis_or_dissertations/47429d66f

Brown, C. E., and Thayer, T. P., 1966, Geologic map of the Canyon City quadrangle, northeastern Oregon: U.S. Geological Survey Miscellaneous Geologic Investigations Map I-447, 1 pl., scale 1:250,000.

Brown, D. E., 1982, Map showing geology and geothermal resources of the southern half of the Burns 15 minute quadrangle, Oregon: Oregon Department of Geology and Mineral Industries Geological Map Series GMS-20, 1 pl., scale 1:24,000. https://www.oregongeology.org/pubs/gms/GMS-020.pdf

Brown, D. E., McLean, G. D., and Black, G. L., 1980a, Preliminary geology and geothermal resource potential of the northern Harney Basin, Oregon: Oregon Department of Geology and Mineral Industries Open-File Report 80-6, 52 p., 4 pl., scale 1:62,500. Zipped file: https://www.oregongeology.org/pubs/ofr/O-80-06.zip

Brown, D. E., McLean, G. D., and Black, G. L., 1980b, Preliminary geology and geothermal resource potential of the southern Harney Basin, Oregon: Oregon Department of Geology and Mineral Industries Open-File Report 80-7, 90 p. 8 pl. Zipped file: https://www.oregongeology.org/pubs/ofr/O-80-07.zip

Butler, R. F., 1992, Origins of natural remanent magnetism, chap. 3 *of* Paleomagnetism: Magnetic domains to geologic terranes: Boston, Mass., Blackwell Scientific Publications, p. 31–63. Available from https://websites.pmc.ucsc.edu/~njarboe/pmagresource/ButlerPaleomagnetismBook.pdf

Cahoon, E. B., and Streck, M. J., 2017, Picture gorge basalt, eastern Oregon: Extended distribution and petrogenetic connections to Steens basalt and Strawberry Volcanics: Geological Society of America Abstracts with Programs, v. 49, no. 6. doi: 10.1130/abs/2017AM-304582. https://gsa.confex.com/gsa/2017AM/webprogram/Paper304582.html

Cahoon, E.B., Streck, M.J., Koppers, A.A.P., and Miggins, D.P., 2020, Reshuffling the Columbia River Basalt chronology—Picture Gorge Basalt, the earliest- and longest-erupting formation: Geology, v. 48, p. 348–352. https://doi.org/10.1130/G47122.1.

Camp, V. E., Ross, M. E., and Hanson, W. E., 2003, Genesis of flood basalts and Basin and Range volcanic rocks from Steens Mountain to the Malheur River Gorge, Oregon: Geological Society of America Bulletin, v. 115, no. 1, p. 105–128. https://doi.org/10.1130/0016-7606(2003)115<0105:GOFBAB>2.0.CO;2

Camp, V. E., Ross, M. E., Duncan, R. A., Jarboe, N. A., Coe, R. S., Hanan, B. B., and Johnson, J. A., 2013, The Steens Basalt: Earliest lavas of the Columbia River Basalt Group, *in* Reidel, S. P., Camp, V. E., Ross, M. E., Wolff, J. A., Martin, B. S., Tolan, T. L., and Wells, R. E., The Columbia River Flood Basalt Province: Geological Society of America Special Paper 497, p. 87–116. https://doi.org/10.1130/2013.2497(04)

Cande, S. C., and Kent, D. V., 1992, A new geomagnetic polarity time scale for the Late Cretaceous and Cenozoic: Journal of Geophysical Research, v. 97, no. B10, p. 13,917–13,951. https://doi.org/10.1029/92JB01202

Cohen, K. M., Finney, S. C., Gibbard, P. L., and Fan, J.-X., 2018, The ICS International Chronostratigraphic Chart: Episodes, v. 36, no. 3, 199–204. Available at http://www.stratigraphy.org/ICSchart/Cohen2013_Episodes.pdf

Conrey, R.M., Taylor, E.M., Donnelly-Nolan, J.M., and Sherrod, D.R., 2002, North-central Oregon Cascades: Exploring petrologic and tectonic intimacy in a propagating intra-arc rift, *in* Moore, G. W., ed., Field guide to geologic processes in Cascadia: Oregon Department of Geology and Mineral Industries Special Paper 36, p. 47–90. https://www.oregongeology.org/pubs/sp/p-SP.htm.

Cox, K.G., Bell, J.D., and Pankhurst, R.J., 1979, The interpretation of igneous rocks: London, George Allen and Unwin, 450 p.

Cruz, M., 2017, Field mapping investigation and geochemical analysis of volcanic units within the Dinner Creek Tuff Eruptive Center, Malheur County, eastern Oregon: Portland, Oreg,: Portland State University, M.S. thesis. http://dx.doi.org/10.15760/etd.5731

Donath, F. A., 1962, Analysis of basin-range structure, south-central Oregon: Geological Society of America Bulletin, v. 73, p. 1–16. https://doi.org/10.1130/0016-7606(1962)73[1:AOBSSO]2.0.CO;2

Ferns, M. L., and McClaughry, J. D., 2013, Stratigraphy and volcanic evolution of the middle Miocene to Pliocene La Grande–Owyhee eruptive axis in eastern Oregon, *in* Reidel, S. P., Camp, V. E., Ross, M. E., Wolff, J. A., Martin, B. S., Tolan, T. L., and Wells, R. E., eds., The Columbia River Flood Basalt Province: Geological Society of America Special Paper 497, p. 401–427. https://doi.org/10.1130/2013.2497(16)

Ferns, M. L., Brooks, H. C., Evans, J. G., and Cummings, M. L., 1993, Geologic map of the Vale 30 × 60 minute quadrangle, Malheur County, Oregon, and Owyhee County, Idaho: Oregon Department of Geology and Mineral Industries Geologic Map Series GMS-77, 1 pl., scale 1:100,000. https://www.oregongeology.org/pubs/gms/GMS-077.pdf

Ford, M. T., 2012, Rhyolitic magmatism of the High Lava Plains and adjacent northwest Basin and Range, Oregon: Implications for the evolution of continental crust: Corvallis, Oreg., Oregon State University, Ph.D. dissertation, 111 p. https://ir.library.oregonstate.edu/concern/graduate_thesis_or_dissertations/p5547t57d

Ford, M. T., Grunder, A. L., and Duncan, R. A., 2013, Bimodal volcanism of the High Lava Plains and northwestern Basin and Range of Oregon: Distribution and tectonic implications of age-progressive rhyolites: Geochemistry, Geophysics, Geosystems, v. 14, no. 8, p. 2837–2857. https://doi.org/10.1002/ggge.20175

Geological Society of America Rock-Color Chart Committee, 1991, Rock color chart, 7th printing: Boulder, Colo.

Gillespie, M. R., and Styles, M. T., 1999, BGS rock classification scheme, v. 1, Classification of igneous rocks: Keyworth, U.K., British Geological Survey Research Report RR 99-06 (reformatted), 52 p. http://nora.nerc.ac.uk/3223/1/RR99006.pdf

Gonthier, J. B., 1985, A description of aquifer units in eastern Oregon: U.S. Geological Survey Water-Resources Investigations Report 84-4095, 39 p., 4 pl., scale 1:500,000. https://doi.org/10.3133/wri844095

Gradstein, F. M., and others. 2004, A geologic time scale 2004: Cambridge University Press, 589 p.

Gray, J. J., Peterson, N. V., Clayton, J., and Baxter, G. L., 1983, Geology and mineral resources of 18 BLM Wilderness, Harney and Malheur counties: Oregon Department of Geology and Mineral Industries Open-File Report 83-2, 106 p., scale 1:63,360. https://www.oregongeology.org/pubs/ofr/O-83-02.pdf

Greene, R. C., 1972, Preliminary geologic map of the Burns and West Myrtle Butte 15-minute quadrangles, Oregon: U.S. Geological Survey Miscellaneous Field Studies Map MF-320, scale 1:62,500. https://ngmdb.usgs.gov/Prodesc/proddesc_2743.htm

Greene, R. C., 1973, Petrology of the welded tuff of Devine Canyon, southeast Oregon: U.S. Geological Survey Professional Paper 797, 26 p. https://doi.org/10.3133/pp797

Greene, R. C., Walker, G. W., and Corcoran, R. E., 1972, Geologic map of the Burns quadrangle, Oregon: U.S. Geological Survey Miscellaneous Geologic Investigations Map I-680, scale 1:250,000. https://ngmdb.usgs.gov/Prodesc/proddesc_9455.htm

Haddock, G. H., 1967, The Dinner Creek welded ash-flow tuff of the Malheur Gorge area: Eugene, Oreg., University of Oregon, Ph.D. thesis, 111 p.

Hallsworth, C. R., and Knox, R. W. O'B., 1999, BGS rock classification scheme, v. 3, Classification of sediments and sedimentary rocks: Keyworth, U.K., British Geological Survey Research Report RR 99-03, 44 p. http://nora.nerc.ac.uk/3227/1/RR99003.pdf

Houston, R. A., McClaughry, J. D., Duda, C. J. M., and Niewendorp, C. A., 2018, Geologic map of the Devine Ridge North 7.5′ quadrangle, Harney County, Oregon: Oregon Department of Geology and Mineral Industries Geologic Map Series 121, scale 1:24,000. https://www.oregongeology.org/pubs/gms/p-GMS-121.htm

Iademarco, M. J., 2009, Volcanism and faulting along the northern margin of Oregon's High Lava Plains: Hampton Butte to Dry Mountain: Corvallis, Oreg., Oregon State University, M.S. thesis, 158 p., 1 pl. https://ir.library.oregonstate.edu/concern/graduate_thesis_or_dissertations/t435gj391

Isom, S. L., 2017, Compositional and physical gradients in the magmas of the Devine Canyon Tuff, eastern Oregon: constraints for evolution models of voluminous high-silica rhyolites: Portland, Oreg., Portland State University, M.S. thesis, 147 p. https://pdxscholar.library.pdx.edu/open_access_etds/3885/

Johnson, D. M., Hooper, P. R., and Conrey, R. M., 1999, XRF analysis of rocks and minerals for major and trace elements on a single low dilution Li-tetraborate fused bead: Advances in X-ray Analysis, v. 41, p. 843–867. Available at: https://s3.wp.wsu.edu/uploads/sites/2191/2017/06/Johnson-Hooper-and-Conrey.pdf

Johnson, J. A., 1994, Geologic map of the Krumbo Reservoir quadrangle, Harney County, southeastern Oregon: U.S. Geological Survey Miscellaneous Field Studies Map MF-2267, 11 p., 1 pl., scale 1:24,000. https://pubs.er.usgs.gov/publication/mf2267

Johnson, J. A., 1996, Geologic map of the Page Springs quadrangle, Harney County, southeastern Oregon: U.S. Geological Survey Open-File Report OF-96-675, 1 pl., scale 1:24,000. https://ngmdb.usgs.gov/Prodesc/proddesc_18672.htm

Johnson, J.A., Hooper, P.R., Hawkesworth, C. J., and Binger, G. B., 1998a, Geologic map of the Stemler Ridge quadrangle, Malheur County, southeastern Oregon: U.S. Geological Survey Open-File Report OF-98-105, 1 pl., scale 1:24,000. https://ngmdb.usgs.gov/Prodesc/proddesc_16445.htm

Johnson, J. A., Hawkesworth, C. J., Hooper, P. R., and Binger, G. B., 1998b, Major- and trace-element analyses of Steens Basalt, southeastern Oregon: U.S. Geological Survey Open-File Report 98-482, 30 p. https://doi.org/10.3133/ofr98482

Jordan, B. T., 2001, Basaltic volcanism and tectonics of the High Lava Plains, southeastern Oregon: Corvallis, Oreg., Oregon State University, Ph.D. dissertation, 218 p., https://ir.library.oregonstate.edu/concern/graduate_thesis_or_dissertations/nv935579s?locale=en

Jordan, B. T., Streck, M. J., and Grunder, A. L., 2002, Bimodal volcanism and tectonism of the High Lava Plains, Oregon, *in* Moore, G. W., ed., Field guide to geologic processes in Cascadia, Field trips to accompany the 98th Annual Meeting of the Cordilleran Section of the Geological Society of America, May 13–15, 2002, Corvallis, Oregon: Oregon Department of Geology and Mineral Industries Special Paper 36, p. 23–46. https://www.oregongeology.org/pubs/sp/SP-36.pdf

Jordan, B. T., Grunder, A. L., Duncan, R. A., and Deino, A. L., 2004, Geochronology of age-progressive volcanism of the Oregon High Lava Plains: Implications for the plume interpretation of Yellowstone: Journal of Geophysical Research, v. 109, no. B10, B10202, 19 p. https://doi.org/10.1029/2003JB002776

Kamb, W.B., 1959., Ice Petrofabric Observations from Blue Glacier, Washington, in Relation to Theory and Experiment: Journal of Geophysical Research, v. 64, no. 11, p. 1891-1909.

Khatiwada, M., and Keller, G. R., 2015, An integrated geophysical imaging of the upper crustal features in the Harney Basin, southeast Oregon: Geosphere, v. 11, no. 1, p. 185–200. https://doi.org/10.1130/GES01046.1

Kittleman, L. R., Green, A. R., Hagood, A. R., Johnson, A. M., McMurray, J. M., Russell, R. G., and Weeden, D. A., 1965, Cenozoic stratigraphy of the Owyhee region, southeastern Oregon: University of Oregon, Museum of Natural History Bulletin, no. 1, 45 p. Available at http://hdl.handle.net/1794/19996

Lawrence, R. D., 1976, Strike-slip faulting terminates the Basin and Range province in Oregon: Geological Society of America Bulletin, v. 87, no. 6, p. 846–850. https://doi.org/10.1130/0016-7606(1976)87<846:SFTTBA>2.0.CO;2

Le Bas, M. J., and Streckeisen, A. L., 1991, The IUGS systematics of igneous rocks: Journal of the Geological Society, v. 148, no. 5, p. 825–833. https://doi.org/10.1144/gsjgs.148.5.0825

Le Bas, M. J., Le Maitre, R. W., Streckeisen, A., and Zanettin, B., 1986, A chemical classification of volcanic rocks based on the total alkali-silica diagram: Journal of Petrology, v. 27, no. 3, p. 745–750. https://doi.org/10.1093/petrology/27.3.745

Le Maitre, R. W. (ed.), and others, 2004, Igneous rocks: a classification and glossary of terms: recommendations of the International Union of Geological Sciences, Subcommission on the Systematics of Igneous Rocks: Cambridge, Cambridge University Press, 236 p.

Leonard, A. R., 1970, Ground-water resources in Harney Valley, Harney County, Oregon: Salem, Oreg., Oregon Water Resources Department, Ground Water Report 16, 65 p., 3 pl., scale 1:125,000. https://www.oregon.gov/owrd/wrdreports/gw_report_16_harney.pdf

Mackenzie, W. S., Donaldson, C. H., and Guilford, C., 1997, Atlas of igneous rocks and their textures (7th ed.): Addison Wesley Longman, 148 p.

MacLean, J. W., 1994, Geology and geochemistry of Juniper Ridge, Horsehead Mountain, and Burns Butte: implications for the petrogenesis of silicic magma on the high lava plains, southeastern Oregon: Corvallis, Oreg., Oregon State University, M.S. thesis, 141 p. https://ir.library.oregonstate.edu/concern/graduate_thesis_or_dissertations/zp38wf64g?locale=en

MacLeod, N. S., Walker, G. W., and McKee, E. H., 1976, Geothermal significance of eastward increase in age of upper Cenozoic rhyolitic domes in southeastern Oregon, *in* Second United Nations Symposium on the Development and Use of Geothermal Resources, v. 1: Washington D.C., Government Printing Office, p. 465–474.

McClaughry, J.D., Duda, C.J.M., and Ferns, M.L., 2019, Geologic map of the Poison Creek and Burns 7.5′ quadrangles, Harney County, Oregon: Oregon Department of Geology and Mineral Industries Geological Map Series GMS 123, 127 p., 2 plates, scale 1:24,000, Esri format geodatabase; shapefiles, metadata; spreadsheet (4 sheets). https://www.oregongeology.org/pubs/gms/p-GMS-123.htm

McClaughry, J.D., Duda, C.J.M., and Ferns, M.L., 2020, Geologic map of the Burns Butte 7.5′ quadrangle, Harney County, Oregon: Oregon Department of Geology and Mineral Industries Geological Map Series GMS 125, 168 p., 1 plate, scale 1:24,000, Esri format geodatabase; shapefiles, metadata; spreadsheet (4 sheets). https://www.oregongeology.org/pubs/gms/p-GMS-125.htm

McClaughry, J. D., Niewendorp, C.A., Franczyk, J. J., Duda, C. J. M., and Madin, I. P., 2020, Mineral Information Layer for Oregon, release 3 [MILO-3]: Oregon Department of Geology and Mineral Industries Digital Data Series MILO-3, Esri geodatabase. https://www.oregongeology.org/milo/index.htm

McClaughry, J.D., Wiley, T.J., Conrey, R.C., Jones, C.B., and Lite, K.E., 2012, Digital geologic map of the Hood River Valley, Hood River and Wasco counties, Oregon: Oregon Department of Geology and Mineral Industries Open-File Report O-12-03, 142 p., 1 pl., scale 1:36,000, Esri ArcGIS™ geodatabase, GIS files, spreadsheets. https://www.oregongeology.org/pubs/ofr/p-O-12-03.htm.

McGrane, D, J., 1985, Geology of the Idol City area: a volcanic-hosted, disseminated precious-metal occurrence in east-central Oregon: Missoula, Mont., University of Montana, M.S. thesis, 88 p. https://scholarworks.umt.edu/etd/7536

Meigs, A., Scarberry, K., Grunder, A., Carlson, R., Ford, M. T., Fouch, M., Grove, T., Hart, W. K., Iademarco, M., Jordan, B., and Milliard, J., 2009, Geological and geophysical perspectives on the magmatic and tectonic development, High Lava Plains and northwest Basin and Range, *in* O'Connor, J. E., Dorsey, R. J., and Madin, I. P., GSA Field Guide 15, Volcanoes to Vineyards: Boulder, Colo., Geological Society of America. https://doi.org/10.1130/2009.fld015(21)

Milliard, J. B., 2010, Two-stage opening of the northwestern Basin and Range in eastern Oregon: Evidence from the Miocene Crane Bbasin: Corvallis, Oreg., Oregon State University, M.S. thesis, 82 p.

Minor, S. A., Rytuba, J. J., Grubensky, M. J., Meulen, D. B. V., Goeldner, C. A., and Tegtmeyer, K. J., 1987a, Geologic map of the High Steens and Little Blitzen Gorge Wilderness Study areas, Harney County, Oregon: U.S. Geological Survey Miscellaneous Field Studies Map MF-1876, 1 pl., scale 1:24,000. https://ngmdb.usgs.gov/Prodesc/proddesc_7460.htm

Minor, S. A., Rytuba, J. J., Vander Meulen, D. B., Grubensky, M. J., and Tegtmeyer, K. J., 1987b, Geologic map of the Wildhorse Lake quadrangle, Harney County, Oregon: U.S. Geological Survey Miscellaneous Field Studies Map MF-1915, 1 pl., scale 1:24,000. https://ngmdb.usgs.gov/Prodesc/proddesc_5480.htm

NCGMP (USGS National Cooperative Geologic Mapping Program), 2010, NCGMP09—Draft standard format for digital publication of geologic maps, version 1.1, *in* Soller, D. R., ed., Digital Mapping Techniques '09—Workshop Proceedings: U.S. Geological Survey Open-File Report 2010–1335, p. 93–146. https://pubs.usgs.gov/of/2010/1335/pdf/usgs_of2010-1335.pdf

Niem, A. R., 1974, Wright's Point, Harney County, Oregon: an example of inverted topography: Ore Bin, v. 36, no. 3, 33–49. https://www.oregongeology.org/pubs/OG/OBv36n03.pdf

Niewendorp, C. A., Duda, C. J. M., Houston, R. A., and McClaughry, J. D., 2018, Geologic map of the Devine Ridge South 7.5 minute quadrangle, Harney County, Oregon: Oregon Department of Geology and Mineral Industries Geologic Map Series GMS-120, 65 p., 1 pl., scale 1:24,000. https://www.oregongeology.org/pubs/gms/p-GMS-120.htm

Ogg, J. G., Ogg, G., and Gradstein, F. M., 2008, The concise geologic time scale: Cambridge University Press, 150 p.

Parker, D. J., 1974, Petrology of selected volcanic rocks of the Harney Basin, Oregon: Corvallis, Oreg., Oregon State University, Ph.D. dissertation, 153 p., 1 pl. https://ir.library.oregonstate.edu/concern/graduate_thesis_or_dissertations/r494vn606

Piper, A. M., Robinson, T. W., and Park C. F., 1939, Geology and ground-water resources of the Harney Basin, Oregon: U.S. Geological Survey Water Supply Paper 841, 189 p., 1 pl., scale 1:125,000. https://pubs.er.usgs.gov/publication/wsp841

Robertson, S., 1999, BGS rock classification scheme, v. 2, Classification of metamorphic rocks: Keyworth, U.K., British Geological Survey Research Report RR 99-02, 24 p. http://nora.nerc.ac.uk/id/eprint/3226/1/RR99002.pdf

Russell, I. C., 1884, A geological reconnaissance in southern Oregon: U.S. Geological Survey Annual Report 4 (1882-1883), p. 431–464. https://doi.org/10.3133/ar4

Sheppard, R. A., 1994, Zeolitic diagenesis of tuffs in Miocene lacustrine rocks near Harney Lake, Harney County, Oregon: U.S. Geological Survey Bulletin 2108, 28 p. https://pubs.usgs.gov/bul/2108/report.pdf

Sherrod, D. R., and Johnson, J. A., 1994, Geologic map of the Irish Lake quadrangle, Harney County, south-central Oregon: U.S. Geological Survey Miscellaneous Field Studies Map MF-2256, 1 sheet, scale 1:24,000. https://ngmdb.usgs.gov/Prodesc/proddesc_5877.htm

Smith, G. A., 1986a, Stratigraphy, sedimentology, and petrology of Neogene rocks in the Deschutes Basin, central Oregon: a record of continental margin volcanism and its influence on fluvial sedimentation in an arc-adjacent basin: Corvallis, Oreg., Oregon State University, Ph.D. dissertation, 467 p, 3 pl., scale 1:24,000.

Smith, G. A., 1986b, Stratigraphy, sedimentology, and the petrology of Neogene rocks in the Deschutes Basin, central Oregon: A record of continental-margin volcanism and its influence on fluvial sedimentation in an arc-adjacent basin: Richland, Wash., U.S. Department of Energy Basalt Waste Isolation Project, Rockwell Hanford Operations Publication RHO-BW-SA-555 P, 1 pl., scale 1:24,000.

Smith, J. V., and MacKenzie, W. S., 1958, The cooling history of high-temperature sodium-rich feldspars, pt. 4 *of* The alkali feldspars: Am. Mineralogist, v. 43, no. 9-10, p. 872–889.

Smith, R. L., and Roe, W. P., 2015, Oregon geologic data compilation [OGDC], release 6 (statewide): Oregon Department of Geology and Mineral Industries Digital Data Series OGDC-6, geodatabase. https://www.oregongeology.org/pubs/dds/p-OGDC-6.htm

Streck, M. J., 1994, Volcanology and petrology of the Rattlesnake Ash-Flow Tuff, eastern Oregon: Corvallis, Oreg., Oregon State University, Ph.D. dissertation, 184 p.

Streck, M., and Ferns, M., 2004, The Rattlesnake Tuff and other Miocene silicic volcanism in eastern Oregon, chap. 1 *of* Haller, K. M., and Wood, S. H., Geological field trips in southern Idaho, eastern Oregon, and northern Nevada: U.S. Geological Survey Open-File Report 2004-1222, p. 4–19. https://pubs.usgs.gov/of/2004/1222/

Streck, M. J., and Grunder, A. L., 1995, Crystallization and welding variations in a widespread ignimbrite sheet; the Rattlesnake Tuff, eastern Oregon, USA: Bulletin of Volcanology, v. 57, no. 3, p. 151–169. https://doi.org/10.1007/BF00265035

Streck, M. J., and Grunder, A. L., 2008, Phenocryst-poor rhyolites of bimodal, tholeiitic provinces: The Rattlesnake Tuff and implications for mush extraction models: Bulletin of Volcanology, v. 70, no. 3, p. 385–401. https://doi.org/10.1007/s00445-007-0144-3

Streck, M. J., Ferns, M. L., and McIntosh, W., 2015, Large, persistent rhyolitic magma reservoirs above Columbia River Basalt storage sites: The Dinner Creek Tuff Eruptive Center, eastern Oregon: Geological Society of America, Geosphere, v. 11, no. 2, 226–235. doi:10.1130/GES01086.1

Streck, M. J., Johnson, J. A., and Grunder, A. L., 1999, Field guide to the Rattlesnake Tuff and High Lava Plains near Burns, Oregon: Ore Bin, v. 61, no. 3, 64–76. https://www.oregongeology.org/pubs/og/OGv61n03.pdf

Thompson, G. A., and Burke, D. B., 1974, Regional geophysics of the Basin and Range province: Ann. Rev. Earth Planet. Sci., v. 2, 213-238. https://doi.org/10.1146/annurev.ea.02.050174.001241

Thormahlen, D. J., 1984, Geology of the northwest one-quarter of the Prineville quadrangle, central Oregon: Corvallis, Oreg., Oregon State University, M.S. thesis, 106 p. 1 pl., scale 1:24,000.

Trench, D., 2008, The termination of the Basin and Range Province into a clockwise rotating region of transtension and volcanism, central Oregon: Corvallis, Oreg., Oregon State University, M.S. thesis, 64 p.

Walker, G. W., 1970, Cenozoic ash-flow tuffs of Oregon: Ore Bin, v. 32, no. 6, 97–115. https://www.oregongeology.org/pubs/OG/OBv32n06.pdf

Walker, G. W., 1974, Some implications of Late Cenozoic volcanism to geothermal potential in the High Lava Plains of south-central Oregon: Ore Bin, v. 36, no. 7, p. 109–119. https://www.oregongeology.org/pubs/og/OBv36n07.pdf

Walker, G. W., 1977, Geologic map of Oregon east of the 121st meridian: U.S. Geological Survey Miscellaneous Investigations Map I-902, 2 sheets, scale 1:500,000. https://ngmdb.usgs.gov/Prodesc/proddesc_9795.htm

Walker, G. W., 1979, Revisions to the Cenozoic stratigraphy of Harney Basin, southeastern Oregon: U.S. Geological Survey Bulletin 1475, 35 p., 1 pl. https://doi.org/10.3133/b1475

Walker, G. W., and MacLeod, N. S., 1991, Geologic map of Oregon: U.S. Geological Survey, scale 1:500,000. https://ngmdb.usgs.gov/Prodesc/proddesc_16259.htm

Walker, G. W., and Repenning, C. A., 1965, Reconnaissance geologic map of the Adel quadrangle, Lake, Harney, and Malheur Counties, Oregon: U.S. Geological Survey, Miscellaneous Geologic Investigations Map IMAP-446, 1 pl., scale 1:250,000. https://doi.org/10.3133/i446

Wallace, R. E., and Calkins, J. A., 1956, Reconnaissance geologic map of the Izee and Logdell quadrangles, Oregon: U.S. Geological Survey Miscellaneous Field Studies Map MF-82, scale 1:62,500. https://ngmdb.usgs.gov/Prodesc/proddesc_2988.htm

Wentworth, C. K., 1922, A scale of grade and class terms of clastic sediments: Journal of Geology, v. 30, no. 5, p. 377–392.

Whitehead, R. L., 1994, Ground water atlas of the United States: Segment 7, Idaho, Oregon, Washington: U.S. Geological Survey Hydrologic Atlas 730-H, 31 p. https://doi.org/10.3133/ha730H

Woods, J. D., 1976, The geology of the Castle Rock area, Grant, Harney, and Malheur counties, Oregon: Portland, Oreg., Portland State University, M.S. thesis, 89 p. http://dx.doi.org/10.15760/etd.2606

12.0 APPENDIX

This appendix contains a summary of the geodatabase along with a description of analytical and field methods and the list of attribute fields for spreadsheets (see page 7 of this report). The appendix is divided into two sections:

- Section 12.1 describes the digital databases included with this publication.
- Section 12.2 contains a summary of analytical and field methods. Accompanying tables, explain the fields listed in various spreadsheets.

12.1 Geographic Information Systems (GIS) database

Geodatabase specifications

Digital data created for the Harney 7.5′ quadrangle are stored in an Esri format geodatabase. The geodatabase structure follows that outlined by the U.S. Geological Survey (USGS) National Cooperative Geologic Mapping Program 2009 draft standard format for digital publication of geologic maps, version 1.1 (NCGMP, 2010). The following information describes the overall database structure, the feature classes, and supplemental tables (**Figure 12-1**, **Figure 12-2**, **Figure 12-3**, **Table 12-1**, and **Table 12-2**).

The data are stored in a file geodatabase feature dataset (GeologicMap). Accessory file geodatabase tables (DataSources, DescriptionOfMapUnits, Glossary) were created by using ArcGIS version 10.2.2 (SP 1). The GeologicMap feature dataset contains all the spatially oriented data (feature classes) created for the Harney 7.5′ quadrangle. The file geodatabase tables are used to hold additional geologic attributes.

Figure 12-1. Harney 7.5′ quadrangle geodatabase feature datasets and data tables.

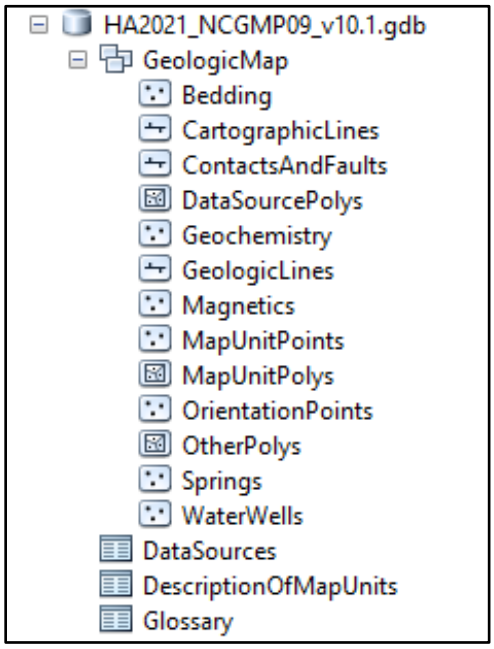

Geodatabase feature class specifications

Each feature class within the GeologicMap feature dataset in the geodatabase contains detailed metadata. Please see the metadata for detailed information such as process descriptions, accuracy specifications, and entity attribute descriptions.

Figure 12-2. Harney 7.5’ quadrangle geodatabase feature classes.

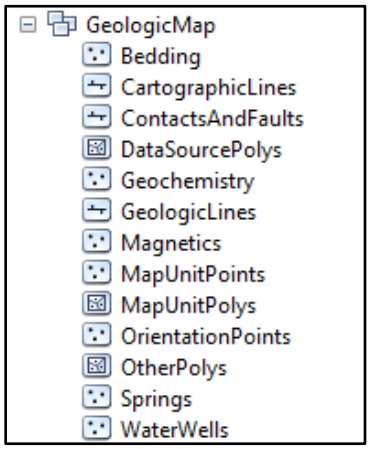

Table 12-1. Feature class descriptions.

Name	Description
Bedding	This feature class represents point locations in the quadrangle where bedding measurements were made or were compiled from previous studies. These data are also contained in the bedding (strike and dip) spreadsheet described in more detail below.
CartographicLines	Vector lines that have no real-world physical existence and do not participate in map-unit topology. The feature class includes cross section lines used for cartography for the quadrangle.
ContactsAndFaults	The vector lines in this feature class contains geologic content including contacts and fault locations used to create the map unit polygon boundaries. The existence and location confidence values for the contacts and faults are provided in the feature class attribute table.
DataSourcePolys	This feature class contains polygons that delineate data sources for all parts of the geologic map. These sources may be a previously published map, new mapping, or mapping with a certain technique. For a map with one data source, for example all new mapping, this feature class contains one polygon that encompasses the study area.
Geochemistry	This feature class represents point locations where whole-rock samples have been analyzed by X-ray fluorescence (XRF) techniques in the quadrangle. Includes data collected by the authors during this study or compiled from previous studies. These data are also contained in the geochemistry spreadsheet.
GeologicLines	These vector lines represent known fold axis locations in the quadrangle. The existence and location confidence for the fold axes are provided in the feature class attribute table.
Magnetics	This feature class represents point locations where measurements of natural remanent magnetization have been obtained for strongly magnetized lavas in the quadrangle. Includes data collected by the authors during the course of this study. These data are also contained in the magnetic polarity spreadsheet.
MapUnitPoints	This feature class represents points used to generate the MapUnitPolys feature class from the ContactsAndFaults feature class.
MapUnitPolys	This polygon feature class represents the geologic map units as defined by the authors.
OrientationPoints	This feature class represents point locations in the quadrangle where bedding measurements were made or were compiled from previous studies. These data are also contained in the bedding (strike and dip) spreadsheet.
OtherPolys	This feature class depicts the reference map for the quadrangle study area.
Springs	This feature class represents point locations where springs were in the quadrangle. Includes data observed or inferred by the authors or obtained by the authors from the Pacific Northwest Hydrography Framework (PNWHF). These data are also contained in the Springs spreadsheet.
WaterWells	This feature class represents point locations of water wells in the quadrangle. Includes data obtained by the authors from the Oregon Department of Water Resources (OWRD). These data are also contained in the WaterWell spreadsheet.

Geodatabase table specifications

Figure 12-3. Harney 7.5’ quadrangle geodatabase data tables.

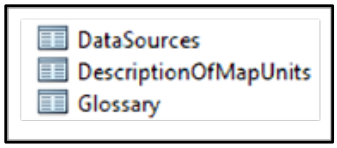

Table name descriptions

Table 12-2. Geodatabase data table descriptions.

Name	Description
DataSources	Data table that contains information about data sources used to compile the geology of the area.
DescriptionOfMapUnits	Data table that captures the content of the Description of Map Units (DMU), or equivalent List of Map Units and associated pamphlet text, included in a geologic map.
Glossary	Data table that contains information about the definitions of terms used in the geodatabase.

Geodatabase projection specifications

All spatial data are stored in the Oregon Statewide Lambert Conformal Conic projection. The datum is NAD83 HARN. The linear unit is international feet. See detailed projection parameters below:

Projection: Lambert_Conformal_Conic
False_Easting: 1312335.958005
False_Northing: 0.000000
Central_Meridian: -120.500000
Standard_Parallel_1: 43.000000
Standard_Parallel_2: 45.500000
Latitude_Of_Origin: 41.750000
Linear Unit: Foot (0.304800)

Geographic Coordinate System: GCS_North_American_1983_HARN
Angular Unit: Degree (0.0174532925199433299)
Prime Meridian: Greenwich (0.000000000000000000)
Datum: D_North_American_1983_HARN
Spheroid: GRS_1980
Semimajor Axis: 6378137.000000000000000000
Semiminor Axis: 6356752.314140356100000000
Inverse Flattening: 298.257222101000020000

Geologic map

This report is accompanied by a map plate displaying surficial and bedrock geology at a scale of 1:24,000 and geologic cross sections for the Harney 7.5′ quadrangle (**Figure 12-4**). The map plate was generated from detailed geologic data (scale of 1:24,000 or better) contained in the accompanying Esri format geodatabase. Both bedrock and surficial geologic interpretations can be recovered from the geodatabase and can be used to create a variety of additional thematic maps.

Figure 12-4. Plate reproduction, geologic map of the Harney 7.5′ quadrangle, Harney County, Oregon. Plate dimensions are 36 by 44 inches.

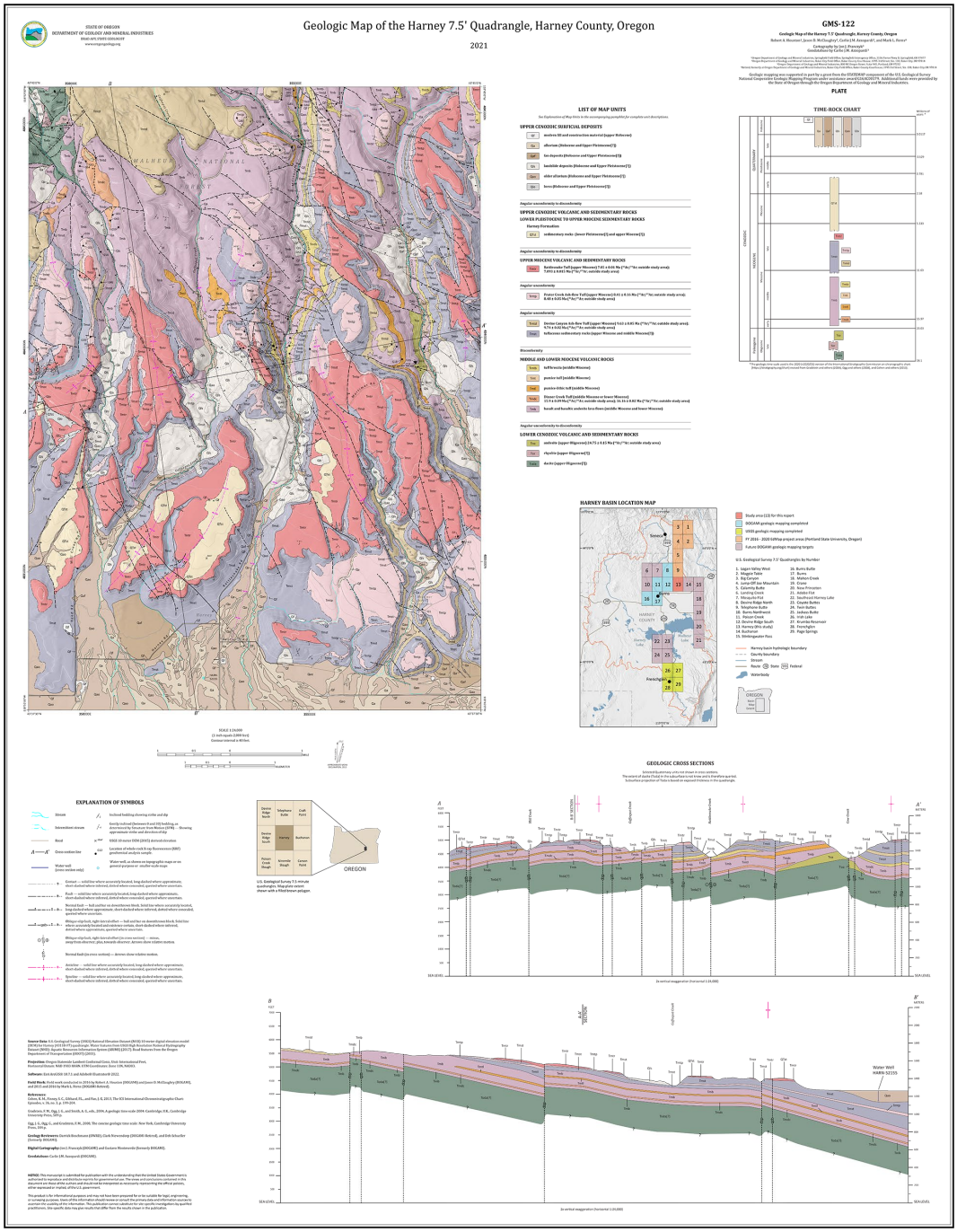

12.2 Methods

Geochemical analytical methods

Geologic mapping in the Harney 7.5′ quadrangle was supported by numerous new and compiled X-ray fluorescence (XRF) geochemical analyses of whole-rock samples. Descriptive rock unit names for igneous rocks are based on normalized major element analyses plotted on the total alkalis ($Na_2O + K_2O$) versus silica (SiO_2) diagram (TAS) of Le Bas and others (1986), Le Bas and Streckeisen (1991), and Le Maitre and others (2004). New and compiled XRF-geochemical analyses are included in the geodatabase, in a separate shapefile named HA2021_Geochemistry.shp, and in a Microsoft Excel® spreadsheet named HA2021_Geochemistry.xlsx. **Table 12-3** describes the fields listed in the spreadsheet. The locations of all geochemical samples are given in five coordinate systems: UTM Zone 11 (datum = NAD 27, NAD 83, units = meters), Geographic (datum = NAD 27, NAD 83, units = decimal degrees), and Oregon Lambert (datum = NAD 83, HARN, units = international feet).

Samples denoted by lab abbreviation WSU were analyzed by XRF at the Washington State University GeoAnalytical Lab, Pullman, Washington. Analytical procedures for the Washington State University GeoAnalytical Lab are described by Johnson and others (1999) and can be obtained online at https://s3.wp.wsu.edu/uploads/sites/2191/2017/06/Johnson-Hooper-and-Conrey.pdf. Notes for spreadsheet: nd, no data; original field sample locations in UTM Zone 11 (datum = NAD 83) coordinates.

Table 12-3. Geochemistry spreadsheet field names and descriptions.

Field	Description
SAMPLE_NO	A unique number identifying the sample. e.g., 18 HAH101-16.
WELL_ID	Well log number for wells. Wells in Harney County preceded by acronym HARN. e.g., HARN 152.
MAP_NO	A unique number identifying the sample on the map plates.
QUADRANGLE	The USGS 7.5’ quadrangle in which the sample is located. e.g., Harney.
ELEV_FT	Elevation of sample location in feet. e.g., 1928.
UTMN_NAD27	Meters north in NAD 27 UTM projection, zone 11.
UTME_NAD27	Meters east in NAD 27 UTM projection, zone 11.
LAT_NAD27	Latitude in NAD 27 geographic coordinates.
LONG_NAD27	Longitude in NAD 27 geographic coordinates.
UTMN_NAD83	Meters north in NAD 83 UTM projection, zone 11.
UTME_NAD83	Meters east in NAD 83 UTM projection, zone 11.
LAT_NAD83	Latitude in NAD 83 geographic coordinates.
LONG_NAD83	Longitude in NAD 83 geographic coordinates.
N_83HARN	Feet north in Oregon Lambert NAD 83, HARN, international feet.
E_83HARN	Feet east in Oregon Lambert NAD 83, HARN, international feet.
TERRANE_GR	Geologic group that the sample is assigned to. See GeologicMap, MapUnitPolys in the geodatabase. e.g., Columbia River Basalt Group. See pamphlet and DescriptionOfMapUnits table in the geodatabase.
FORMATION	Geologic formation that the sample is assigned to. See GeologicMap, MapUnitPolys in the geodatabase. e.g., Dalles Formation. See pamphlet and DescriptionOfMapUnits table in the geodatabase.
MEMBER	Geologic member that the sample is assigned to. See GeologicMap, MapUnitPolys in the geodatabase. e.g., Frenchman Springs. See pamphlet and DescriptionOfMapUnits table in the geodatabase.
MAP_UNIT_N	Geologic unit that the sample is assigned to. See GeologicMap, MapUnitPolys in the geodatabase. e.g., Basalt of Gingko. See pamphlet and DescriptionOfMapUnits table in the geodatabase.
MAP_UNIT_L	Unique label identifying the geologic unit that the sample is assigned to. See GeologicMap, MapUnitPolys in the geodatabase. e.g., Tmtr. See pamphlet and DescriptionOfMapUnits table in the geodatabase.
VOLCANIC_FIELD	Volcanic field that the unit is assigned to. In igneous provinces, a well-defined area covered with volcanic rocks with a common geologic history.
TAS_LITHOLOGY	Rock name assigned based on the total alkalis ($Na_2O + K_2O$) versus silica (SiO_2) diagram (TAS) of Le Bas and others (1986), Le Bas and Streckeisen (1991), and Le Maitre and others (2004). e.g., Basalt, Rhyolite.
[MAJOR ELEMENTS]	SiO_2, Al_2O_3, TiO_2, FeO*, MnO, CaO, MgO, K_2O, Na_2O, P_2O_5. In wt.%.
[TRACE ELEMENTS]	Ni, Cr, Sc, V, Ba, Rb, Sr, Zr, Y, Nb, Ga, Cu, Zn, Pb, La, Ce, Th, Nd, U, Cs, Co, Hf, Sm, Eu, Yb, Lu. In ppm.
LOI	Value for loss on ignition as reported by lab.
FE_2O_3	Iron (III) oxide or ferric oxide reported in original analysis.
FeO	Iron (II) oxide or ferrous oxide reported in original analysis.
REFERENCE	Publication reference, keyed to the reference list in this report.
METHOD	Analytical method used by laboratory that analyzed the sample. e.g., XRF.
LABORATORY	Analytical laboratory that analyzed the sample. e.g., F & M.
NOTES	Special information (e.g., alteration) about certain samples.

Natural remanent magnetization (magnetic polarity) methods

Field measurements of natural remanent magnetization (the magnetic field of a sample measured when induced magnetic fields are absent or zeroed out by probe [Butler, 1992]) were determined from strongly magnetized lavas exposed in the Harney 7.5′ quadrangle during the course of this study in order to distinguish between flow units with normal and reversed magnetic polarity. Magnetic polarity also serves as a check on the permissible age of radiometrically dated samples, when compared to the paleomagnetic time scale of Cande and Kent (1992). This method of constraining radiometric ages by magnetic polarity determinations is most effective when the analytical error is less than 0.20 m.y. Larger errors reported for radiometric ages may overlap so many polarity subchrons that no constraint is provided by knowing a sample's magnetic polarity. Magnetic polarity values reported were determined using a MEDA, Inc. μMag handheld digital fluxgate magnetometer. The measured point data are included in the geodatabase, a separate shapefile named HA2021_Magnetics.shp, and as a Microsoft Excel® spreadsheet named HA2021_Magnetics.xlsx. **Table 12-4** describes the fields listed in the spreadsheet. The locations of these point data are given in five coordinate systems: UTM Zone 11 (datum = NAD 27, NAD 83, units = meters), Geographic (datum = NAD 27, NAD 83, units = decimal degrees), and Oregon Lambert (datum = NAD 83, HARN, units = international feet).

The natural remanent magnetization (magnetic polarity) of strongly magnetized lavas was determined using the following method (also see **Figure 12-5**):

- A north-pointing arrow and near-horizontal line were drawn on and around (to the extent possible) an approximately fist-sized equidimensional sample that was then removed from the outcrop (**Figure 12-5**). Next, a line is drawn from the south end of the sample to the north end at an angle approximating the magnetic inclination (approximately equivalent to the latitude). For the study area, a line was drawn inclined at ~45° down to the north. This line gives the approximate orientation of the magnetic pole of the sample.
- The magnetometer was placed on the most level ground available in a relatively magnetically clean area. The probe was then placed in a fixed position in the horizontal plane and rotated to null the local magnetic field (μMag reads zero). This procedure was done incrementally beginning with minimum range sensitivity (2,000 mG [milliGauss]), increasing the sensitivity (20 mG) and re-rotating the probe until maximum sensitivity was reached. Magnetic polarity was then checked with the north end of a locked compass needle. Total field value will decrease when the compass needle is moved horizontally toward and remains parallel to the probe.
- The polarity of a sample was determined by placing the oriented sample in a path parallel to the probe. The inclined north-directed line drawn to represent the approximate magnetic pole of the sample was held horizontally (approximately) with the north end facing toward the probe at a distance of at least 10 times further than the measurement distance. A reading was then determined with the sample absent from the probe. The sample was then moved to a point (typically within 1 to 2 cm) toward the probe in order to cause a change of at least several times greater than the minimum resolution of the magnetometer (**Figure 12-5b**). A decrease in the total field value indicated normal-polarity (N); an increase in total field value indicated reversed-polarity (R).
- The sample was then rotated backward (top away from the probe) about a horizontal axis ~45° to see if field strength increased as the sample's inclined magnetic field was rotated into parallel with the probe.
- The polarity of two to ten representative samples from different portions of an outcrop or from different outcrops was determined to verify the repeatability of results. Erratic results, due to

re-magnetization resulting from lighting strikes, obscure post-emplacement alteration, or aberrant declination and inclination are reported as indeterminate (I). Reversed readings should take precedence over normal readings in assigning polarity. Re-magnetization will more likely reset the remnant magnetism to the present-day normal polarity.

Figure 12-5. Procedure for determining natural remanent magnetism of lavas. (A) Ideal sample is selected and oriented in outcrop. North arrow is drawn on upper surface; horizontal lines are drawn around the exposed edges of the sample. Fist-sized sample is then removed. (B) Magnetometer probe is placed in a fixed position in the horizontal plane and rotated to null the local magnetic field. Sample polarity is determined by moving the oriented sample into the path of the probe.

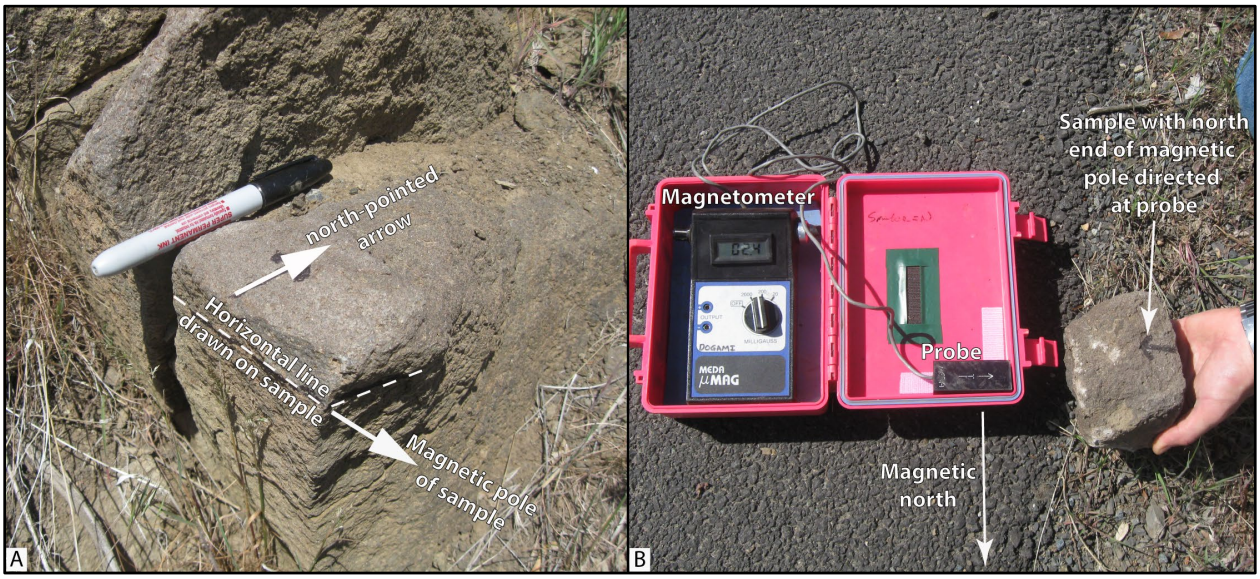

Table 12-4. Magnetics (natural remanent magnetization) spreadsheet field names and descriptions.

Field	Description
SITE	A unique number identifying the sample. e.g., 18DFW.
NRM	N, R, I Natural remanent magnetization of sample as determined from a portable fluxgate magnetometer.
QUADRANGLE	The USGS 7.5’ quadrangle in which the sample is located. e.g., Harney.
ELEV_FT	Elevation of sample location in feet. e.g., 1928.
UTMN_NAD27	Meters north in NAD 27 UTM projection, zone 11.
UTME_NAD27	Meters east in NAD 27 UTM projection, zone 11.
LAT_NAD27	Latitude in NAD 27 geographic coordinates.
LONG_NAD27	Longitude in NAD 27 geographic coordinates.
UTMN_NAD83	Meters north in NAD 83 UTM projection, zone 11.
UTME_NAD83	Meters east in NAD 83 UTM projection, zone 11.
LAT_NAD83	Latitude in NAD 83 geographic coordinates.
LONG_NAD83	Longitude in NAD 83 geographic coordinates
N_83HARN	Feet north in Oregon Lambert NAD 83, HARN, international feet
E_83HARN	Feet east in Oregon Lambert NAD 83, HARN, international feet
TERRANE_GR	Geologic group that the sample is assigned to. See GeologicMap, MapUnitPolys in the geodatabase. e.g., Columbia River Basalt Group. See pamphlet and DescriptionOfMapUnits table in the geodatabase.
FORMATION	Geologic formation that the sample is assigned to. See GeologicMap, MapUnitPolys in the geodatabase. e.g., Dalles Formation. See pamphlet and DescriptionOfMapUnits table in the geodatabase.
MEMBER	Geologic member that the sample is assigned to. See GeologicMap, MapUnitPolys in the geodatabase. e.g., Frenchman Springs. See pamphlet and DescriptionOfMapUnits table in the geodatabase.
MAP_UNIT_N	Geologic unit that the sample is assigned to. See GeologicMap, MapUnitPolys in the geodatabase. e.g., Basalt of Gingko. See pamphlet and DescriptionOfMapUnits table in the geodatabase.
MAP_UNIT_L	Unique label identifying the geologic unit that the sample is assigned to. See GeologicMap, MapUnitPolys in the geodatabase. e.g., Twfg. See pamphlet and DescriptionOfMapUnits table in the geodatabase.
REFERENCE	Publication reference, keyed to the reference list in this report.
METHOD	Method used to determine magnetic polarity of the sample.e.g., Portable fluxgate
NOTES	Special information (e.g., alteration) about certain samples.

Bedding (strike and dip)

Strike and dip measurements of inclined bedding were taken in the study area during this study by traditional compass and clinometer methods. Additional measurements have been compiled from previous workers. Strikes and dips are reported in both quadrant format (e.g., N30W, 15NE) and azimuthal format using the right-hand rule (e.g., 330, 15NE, American convention). Field measured bedding is coded by its appropriate Federal Geographic Data Committee (FGDC) reference number for geologic map symbolization. The measured point data are included in the geodatabase, a separate shapefile named HA2021_Bedding.shp, and as a Microsoft Excel spreadsheet named HA2021_Bedding.xlsx. **Table 12-5** describes the fields listed in the spreadsheet. The locations of these point data are given in five coordinate systems: UTM Zone 11 (datum = NAD 27, NAD 83, units = meters), Geographic (datum = NAD 27, NAD 83, units = decimal degrees), and Oregon Lambert (datum = NAD 83, HARN, units = international feet). Strike and dip symbols can be properly drawn by the Esri ArcMap product by opening the layer properties, categorizing by type, choosing the appropriate symbol, and rotating the symbol based on the "Strike_Azi" field. (The Advanced button allows one to select the rotation field). The rotation style should be set to geographic to maintain the right-hand rule property. Azimuths are given in true north; an additional clockwise correction of about 1.6 degrees is needed to plot strikes and dips properly on the Oregon Lambert conformal conic projection in this area.

DOGAMI has developed a routine and model in Esri ArcGIS Model Builder™ to calculate 3-point solutions for SFM-derived bedding. The modeling process incorporates the use of 1) a 5-m SRM-derived DEM (Digital Elevation Model); 2) the registration of three non-collinear points picked along the trace of a geological plane or contact discernable from a 5-m SFM DEM; 3) updating these points with their SFM-derived elevation values; and 4) creating a TIN (triangular irregular network) facet of the three points. The aspect of the TIN facet is equivalent to the dip direction and the slope corresponds to the dip (0˚ to 90˚ degrees). The strike is then determined from the dip direction, subtracting or adding 90˚ based on the right-hand rule (described in paragraph 1 above).

The factors influencing the certainty of SFM-derived bedding are the subjectivity of the digitizer and the clarity of the feature presumed to be indicative of bedding. Where possible, aerial photography, combined with a contextual knowledge of the geology of the area, was used to verify bedding features interpreted from the SFM. Agreement of the calculated strikes and dips over small areas, taken together with field measurements and data compiled from previous workers, was used as an accuracy gauge.

Table 12-5. Bedding (strike and dip) spreadsheet field names and descriptions.

Field	Description
STRUCTURE	Type of geologic structure from which feature was determined. e.g., Inclined bedding.
FGDC_REF	An attribute code assigned to each feature, derived from the Federal Geographic Data Committee (FGDC) digital standard for geologic map symbolization. e.g., 6.2.
QUADRANGLE	The USGS 7.5’ quadrangle in which the sample is located. e.g., Harney.
ELEV_FT	Elevation of data location in feet. e.g., 22.
UTMN_NAD27	Meters north in NAD 27 UTM projection, zone 11.
UTME_NAD27	Meters east in NAD 27 UTM projection, zone 11.
LAT_NAD27	Latitude in NAD 27 geographic coordinates.
LONG_NAD27	Longitude in NAD 27 geographic coordinates.
UTMN_NAD83	Meters north in NAD 83 UTM projection, zone 11.
UTME_NAD83	Meters east in NAD 83 UTM projection, zone 11.
LAT_NAD83	Latitude in NAD 83 geographic coordinates.
LONG_NAD83	Longitude in NAD 83 geographic coordinates.
N_83HARN	Feet north in Oregon Lambert NAD 83, HARN, international feet.
E_83HARN	Feet east in Oregon Lambert NAD 83, HARN, international feet.
TERRANE_GR	Geologic group that the sample is assigned to. See GeologicMap, MapUnitPolys in the geodatabase. e.g., Columbia River Basalt Group.
FORMATION	Geologic formation that the sample is assigned to. See GeologicMap, MapUnitPolys in the geodatabase. e.g., Rattlesnake Tuff Formation.
MEMBER	Geologic member that the sample is assigned to. See GeologicMap, MapUnitPolys in the geodatabase.
MAP_UNIT_N	Geologic unit that the sample is assigned to. See GeologicMap, MapUnitPolys in the geodatabase. e.g., dacite.
MAP_UNIT_L	Unique label identifying the geologic unit that the sample is assigned to. See GeologicMap, MapUnitPolys in the geodatabase. e.g., Toda.
STRIKE_QUAD	Strike direction of the inclined plane, stated in a north-directed quadrant format. e.g., N35E.
DIP	Amount of dip, degrees from horizontal, with direction. e.g., 45SE.
STRIKE_AZI	Strike direction of the inclined plane, as determined by employing the right-hand rule (American convention). e.g., 035.
DIP_AZIMUT	Azimuthal direction of dip. e.g., 125.
DIP_AMOUNT	Amount of dip, degrees from horizontal. e.g., 45.
REFERENCE	Publication reference, keyed to the reference list in this report.

Water well logs

Well log data are derived from written drillers' logs provided by Oregon Department of Water Resources (OWRD). Well logs vary greatly in completeness and accuracy, so the utility of subsurface interpretations based upon these data can be limited. Water well logs compiled and used for interpretation during this study were not field located. The approximate locations were estimated using tax lot maps, street addresses (coordinates obtained from Google Earth™), and aerial photographs to plot locations on the map. The accuracy of the locations ranges widely, from errors of one-half mile possible for wells located only by section and plotted at the section centroid to a few tens of feet for wells located by address or tax lot number on a city lot with bearing and distance from a corner. At each mapped location the number of the well log is indicated. This number can be combined with the first four letters of the county name (e.g., HARN 5473), to retrieve an image of the well log from the OWRD web site.

Point data are included in the geodatabase, in a separate shapefile named HA2021_WaterWells.shp, and in a Microsoft Excel spreadsheet named HA2021_WaterWells.xlsx. **Table 12-6** describes the fields listed in the spreadsheet. The locations of water well point data are given in six coordinate systems: UTM Zone 11 (datum = WGS 84, NAD 27, NAD 83, units = meters), Geographic (datum = NAD 27, NAD 83, units = decimal degrees), and Oregon Lambert (datum = NAD 83, HARN, units = international feet).

Lithologies in well intervals listed in the well log spreadsheet can alternate between consolidated and unconsolidated and may be listed as alternating between bedrock and surficial geologic units. This may occur where bedrock units are soft, where paleosols or weak zones lie within bedrock, or where cemented or partly cemented zones alternate with unconsolidated zones in surficial deposits.

Lithologic abbreviations used (alphabetical by group)

UNCONSOLIDATED SURFICIAL UNITS	
Abbreviation	**Description**
a	Ash
bd	Boulders
c	Clay
ch	Clay, hard (often logged as claystone but probably not bedrock)
g	Gravel
gc	Cemented gravel
gs	Gravel and sand (also sandy gravel)
m	Mud
s	Sand
sg	Sand and gravel (also gravelly sand)
st	Silt
ROCK, sedimentary	
ar	Argillite
bc	Breccia
cg	Conglomerate
cs	Claystone
pbs	Pebbly sandstone
sh	Shale
sts	Siltstone
ss	Sandstone
ROCK, igneous	
an	Andesite
b	Basalt
ba	Basaltic andesite
cd	Cinders
pu	Pumice
d	Diorite
gb	Gabbro
gr	Granite
l	Lava
r	Rhyolite
sc	Scoria
t	Tuff
v	Volcanic, undivided
vb	Volcanic breccia
Other	
af	Artificial fill
cl	Coal (lignite)
dg	Decomposed granite
o	Other (drillers unit listed in notes column of spreadsheet)
rk	Rock
sl	Soil
u	Unknown (typically used where a well has been deepened)

Table 12-6. Water well log spreadsheet field names and descriptions

Field	*Description and Example
TRS	Two digits for township, two digits for range, and two for section; negative if township is south of Willamette baseline. Exception for township and range if they contain a decimal. e.g., −2132.503.
COUNTY	Harney County. e.g., HARN.
GRID	Well log number for wells. Wells in Harney County preceded by acronym HARN (e.g., HARN 53799). e.g., 53779.
WELL_EL_FT	Wellhead elevation in feet as given by Google Earth™ at corresponding WGS 84 location. e.g., 1978.
LOCATED_BY	Google Earth™ elevation for cursor location at a given address. e.g., Google.
	Google Earth™ elevation at house in vicinity of given address. e.g., House.
	Pad identifying approximate well location, visible in air photo. e.g., Pad.
	Approximate taxlot centroid or other best guess for well location using a combination of taxlot maps and aerial photographs. e.g., Taxlot.
	Owner name. e.g., Owner.
	Wells located by Oregon Water Resources Department (OWRD) using handheld GPS. e.g., OWRD.
	GPS coordinates of wellhead included with well log. e.g., GPS.
	Approximate quarter-quarter-section centroid. e.g., qq.
	Approximate quarter-section centroid. e.g., q.
	Approximate fit to sketch map included with well log. e.g., map
LITHOLOGY	Best interpretation of driller's log using abbreviations above. e.g., g.
BASE_FT	Record base of driller's interval or, if lithology abbreviation would not change, similar intervals, in feet below wellhead. e.g., 17.
TOP_FT	Calculated top of driller's interval or similar intervals, in feet below wellhead. e.g., 14.
TOP_EL_FT	Calculated elevation at top of driller's interval, or similar intervals, in feet above sea level. e.g., 86.
BASE_EL_FT	Calculated elevation at base of driller's interval, or similar intervals, in feet above sea level. e.g., 83.
BEDRK_LITH	Lists bedrock lithologies, when encountered, abbreviations listed above. e.g., b.
BEDRK_ELEV	Calculated elevation at which bedrock or soil over bedrock was first encountered, in feet above sea level. e.g., 1924.
TAX_LOT	Taxlot number. Where it is determined that a taxlot number is used more than once in the section then the appropriate subdivision of the section is indicated in the notes field. e.g., 800.
COLOR	Color of interval as reported by the well driller. e.g., green.
NOTES	Notes about the stratigraphic interval as originally described by the well driller.
MAP_UNIT_L	Geologic unit interpreted in subsurface based on drillers log and designated by map unit label used in accompanying geodatabase. Intervals labeled "suna" (surface unit not applicable) are those where the lithology as interpreted by the original drillers' log do not correspond; also denotes intervals in the subsurface where a precise unit label cannot be applied. e.g., Tb.
QUADRANGLE	The USGS 7.5′ quadrangle in which the sample is located. e.g., Harney.
UTMN_WGS84	Meters north in WGS84 UTM projection, zone 11.
UTME_WGS84	Meters east in WGS84 UTM projection, zone 11.
UTMN_NAD27	Meters north in NAD 27 UTM projection, zone 11.
UTME_NAD27	Meters east in NAD 27 UTM projection, zone 11.
LAT_NAD27	Latitude in NAD 27 geographic coordinates.
LONG_NAD27	Longitude in NAD 27 geographic coordinates.
UTMN_NAD83	Meters north in NAD 83 UTM projection, zone 11.
UTME_NAD83	Meters east in NAD 83 UTM projection, zone 11.
LAT_NAD83	Latitude in NAD 83 geographic coordinates.
LONG_NAD83	Longitude in NAD 83 geographic coordinates.
N_83HARN	Feet north in Oregon Lambert NAD 83, HARN, international feet.
E_83HARN	Feet east in Oregon Lambert NAD 83, HARN, international feet.

*Well location given in six coordinate systems calculated by reprojecting original WGS 84 UTM, zone 11 locations.